Functions of the SLC36 transporter Pathetic in growth control of *Drosophila* sensory neurons

Wen-Yang Lin

A dissertation

submitted in partial fulfillment of the

requirements for the degree of

Doctor of Philosophy

University of Washington

2016

Reading Committee:

Jay Z. Parrish, Chair

Martha M. Bosma

David M. Parichy

Program Authorized to Offer Degree:

Biology

University of Washington

Abstract

Functions of the SLC36 transporter Pathetic in growth control of *Drosophila* sensory neurons

Wen-Yang Lin

Chair of the Supervisory Committee:

Associate Professor Jay Z. Parrish

Department of Biology

Dendrites exhibit enormous diversity in form and can differ in size by several orders of magnitude even in a single animal. However, whether neurons with large dendrite arbors have specialized mechanisms to support their growth demands is unknown. To address this question, we conducted a genetic screen for mutations that differentially affected growth in neurons with different sized dendrite arbors. From this screen, we identified a mutant that selectively affects dendrite growth in neurons with large dendrite arbors without affecting dendrite growth in neurons with small dendrite arbors or the animal overall. This mutant disrupts a putative amino acid transporter, Pathetic (Path), that localizes to the cell surface and endolysosomal compartments in neurons. Although Path is broadly expressed in neurons and non-neuronal cells,

mutation of *path* impinges on nutrient responses and protein homeostasis specifically in neurons with large dendrite arbors, but not in other cells.

To gain insight into the basis of growth control by *path*, we generated additional alleles of *path* and further examined the apparent specificity of growth defects in *path* mutants. We confirm our prior finding that loss of *path* function imposes an upper limit on neuron growth, and additionally report that *path* likely limits overall neurite length rather than dendrite length alone. Besides this, *path* mutant affects presynapse formation in C4da axons and nociceptive escape response. Using a GFP knock-in allele of *path*, we identify additional tissues where *path* likely functions in nutrient sensing and possibly growth control. Moreover, we demonstrate that *path* regulates translational capacity in a cell type that does not normally require *path* for growth, suggesting that *path* may confer robustness on growth programs by buffering translational output. Finally, we discovered that *path* mutant has dramatically shortened life span, but neuronal Path or path expression in other tissues can partially rescue the *path* mutant life span. Altogether, our results demonstrate that specialized molecular mechanisms exist to support growth demands in neurons with large dendrite arbors and define Path as a founding member of this growth program. Moreover, Path is a nutrient sensor with widespread function in Drosophila.

Table of Contents

Chapter 1 Molecular mechanisms of dendrite morphogenesis

1.1 Introduction

1.1.1 The evolution of the nervous system

The highly specialized nervous system enables both invertebrates and vertebrates to sense different environmental events and generate elaborate behaviors. The jellyfish has no true nervous system but specialized nerve nets composed of nerve cells that respond to light and chemicals in the environment (Holland et al., 2003). The earthworm is the first appearance of a segmented nervous system, and specific pairs of 'oscillatory firing neurons projecting to peripheral nerves' conduct octopamine-induced 'earthworm fictive' locomotion (Shimoi et al., 2014). The human brain contains roughly 67 billion brain cells (von Bartheld et al., 2016), and its 'number neurons' are specific for number processing in the brain region of lateral prefrontal cortex and the intraparietal sulcus (Nieder A., 2016).

Although vertebrates have tremendous complexity and diversity in nervous system than invertebrates, almost all of their neurons consist the typical morphology: a soma, a long axon, and multiple branching dendrites. Moreover, neuronal polarity, whereby polarized distribution of information proteins allows the information flows from dendrites toward the soma and to the axon, is highly conserved through Lophotrochozoans (Aplysia), Ecdysozoans (C. elegans and Drosophila), Chordates, and Vertebrates (Rolls et al., 2015). Interestingly, the human 'number neurons' are also present in numerically naïve monkeys, suggesting non-human primates and humans share the elemental quantification system (Nieder A., 2016). Understanding the evolutionary of neurons is critical to understanding how human nervous systems and behavior

arose. It is also very helpful for neuroscientists to know what kind of questions can be asked in the powerful and efficient invertebrate model systems.

Here, I summarize several featured evolutionary events of invertebrate and vertebrate nervous systems from anatomy to molecular mechanism. In the aspect of anatomy, the vertebrate brain has a much larger number of neurons and synapses than the invertebrate brain. Second, the central nervous system (CNS) of vertebrates is protected with skull and vertebral column, while there is no protective covering over invertebrate CNS except exoskeleton. Third, the vertebrate CNS is located on the back or dorsal surface of the body, whereas the invertebrate nerve cord is usually on the ventral side (Arendt et al., 1999). Fourth, in the vertebrate brain, sensory input is transmitted both contralaterally and ipsilaterally, while in invertebrate brain, sensory input is exclusively ipsilateral. Fifth, motor responses in vertebrates are controlled contralaterally, although motor responses in invertebrates are controlled ipsilaterally.

In terms of molecular mechanism, the appearance of vertebrate neural crest is mediated by conserved genetic mechanism involving BMPs, Wnts, and *Dlx* present in the ancestral chordate (Holland et al., 2009). Moreover, the more evolutionarily advanced vertebrates have the larger forebrain comparing to the midbrain and hindbrain, and the midbrain-hindbrain boundary organizer arose within the vertebrate lineage (Holland et al., 2009). Last, recent sequence analysis suggests that protein distribution changes at axon initial segment and differential microtubule polarity in axons and dendrites are likely to present in all bilaterians, including *C.elegans* and *Drosophila* (Ryan et al., 2013; Moroz et al., 2014).

1.1.2 Dendrite morphogenesis

Dendrites are processes of neurons that are specialized for information input. The formation of specialized morphological structures of dendrites is a key step to the establishment of wiring

of neuronal circuits. Throughout development, dendritic arbors must grow to an appropriate size to cover their receptive fields for proper signal inputs (London et al., 2005).

Dendrite morphogenesis can be divided into several stages. In both invertebrates and vertebrates, after exit from the cell cycle and extensive migration, neuron dendrites undergo axo-dendritic polarization, rapid dendritic arbor extension and growth, retraction and pruning, and synapse formation to establish and maintain their mature receptive field (Ramos et al., 2007; Bloss et al., 2016). In vertebrates, especially, while most dendritic branches become stabilized, individual dendritic spines continue to form, prune, and turn over as circuits mature. Dendritic spines are small extensions from the surface of a dendrite and preferentially form postsynaptic sites of most excitatory synapses (Bhatt et al., 2009). Abnormal dendritic arbor or losses of dendritic spine are major factors to mental disorders and neurodegenerative diseases, such as schizophrenia and Alzheimer's disease, respectively (Penzes et al., 2011). Therefore, understanding the molecules and mechanisms that control dendrite morphogenesis can give us a hint about nervous system function and connectivity.

Since the neuronal diversity is thought to arise from the combinatorial expression of a complex array of genetic determinants (Hobert et al. 2010), in this review, I will discuss both cell-intrinsic and cell-extrinsic molecules that regulate vertebrate and invertebrate dendrite growth separately.

1.2 Cell-intrinsic drivers of vertebrate dendrite growth

Recent findings have provided insights into cell-intrinsic molecules that regulate the stability of dendrite branch and dendritic spines, including protein kinases, transcription factors, nuclear calcium, local protein translation, and post-translational modification.

1.2.1 mTOR signaling proteins

An evolutionarily conserved serine/threonine protein kinase mechanistic (formerly 'mammalian') target of rapamycin (mTOR) signaling pathway plays important roles in establishment of dendritic arbors and the density of dendritic spines. mTOR functions in two distinct protein complexes named mTOR complex 1 (mTORC1) and mTOR complex 2 (mTORC2) with different sensitivities to nutrients, different upstream regulators, and different downstream cellular processes (Laplante et al., 2012). mTORC1 responds to stress, oxygen, energy status, growth factors, and most interestingly, amino acids availability in order to positively control protein synthesis through the modulation of mRNA translation (Goberdhan et al., 2016). mTORC2 is insensitive to nutrients but responds to growth factors in order to regulate cell survival, metabolism, and cytoskeleton organization (Renna et al., 2012).

In hippocampal pyramidal neurons of mice and rats, mutations in mTOR regulatory genes, the tuberous sclerosis complex 1 (*TSC1)* or tuberous sclerosis complex 2 (*TSC2)* tumor suppressor genes, cause enlargement of somas and decreased density of dendritic spines (Tavazoie et al. 2005). Activation of both mTORC1 and mTORC2 complexes is essential for the normal dendritic arbor growth of primary rat hippocampal cultures (Urbanska et al. 2012). In the peripheral nervous system of mice, injured dorsal root ganglion neurons activates mTOR signaling and that this activity increases axonal outgrowth capacity *in vitro*. Moreover, deletion

of *TSC2*, the negative regulator of mTOR activity, leads to increased basal level of mTOR activity, which is sufficient to facilitate axonal regrowth *in vivo* (Abe et al. 2012).

1.2.2 Transcription factors

Transcription factors provide complex but tightly regulated control of gene expression for vertebrate dendrite growth. For example, the mouse homologs of the *Drosophila* homeobox transcription factor *Cut, Cux1* and *Cux2* genes, coordinately controls the dendritic branching, formation of the dendritic spines, and functional synapses in layer II-III neurons of cerebral cortex. *Cux1* modulates the development of basal dendritic processes, while *Cux2* preferentially affects apical dendrite differentiation (Cubelos et al., 2015). *Cux* genes directly bind and repress downstream X-linked lymphocyte regulated (*Xlr*) *4b* and *XLR3b*, two chromatin remodeling genes that were implicated in cognitive defects (Cubelos et al., 2010).

A member of FoxO family of forkhead transcription factor, FoxO6, is predominantly expressed in the CA1 and CA3 regions of the mice hippocampus. Knockdown of FoxO6 proteins in mice leads to decreased dendritic spine density in hippocampal neurons *in vivo* (Salih et al., 2012). The member of the basic helix-loop-helix (bHLH) transcription factor, NeuroD, has also been shown to stimulate dendrite growth of rat cerebellar granule neurons. Knockdown of NeuroD in primary rat granule neurons specifically results in loss of total dendritic length but not the growth of axons (Gaudilliere et al., 2004).

1.2.3 Nuclear calcium signaling

Interestingly, nuclear calcium signaling robustly regulates many transcription factors with the role in controlling dendrite growth. For example, in rat cerebellar granule neurons, neuronal depolarization followed by transient calcium entry triggers the activation of calcium/calmodulin-dependent protein kinase (CaMK), CaMKIIα. CaMKIIα stimulates the phosphorylation of

NeuroD at Ser366 and directs downstream NeuroD-dependent transcription and dendrite growth (Gaudilliere et al., 2004). Moreover, in adult mouse hippocampal neurons, nuclear calcium-CaMKIV signaling has been demonstrated to regulate total dendrite length, dendritic complexity, and spine size through a downstream target gene, vascular endothelial growth factor D (VEGFD) (Mauceri et al., 2011).

1.2.4 Local protein translation

In order to response to rapid extension of dendritic arbors, high concentration of certain proteins are synthesized locally using messenger RNAs that are selectively transported into dendrites. Several RNA-binding proteins (RBPs) were found to regulate intracellular mRNA trafficking and translation through the formation of ribonucleo-protein (RNP) complexes with specific mRNA motifs (Doyle et al., 2011). For example, fragile X mental retardation protein (FMRP) binds to a subset of dendritic mRNAs containing a G quartet structure in the mouse brain and reversibly stalls ribosomes specifically on its structural target mRNAs (Brown et al., 2001; Darnell et al., 2011). Loss of function of FMRP causes aberrant growth of dendritic spines in CA1 pyramidal neurons of the mouse hippocampus (Udagawa et al., 2013).

1.2.5 Post-translational modification

It has been shown recently that the very dynamic processes of dendritic growth and maintenance are controlled by several post-translational modifications (PTMs). PTMs can fine-tune the localization and activity of specific dendritic proteins, and therefore control the stability of dendritic structures. For example, mouse poly-ADP-ribose polymerase 6 (PARP6) catalyzes the formation of mono-ADP-ribosylation (MARylation), a reversible PTM process of transfer of ADP-ribose from nicotinamide adenine dinucleotide (NAD^+) to amino acids on proteins. Huang et al. found that PARP6 is highly expressed during dendritic growth and branching in

cultured rat hippocampal neurons. Knockdown of PARP6 significantly reduces rat hippocampal dendrite length and branch points *in vivo* (Huang et al., 2016).

Another PTM that was recently found to regulate the maturation and stability of dendritic spines is neddylation. Neddylation is an ubiquitylation-like pathway that covalently conjugates ubiquitin-like proteins (UBL), such as Nedd8, to specific targets and therefore controls cell cycle and proliferation. Vogl et al. showed that Nedd8 mRNA was the most abundant UBL mRNA in immature and mature mouse hippocampal neurons. Downregulation of Nedd8 pathway in primary hippocampal neurons prevents the development of mature mushroom-like spines. Moreover, in $Nae1^{CamKII\alpha\text{-}CreERT2}$ mice, in which the Nedd8 activating enzyme (NAE) is conditionally ablated in adult excitatory forebrain neurons, the neurons have severe dendritic spine loss and decreased synaptic activity (Vogl et al., 2015).

1.3 Cell-extrinsic drivers of vertebrate dendrite growth

Cell-extrinsic cues also regulate distinct aspects of dendrite morphogenesis from the overall diverse patterns of dendrite branching to their fine structure of dendritic spines in vertebrates. Growth factors, extracellular matrix components, secreted polypeptide, and cell adhesion molecules regulate the growth and scaling of vertebrate dendritic arbors.

1.3.1 Growth factors

Brain-derived neurotrophic factor (BDNF) belongs to a family of secreted proteins, Neurotrophin family, and was found to promote dendrite growth and arborization through binding to the tyrosine receptor kinase (Trk) family (Xu et al., 2000). Knockdown of TrkC in mouse cerebellar Purkinje neurons severely reduces dendritic growth and branching (Joo et al., 2014). Moreover, in highly polarized neurons, intracellular receptor trafficking is essential for neurons to detect various extracellular cues during different stages of morphogenesis (Maeder et al., 2014). Recently, one of the intracellular trafficking proteins, ARHGAP33, was identified to regulate TrkB trafficking to synaptic sites. A*RHGAP33* knockout mice have impaired spine morphogenesis in hippocampal granule cells and exhibit spatial working deficits (Nakazawa et al., 2016).

1.3.2 Extracellular matrix components

About 20% of the vertebrate brain is occupied by extracellular space, and this space is filled with extracellular matrix (ECM) that forms a three-dimensional perineuronal net with surrounding cells (Dityatev et al., 2011). ECM are synthesized and secreted by neurons, glial, astrocytes, and non-neural cells, so its composition varies depending on different brain region (Clarke et al., 2013). Recent studies show that ECM controls the plasticity and maturation of

dendritic spines. For example, disruption of Reelin signaling in the adult mouse hippocampal neurons lead to shorter dendrites with abnormal orientations (Kupferman et al., 2014). Moreover, chondroitin sulfate proteoglycans (CSPGs) inhibits dendritic spine motility and functional plasticity thus stabilizing the mature cortex. After enzymatic digestion of CSPGs, the adult visual cortex shows an increased volume of the spine head (de Vivo et al., 2013).

1.3.3 Other secreted proteins

A secreted protein superfamily, semaphorin, has been implicated in dendrite morphogenesis. Semaphorin 3A (Sema3A), is well known in axon guidance, also acts as a polarizing factor that preferably induce dendrite formation in primary rat hippocampal neurons (Shelly et al., 2011). The Sema3A/Sema3A receptor neuropilin 1 (NRP1) signaling has also been implicated in regulation of basal dendritic arborization in mouse layer V cortical neurons (Tran et al., 2009). Notably, a protein kinase, thousand-and-one-amino acid 2 kinase (TAOK2) was found to interact with Nrp1 and modulate basal dendrite formation in mouse cortical pyramidal neurons (de Anda et al., 2012).

Both EphB receptor tyrosine kinases and ephrin-B ligands are membrane-bound proteins and are known to regulate a several aspect of neurogenesis through cell-cell interactions. Triple knockout of EphB1, EphB2 and EphB3 causes a significant decrease in total dendritic length and a reduction in the number of primary dendrites in primary mouse hippocampal neurons (Hoogenraad et al., 2005).

1.3.4 Cell adhesion molecules

The cell surface receptor Down's syndrome cell adhesion molecule (DSCAM) mediates several recognition events during the development of neural circuits. For example, DSCAM is abundantly expressed in the mouse cortex during the stage of cortical dendrite arborization and spine formation. Lack of DSCAM in spontaneous $DSCAM^{del17}$ mutant specifically impairs dendritic arborization and spine density in cortical pyramidal neurons of the early postnatal mouse (Maynard et al., 2012). Moreover, *Dscam* is expressed in mouse retinal ganglion cells (RGC) and is required for proper dendrite arborization (Fuerst et al., 2009).

The mouse *Protocadherins* (*Pcdhs*) locus is clustered into α-, β- and γ-subclusters (*Pcdha, Pcdhb* and *Pcdhg*), and encodes total 58 related cadherin-like transmembrane proteins (Wu et al., 1999). Deletion of all 22 *Pcdhg* genes disrupts normal dendrite patterning in mouse retinal starburst amacrine cells and cerebellar Purkinje neurons (Lefebvre et al., 2012). Notably, using transgenic and conditional knockout of *Pcdhg mice* reveal that expression of a single γ-Pcdh isoform is sufficient for a cortical neuron to form complex dendritic arbor, but only if surrounding cells express the same isoform. Moreover, increasing γ-Pcdh homophilic matching between astrocytes and pyramidal neurons leads to greater dendrite complexity, while decreasing γ-Pcdh homophilic matching between cells leads to reduced dendrite complexity (Molumby et al., 2016).

1.4 Invertebrate model systems for the research of dendrite growth

The mostly used invertebrate models in studying dendritic morphogenesis are *Caenorbabditis elegans* and *Drosophila melanogaster.* In the *C. elegans*, multidendritic mechanosensory FLP and PVD neurons tile the whole body wall; with FLP neurons cover the head region and PVD neurons cover the body region. Both FLP and PVD neurons extend their dendrites between the hypodermis and internal organs. Genetically, these two neurons follow the similar developmental cues to regulate dendrite morphogenesis. Behaviorally, FLP neurons respond to harsh mechanical force (Li et al., 2011); while PVD neurons respond to not only harsh mechanical force, but also temperature and osmolarity (Chatzigeorgiou et al., 2010). There are well-developed genetic tools and confocal imaging techniques make these neurons a nice system to study the development of dendrites.

In the peripheral nervous system (PNS) of *Drosophila*, dendrites of dendrite arborization (da) sensory neurons have been used as a model system for studying dendrite morphogenesis for several reasons. First, dendrites of these neurons establish their type-specific coverage of the body wall early in larval development and then maintain this coverage throughout later larval stages (Parrish et al., 2009). Second, different functional classes of da neurons have stereotyped class-specific dendritic arbors, which facilitate identification of genes influencing dendrite morphogenesis when conducting genetic screen (Grueber et al., 2002). Last, da neurons have multiple dendritic projections that are spread along the epidermis and accessible to live confocal imaging.

1.5 Cell-intrinsic drivers of invertebrate dendrite growth

1.5.1 mTOR signaling proteins

In Drosophila da neurons, mTORC1 and mTORC2 function distinctly in dendrite development of class IV da (C4da) neurons. Mosaic analysis with a repressible cell marker (MARCM) clones of m*Tor* and ribosomal S6 kinase (*S6K)*, one of the downstream targets of mTORC1, showed a severe simplification of dendritic arbors with significant reductions in the overall size of the receptive field. Moreover, m*Tor* and *S6K* trans-heterozygotes also showed simplified dendrites with significant reductions in dendrite branch number and length (Koike-Kumagai et al., 2009). In contrast, mTORC2 components regulate dendrite tiling and self-recognition, showing that mTORC1 and mTORC2 differentially control dendrite development in class IV neurons.

1.5.2 Transcription factors

In *C. elegans*, *mec-3* encodes a LIM homeodomain transcription factor and is required for distinct morphologies of sensory neurons in different expression levels (Albeg et al., 2011). Take the PVD neurons for instance, low levels of MEC-3 defines their elaborate lateral branches (Smith et al., 2010). Moreover, MEC-3 regulates the growth of PVD dendrites in combination with another conserved transcription factor aryl hydrocarbon receptor (AHR-1). AHR-1 blocks the expression of MEC-3 downstream targets, such as the claudin-like membrane protein HPO-30, which promotes the complex dendritic branching pattern of PVD neurons (Smith et al., 2013).

In *Drosophila*, class-specific expression patterns of the transcription factors Abrupt, Cut (the Cux1 and Cux2 homolog), Knot, Polycomb group, and Spineless (the AHR-1 homolog)

regulate the dendritic morphology of da neurons. Class I da (C1da) neurons express the BTB-zinc finger protein Abrupt, which defines their simple dendrite arbor (Sugimura et al., 2004). Abrupt uses Centrosomin, a centrosome-associated protein for mitotic spindle maturation, as a dendritic microtubule regulator to repress dendrite branch formation (Cagri et al., 2015). Class IV da neurons express the homeodomain protein Cut and early B cell factor/olfactory 1 protein Knot, which promotes their complex dendrite arbor (Grueber et al., 2003; Hattori et al., 2013). The cell adhesion molecule Ten-m is co-regulated by both Abrupt and Knot to control the branch outgrowth in C1da and C4da neurons correspondingly (Hattori et al., 2013). The Polycomb repressor complexes bind to methylated histone tails of homeobox transcription factors, and regulate the dendrite complexity of C4da neurons (Parrish et al., 2007). The basic helix–loop–helix-PAS protein Spineless (ss) is expressed in all da neurons and loss of ss reduces dendrite diversity (Kim et al., 2006).

1.5.3 Intracellular calcium signaling

In *Drosophila*, larval C4da neurons refine their connections through dendrite pruning during early metamorphosis (Emote, 2012). Intracellular calcium transients are found to compartmentalize in specific dendritic branches before elimination happens. Moreover, neuronal voltage-gated calcium channels (VGCCs) are responsible for generating the compartmentalized calcium influxes (Kanamori et al., 2013). In *Drosophila* larval motoneurons, activity-dependent calcium influx is required for normal dendrite growth of the monopolar motoneuron5 (MN5). Dα7 nicotinic acetylcholine receptors (nAChRs) are highly permeable to calcium and broadly expressed in MN5 prior to the onset of the dendrite development (Vonhoff et al., 2013).

Few studies have addressed the role of neuronal activity during dendritic development in the *Drosophila* nervous system due to the absence of suitable tools. Recently, Gao et al. designed

a transcriptional reporter of intracellular calcium (TRIC) in *Drosophila* that uses the *UAS-GAL4* binary system to report calcium-dependent interactions between calmodulin (CaM) and its target peptide. CaM is fused with a transcriptional activation domain; while CaM target peptide is fused with a DNA-binding domain. The binding of two fusion proteins depends on calcium concentration, and only in the presence of Ca^{2+}, the reconstituted transcription factor is able to express an effector. TRIC will allow both monitoring and manipulation of neuronal activity through the place of appropriate effectors (Gao et al., 2015).

1.5.4 Local protein translation

The development and maintenance of highly polarized dendrites, which extend long distances from the cell body, require finely tuned spatiotemporal control of gene expression. Recent genome-wide screen of novel localized transcripts in *Drosophila* C4da neurons reveals 55 transcripts that are particularly enriched in dendrites. Among these, 47 genes encode molecularly diverse proteins, and are enriched for genes that function in neuronal development and physiology. Transport of mRNAs encoded by these genes into the dendrites allows on-site mRNA translation during the dynamic developmental processes of dendrite growth (Misra et al., 2016).

For example, several RNA-binding proteins, such as Nanos, Pumilio, Glorund, and Smaug, involve in translation control in dendrite morphogenesis in Drosophila C4da neurons. Nanos and Pumilio together form a translational repression complex and localize to RNA granules in dendrites. The function of Nanos/Pumilio complex is required for the elaboration of high-order dendritic branches of C4da neurons (Ye et al., 2004). Glorund and Smaug further regulate the localization and translation of *nanos* mRNA in C4da dendrite terminals by binding to the stem loops structure in the 3′ untranslated region of nanos mRNA (Brechbiel et al., 2008).

1.6 Cell-extrinsic drivers of invertebrate dendrite growth

1.6.1 Steroid hormones

Steroid hormones are organic compound and play conserved roles in controlling the developmental transition across animal phyla. In *Drosophila*, ecdysteroids are the only steroid hormones, and they govern dendrite pruning of ddaC neurons during early metamorphosis (Kirilly et al., 2009). Two ecdysteroid receptors (EcR), EcRA and EcRB1, are expressed in C4da dendrites by third instar larvae before pruning happens (McParland et al., 2015). Moreover, several intrinsic factors, such as Brahma (Brm)-containing chromatin remodeler and a histone acetyltransferase CREB-binding protein (CBP) specifically activate a key ecdysteroid response gene, *sox14* in initiating dendrite pruning (Kirilly et al., 2011). Interestingly, recent research identified that the biosynthesis of ecdysteroids is regulated by a subset of serotonergic neurons in *Drosophila.* These neurons directly innervate the ecdyteroid-producing organ, prothoracic gland (PG), and modify their axon terminal morphology to nutrient conditions (Shimada-Niwa et al., 2014).

1.6.2 Extracellular matrix components

In Drosophila, C4da neurons tile the whole larval body wall with most dendrites distributed in a 2D space between the epidermal basal surface and the ECM secreted by the epidermis. Blocking epidermal production of laminins, one of the components of the ECM, causes dendrites to grow into the epidermis. Moreover, knocking out of neuronal integrins, the cell membrane receptor of laminins, also leads to increased epidermal enclosing and aberrant dendritic crossings. These studies suggest that epidermis-derived laminins function as ligands of neuronal integrins, and the laminin-integrin interaction mediates the attachment of dendrites to a 2D plane (Han et al., 2012).

1.6.3 Other secreted proteins

As mentioned above, the ECM-dendrite adhesion is critical for *Drosophila* larval C4da dendrites to grow into a 2D space. A recent study in the same system have found that epidermal secreted semaphorin ligand Sema-2b facilitates this contact-mediated dendrite patterning. The mutations in the *sema-2b* lead to a progressive increase in detachment of terminal dendrites from the ECM. Moreover, Sema-2b signals through the Plexin B receptor in neighboring C4da dendrites. Furthermore, from co-immunoprecipitation assay, β subunit of integrin is found to physically associate with the Plesin B receptor in dendrites for mediating downstream signaling pathway (Meltzer et al., 2016).

In *C.elegans*, a skin-derived conserved protein, MNR-1 (menorin), is required for the proper growth of PVD dendrites. MNR-1 physically interacts with the ligand complex SAX-7/L1CAM in the skin to promote higher-order branch formation (Salzberg et al., 2013). Besides the skin-derived diffusible cue, a body-wall muscle-derived conserved protein, LECT-2, which is homologous to vertebrate leukocyte cell-derived chemotaxin 2, is also required for patterning of PVD dendrites. The localization of LECT-2 is dependent on SAX-7/L1CAM, and LECT-2 functions genetically downstream of MNR-1–SAX-7/L1CAM adhesion complex. These findings suggest that during dendrite development of PVD neurons, diffusible signals from both skin and muscle orchestrate the molecular interactions of these three tissues (Díaz-Balzac et al., 2016).

1.6.4 Cell adhesion molecules

A few cell adhesion molecules are identified to play important roles in invertebrate dendrite patterning. In *C. elegans*, the ligand complex SAX-7/L1CAM on the hypodermal cells physically interacts with the cognate receptor DMA-1 on the PVD neuron to instruct the branching of PVD dendrites. Mutations in sax-7, mnr-1, or dma-1 lead to dramatic defects in

dendrite morphology (Dong et al., 2013).

In *Drosophila*, the atypical cadherin Flamingo (Fmi) is required in C4da neurons to repress abnormal dendritic crossing. Fmi forms a complex with the LIM domain protein Espinas (Esn) in C4da neurons and genetically interacts with downstream molecules regulating cell polarity such as Van Gogh (Vang) and Rho (Horiuchi et al., 2011). Moreover, similarly to mouse protocadherins, *Drosophila* DSCAM regulates dendrite patterning through homophilic binding. Interestingly, alternative splicing of *Drosophila Dscam* gene can generate up to 38,016 different receptor isoforms (Wojtowicz et al., 2004). Therefore, different da neurons express diverse DSCAM isoforms, which allow individual dendrites to repel each other through isoform-specific DSCAM-DSCAM interactions (Hughes et al., 2007).

1.7 References

Abe, N., Borson, S. H., Gambello, M. J., Wang, F. & Cavalli, V. Mammalian target of rapamycin (mTOR) activation increases axonal growth capacity of injured peripheral nerves. *J. Biol. Chem.* **285**, 28034–28043 (2010).

Albeg A, C.J. Smith, M. Chatzigeorgiou, D.G. Feitelson, D.H. Hall, W.R. Schafer, D.M. Miller 3rd, M. Treinin. C. elegans multi-dendritic sensory neurons: morphology and function. *Mol. Cell. Neurosci.* **46**, 308–317 (2011).

Arendt D, Nübler-Jung K. Comparison of early nerve cord development in insects and vertebrates. *Development*. **126**, 2309-25 (1999).

Brechbiel JL, Gavis ER. Spatial regulation of nanos is required for its function in dendrite morphogenesis. *Curr Biol.* **18**, 745-50 (2008).

Bhatt DH, Zhang S, Gan WB. Dendritic spine dynamics. *Annu Rev Physiol*. **71**, 261-82 (2009).

Bloss EB, Cembrowski MS, Karsh B, Colonell J, Fetter RD, Spruston N. Structured Dendritic Inhibition Supports Branch-Selective Integration in CA1 Pyramidal Cells. *Neuron*. **89**, 1016-30 (2016).

Brown, V. *et al*. Microarray identification of FMRP-associated brain mRNAs and altered mRNA translational profiles in fragile X syndrome. *Cell* **107**, 477–487 (2001).

Chatzigeorgiou M., S. Yoo, J.D. Watson, W.H. Lee, W.C. Spencer, K.S. Kindt, S.W. Hwang, D.M. Miller 3rd, M. Treinin, M. Driscoll, W.R. Schafer. Specific roles for DEG/ENaC and TRP channels in touch and thermosensation in C. elegans nociceptors. *Nat. Neurosci*. **13**, 861–868 (2010).

Clarke LE, Barres BA. Emerging roles of astrocytes in neural circuit development. *Nat Rev Neurosci.* **14**, 311-21 (2013).

Cubelos, B., Sebastián-Serrano, A., Beccari, L., Calcagnotto, M. E., Cisneros, E., Kim, S., Dopazo, A., Alvarez-Dolado, M., Redondo, J. M., Bovolenta, P. et al. Cux1 and Cux2 regulate dendritic branching, spine morphology, and synapses of the upper layer neurons of the cortex. *Neuron* **66**, 523-535 (2010).

Cubelos B., Briz C. G., Esteban-Ortega G. M., Nieto M. Cux1 and Cux2 selectively target basal and apical dendritic compartments of layer II-III cortical neurons. *Dev Neurobiol.* **75**, 163-72 (2015).

Darnell, J. C. *et al*. FMRP stalls ribosomal translocation on mRNAs linked to synaptic function and autism. *Cell.* **146**, 247–261 (2011).

de Anda FC, Rosario AL, Durak O, Tran T, Gräff J, Meletis K, Rei D, Soda T, Madabhushi R, Ginty DD, Kolodkin AL, Tsai LH. Autism spectrum disorder susceptibility gene TAOK2 affects basaldendrite formation in the neocortex. *Nat Neurosci.* **15**, 1022-31 (2012).

de Vivo L, Landi S, Panniello M, Baroncelli L, Chierzi S, Mariotti L, Spolidoro M, Pizzorusso T, Maffei L, Ratto GM. Extracellular matrix inhibits structural and functional plasticity of dendritic spines in the adult visual cortex. *Nat Commun*. **4**, 1484 (2013).

Díaz-Balzac CA, Rahman M, Lázaro-Peña MI, Martin Hernandez LA, Salzberg Y, Aguirre-Chen C, Kaprielian Z, Bülow HE. Muscle- and Skin-Derived Cues Jointly Orchestrate Patterning of Somatosensory Dendrites. *Curr Biol.* **[Epub ahead of print]** (2016).

Dityatev A, Schachner M, Sonderegger P. The dual role of the extracellular matrix in synaptic plasticity and homeostasis. *Nat Rev Neurosci*. **11**, 735-46 (2010).

Dong X, Liu OW, Howell AS, Shen K. An Extracellular Adhesion Molecule Complex Patterns Dendritic Branching and Morphogenesis. *Cell*. **155**, 296-307 (2013).

Doyle, M. & Kiebler, M. A. Mechanisms of dendritic mRNA transport and its role in synaptic tagging. *EMBO J.* **30**, 3540–3552 (2011).

Emoto K. Signaling mechanisms that coordinate the development and maintenance of dendritic fields. *Curr. Opin. Neurobiol*. 22, 805 (2012).

Fuerst PG, Bruce F, Tian M, Wei W, Elstrott J, Feller MB, Erskine L, Singer JH, Burgess RW. DSCAM and DSCAML1 function in self-avoidance in multiple cell types in the developing mouse retina. *Neuron.* **64**, 484-97 (2009).

Huang JY, Wang K, Vermehren-Schmaedick A, Adelman JP, Cohen MS. PARP6 is a Regulator of Hippocampal Dendritic Morphogenesis. *Sci Rep*. **6**, 18512 (2016).

Gao XJ, Riabinina O, Li J, Potter CJ, Clandinin TR, Luo L. A transcriptional reporter of intracellular Ca(2+) in Drosophila. *Nat Neurosci.* **18**, 917-25 (2015).

Gaudillière B, Konishi Y, de la Iglesia N, Yao Gl, Bonni A. A CaMKII-NeuroD signaling pathway specifies dendritic morphogenesis. *Neuron*. **41**, 229–241 (2004).

Goberdhan DC, Wilson C, Harris AL. Amino Acid Sensing by mTORC1: Intracellular Transporters Mark the Spot. *Cell Metab*. **23**, 580-589 (2016).

Han C, Wang D, Soba P, Zhu S, Lin X, Jan LY, Jan YN. Integrins regulate repulsion-mediated dendritic patterning of drosophila sensory neurons by restricting dendrites in a 2D space. *Neuron.* **73**, 64-78 (2012).

Hattori Y, Usui T, Satoh D, Moriyama S, Shimono K, Itoh T, Shirahige K, Uemura T. Sensory-neuron subtype-specific transcriptional programs controlling dendrite morphogenesis: genome-wide analysis of Abrupt and Knot/Collier. *Dev Cell.* **27**, 530-44 (2013).

Holland LZ. Chordate roots of the vertebrate nervous system: expanding themolecular toolkit. *Nat Rev Neurosci*. **10**, 736-46 (2009).

Holland ND. Early central nervous system evolution: an era of skin brains? *Nat Rev Neurosci*. **4**, 617-27 (2003).

Hoogenraad CC, Milstein AD, Ethell IM, Henkemeyer M, Sheng M. GRIP1 controls dendrite morphogenesis by regulating EphB receptor trafficking. *Nat Neurosci.* **8**, 906-15 (2005).

Hughes ME, Bortnick R, Tsubouchi A, Bäumer P, Kondo M, Uemura T, Schmucker D. Homophilic Dscam interactions control complex dendrite morphogenesis. *Neuron*. **54**, 417–27 (2007).

Huntley GW. Synaptic circuit remodelling by matrix metalloproteinases in health and disease. *Nat Rev Neurosci*. **13**, 743-57 (2012).

Joo W, Hippenmeyer S, Luo L. Dendrite morphogenesis depends on relative levels of NT-3/TrkC signaling. *Science*. **346**, 626–629 (2014).

Kupferman JV, Basu J, Russo MJ, Guevarra J, Cheung SK, Siegelbaum SA.
Reelin signaling specifies the molecular identity of the pyramidal neuron distal dendritic compartment. *Cell*. **158**, 1335-47 (2014).

Kanamori T, Kanai MI, Dairyo Y, Yasunaga K, Morikawa RK,Emoto K. Calcium transients trigger dendrite pruning in Drosophila sensory neurons. *Science*. **340**, 1475-8 (2013).

Kim MD, Jan LY, Jan YN. The bHLH-PAS protein Spineless is necessary for the diversification of dendrite morphology of Drosophila dendritic arborization neurons. *Genes Dev*. **20**, 2806-19 (2006).

Kirilly D, Gu Y, Huang Y, Wu Z, Bashirullah A, Low BC, Kolodkin AL, Wang H, Yu F. A genetic pathway composed of Sox14 and Mical governs severing of dendrites during pruning *Nat Neurosci*. **12**, 1497-505 (2009).

Kirilly D, Wong JJ, Lim EK, Wang Y, Zhang H, Wang C, Liao Q, Wang H, Liou YC, Wang H. Intrinsic epigenetic factors cooperate with the steroid hormone ecdysone to govern dendrite pruning in Drosophila. *Neuron*. 72, 86-100 (2011).

Laplante, M., and Sabatini, D.M. mTOR signaling in growth control and disease. *Cell.* **149**, 274-293 (2012).

Lefebvre JL, Kostadinov D, Chen WV, Maniatis T, Sanes JR. Protocadherins mediate dendritic self-avoidance in the mammalian nervous system. *Nature.* **488**, 517-21 (2012).

Li, W., L. Kang, B.J. Piggott, Z. Feng, X.Z. Xu. The neural circuits and sensory channels mediating harsh touch sensation in Caenorhabditis elegans. *Nat. Commun*. **2**, 315 (2011).

London M, Häusser M. Dendritic computation. *Annu Rev Neurosci*. **28**, 503-32 (2005).
Mackie G. O. Central neural circuitry in the jellyfish Aglantha: a model 'simple nervous system'. *Neurosignals*. **13**, 5-19 (2004).

Maeder, C. I., Shen, K. & Hoogenraad, C. C. Axon and dendritic trafficking. *Curr. Opin. Neurobiol.* **27**, 165–170 (2014).

Matsubara D, Horiuchi SY, Shimono K, Usui T, Uemura T. The seven-pass transmembrane cadherin Flamingo controls dendritic self-avoidance via its binding to a LIM domain protein, Espinas, in *Drosophila* sensory neurons. *Genes Dev.* **25**, 1982–96 (2011).

Mauceri, D., Freitag, H. E., Oliveira, A.M., Bengtson, C.P., Bading, H. Nuclear calcium-VEGFD signaling controls maintenance of dendrite arborization necessary for memory formation. *Neuron*. **71**, 117–130 (2011).

Maynard KR, Stein E. DSCAM contributes to dendrite arborization and spine formation in the developing cerebral cortex. *J Neurosci*. **32**, 16637-50 (2012).

McParland AL, Follansbee TL, Vesenka GD, Panaitiu AE, Ganter GK. Steroid Receptor Isoform Expression in Drosophila Nociceptor Neurons Is Required for Normal Dendritic Arbor and Sensitivity. *PLoS One.* **10**, e0140785 (2015).

Meltzer S, Yadav S, Lee J, Soba P, Younger SH, Jin P, Zhang W, Parrish J, Jan LY, Jan YN. Epidermis-Derived Semaphorin Promotes Dendrite Self-Avoidance by Regulating Dendrite-Substrate Adhesion in Drosophila Sensory Neurons. *Neuron*. **89**, 741-55 (2016).

Misra M, Edmund H, Ennis D, Schlueter MA, Marot JE, Tambasco J, Barlow I, Sigurbjornsdottir S, Mathew R, Vallés AM, Davis I, Leptin M, Gavis ER. A Genome-Wide Screen for Dendritically Localized RNAs Identifies Genes Required for Dendrite Morphogenesis. *G3 (Bethesda).* **[Epub ahead of print]** (2016).

Molumby MJ, Keeler AB, Weiner JA. Homophilic Protocadherin Cell-Cell Interactions Promote Dendrite Complexity. *Cell Rep***. 15,** 1037-50 (2016).

Moroz LL, Kocot KM, Citarella MR, Dosung S, Norekian TP, Povolotskaya IS, Grigorenko AP, Dailey C, Berezikov E, Buckley KM, Ptitsyn A, Reshetov D, Mukherjee K, Moroz TP, Bobkova Y, Yu F, Kapitonov VV, Jurka J, Bobkov YV, Swore JJ, Girardo DO, Fodor A, Gusev F, Sanford R, Bruders R, Kittler E, Mills CE, Rast JP, Derelle R, Solovyev VV, Kondrashov FA, Swalla BJ, Sweedler JV, Rogaev EI, Halanych KM, Kohn AB. The ctenophore genome and the evolutionary origins of neural system. *Nature*. **510**, 109-14 (2014).

Nakazawa T, Hashimoto R, Sakoori K, Sugaya Y, Tanimura A, Hashimotodani Y, Ohi K, Yamamori H, Yasuda Y, Umeda-Yano S, Kiyama Y, Konno K, Inoue T, Yokoyama K, Inoue T, Numata S, Ohnuma T, Iwata N, Ozaki N, Hashimoto H, Watanabe M, Manabe T, Yamamoto T, Takeda M, Kano M. Emerging roles of ARHGAP33 in intracellular trafficking of TrkB and pathophysiology of neuropsychiatric disorders. *Nat Commun.* **7**:10594 (2016).

Nieder A. The neuronal code for number. *Nat Rev Neurosci*. **17**,366-82 (2016).

Parrish JZ, Emoto K, Jan LY, Jan YN. Polycomb genes interact with the tumor suppressor genes hippo and warts in the maintenance of Drosophila sensory neuron dendrites. *Genes Dev*. **21**, 956-72 (2007).

Parrish JZ, Xu P, Kim CC, Jan LY, Jan YN. The microRNA bantam functions in epithelial cells to regulate scaling growth of dendrite arbors in drosophila sensory neurons. *Neuron*. **63**, 788-802 (2009).

Penzes P, Cahill ME, Jones KA, VanLeeuwen JE, Woolfrey KM. Dendritic spine pathology in neuropsychiatric disorders. *Nat Neurosci*.**14**, 285-93 (2011).

Ramos B, Gaudillière B, Bonni A, Gill G. Transcription factor Sp4 regulates dendritic patterning during cerebellar maturation. *Proc Natl Acad Sci*. **104**, 9882-9887 (2007).

Renna M, Bento CF, Fleming A, Menzies FM, Siddiqi FH, Ravikumar B, Puri C, Garcia-Arencibia M, Sadiq O, Corrochano S, Carter S, Brown SD, Acevedo-Arozena A, Rubinsztein DC. IGF-1 receptor antagonism inhibits autophagy. *Hum Mol Genet*. **22**, 4528-44 (2013).

Rui Y, Myers KR, Yu K, Wise A, De Blas AL, Hartzell HC, Zheng JQ. Activity-dependent regulation of dendritic growth and maintenance by glycogen synthase kinase 3beta. *Nat. Commun*. **4**, 2628 (2013).

Ryan JF, Pang K, Schnitzler CE, Nguyen AD, Moreland RT, Simmons DK, Koch BJ, Francis WR, Havlak P; NISC Comparative Sequencing Program, Smith SA, Putnam NH, Haddock SH, Dunn CW, Wolfsberg TG, Mullikin JC, Martindale MQ, Baxevanis AD. The genome of the ctenophore Mnemiopsis leidyi and its implications for cell type evolution. *Science*. **342**, 1242592 (2013).

Salih, DAM; Rashid, AJ; Colas, D; de la Torre-Ubieta, L; Zhu, RP; Morgan, AA; Santo, EE. FoxO6 regulates memory consolidation and synaptic function. *Genes & Development* **26**, 2780-2801 (2012).

Salzberg Y, Díaz-Balzac CA, Ramirez-Suarez NJ, Attreed M, Tecle E, Desbois M, Kaprielian Z, Bülow HE. *Skin-derived cues control arborization of sensory dendrites in Caenorhabditis elegans. Cell*. **155**, 308-20 (2013).

Shelly M, Cancedda L, Lim BK, Popescu AT, Cheng PL, Gao H, Poo MM. Semaphorin3A regulates neuronal polarization by suppressing axon formation and promoting dendrite growth. *Neuron.* **71**, 433-46 (2011).

Shimada-Niwa Y, Niwa R. Serotonergic neurons respond to nutrients and regulate the timing of steroid hormone biosynthesis in Drosophila. *Nat Commun*. **5**:5778 (2014).

Shimoi T, Mizutani K, Kojima D, Kitamura Y, Hotta K, Ogawa H, Oka K. Identification of oscillatory firing neurons associated with locomotion in the earthworm through synapse imaging. *Neuroscience*. **268**, 149-58 (2014).

Smith CJ, J.D. Watson, W.C. Spencer, T. O'Brien, B. Cha, A. Albeg, M. Treinin, D.M. Miller 3rd. Time-lapse imaging and cell-specific expression profiling reveal dynamic branching and molecular determinants of a multi-dendritic nociceptor in C. elegans. *Dev. Biol.* **345**, 18–33 (2010).

Smith CJ, O'Brien T, Chatzigeorgiou M, Spencer WC, Feingold-Link E, Husson SJ, Hori S, Mitani S, Gottschalk A, Schafer WR, Miller DM 3rd. Sensory neuron fates are distinguished by a transcriptional switch that regulates dendrite branch stabilization. *Neuron.* **79**, 266–280 (2013).

Sugimura, K., Satoh, D., Estes, P., Crews, S., Uemura, T. Development of morphological diversity of dendrites in *Drosophila* by the BTB-zinc finger protein Abrupt. *Neuron*. **43**,809–822 (2004).

Tavazoie, S. F., Alvarez, V. A., Ridenour, D. A., Kwiatkowski, D. J. & Sabatini, B. L. Regulation of neuronal morphology and function by the tumor suppressors Tsc1 and Tsc2. *Nat. Neurosci.* **8**, 1727–1734 (2005).

Tran TS, Rubio ME, Clem RL, Johnson D, Case L, Tessier-Lavigne M, Huganir RL, Ginty DD, Kolodkin AL. Secreted semaphorins control spine distribution and morphogenesis in the postnatal CNS. *Nature* **462**, 1065–1069 (2009).

Udagawa T, Farny NG, Jakovcevski M, Kaphzan H, Alarcon JM, Anilkumar S, Ivshina M, Hurt JA, Nagaoka K, Nalavadi VC, Lorenz LJ, Bassell GJ, Akbarian S, Chattarji S, Klann E, Richter JD. Genetic and acute CPEB1 depletion ameliorate fragile X pathophysiology. *Nat Med.* **19**, 1473-1477 (2013).

Urbanska, M.1, Gozdz, A., Swiech, L. J. & Jaworski, J. Mammalian target of rapamycin complex 1 (mTORC1) and 2 (mTORC2) control the dendritic arbor morphology of hippocampal neurons. *J. Biol. Chem.* **287**, 30240–30256 (2012).

van Beuningen SF, Hoogenraad CC. Neuronal polarity: remodeling microtubule organization. *Curr Opin Neurobiol*. **39**, 1-7 (2016).

Vogl AM, Brockmann MM, Giusti SA, Maccarrone G, Vercelli CA, Bauder CA, Richter JS, Roselli F, Hafner AS, Dedic N, Wotjak CT, Vogt-Weisenhorn DM, Choquet D, Turck CW, Stein V, Deussing JM, Refojo D. Neddylation inhibition impairs spine development, destabilizes synapsesand deteriorates cognition. *Nat Neurosci*. **18**, 239-251 (2015).

von Bartheld CS, Bahney J, Herculano-Houzel S. The Search for True Numbers of Neurons and Glial Cells in the HumanBrain: A Review of 150 Years of Cell Counting. *J Comp Neurol*. **[Epub ahead of print]** (2016).

Vonhoff F, Kuehn C, Blumenstock S, Sanyal S, Duch C. Temporal coherency between receptor expression, neural activity and AP-1-dependent transcription regulates *Drosophila* motoneuron dendrite development. *Development.* **140**, 606-16 (2013).

Wojtowicz W.M., J.J. Flanagan, S.S. Millard, S.L. Zipursky, J.C. Clemens. Alternative splicing of Drosophila Dscam generates axon guidance receptors that exhibit isoform-specific homophilic binding. *Cell*. **118**, 619–633 (2004).

Wu, Q. & Maniatis, T. A striking organization of a large family of human neural cadherin-like cell adhesion genes. *Cell.* **97**, 779–790 (1999)

Xu B, Zang K, Ruff NL, Zhang YA, McConnell SK, Stryker MP, Reichardt LF. Cortical degeneration in the absence of neurotrophin signaling: dendritic retraction and neuronal loss after removal of the receptor TrkB. *Neuron*. **26**, 233-245 (2000).

Yalgin Cagri, Saman Ebrahimi, Caroline Delandre, Li Foong Yoong, Saori Akimoto, Heidi Tran, Reiko Amikura, Rebecca Spokony, Benjamin Torben-Nielsen, Kevin P White, Adrian W Moore. Centrosomin represses dendrite branching by orienting microtubule nucleation. *Nat Neurosci.* **18**, 1437-45 (2015).

Ye B, Petritsch C, Clark IE, Gavis ER, Jan LY, Jan YN. Nanos and Pumilio are essential for dendrite morphogenesis in *Drosophila* peripheral neurons. *Curr. Biol.* **14**, 314–321 (2004).

Chapter 2 The SLC36 transporter Pathetic is required for extreme dendrite growth in *Drosophila* sensory neurons

2.1 Abstract

Dendrites exhibit enormous diversity in form and can differ in size by several orders of magnitude even in a single animal. However, whether neurons with large dendrite arbors have specialized mechanisms to support their growth demands is unknown. To address this question, we conducted a genetic screen for mutations that differentially affected growth in neurons with different sized dendrite arbors. From this screen, we identified a mutant that selectively affects dendrite growth in neurons with large dendrite arbors without affecting dendrite growth in neurons with small dendrite arbors or the animal overall. This mutant disrupts a putative amino acid transporter, Pathetic (Path), that localizes to the cell surface and endolysosomal compartments in neurons. Although Path is broadly expressed in neurons and non-neuronal cells, mutation of *path* impinges on nutrient responses and protein homeostasis specifically in neurons with large dendrite arbors, but not in other cells. Altogether, our results demonstrate that specialized molecular mechanisms exist to support growth demands in neurons with large dendrite arbors and define Path as a founding member of this growth program.

2.2 Introduction

How cells achieve their correct size and how this relates to organ size control is a fundamental, unresolved question in biology. As animals grow, most organs scale proportional to animal growth by addition of new cells (Hall et al. 2004). By contrast, nervous system growth largely entails growth of existing cells. For example, many types of sensory neurons are born early and must grow continuously during animal development to maintain coverage of a growing

receptive field (Parrish et al. 2009; Bloomfield and Hitchcock 1991). Within the nervous system, different types of neurons have different growth requirements, depending on the size and complexity of their dendrite and axon arbors. For example, mature cerebellar Purkinje neurons have dendrites that are more than two orders of magnitude longer than dendrites of nearby granule cells (Fiala et al. 2008). Likewise, dendrite arbor size scales with increased body size for many types of neurons across phylogeny (Purves and Lichtman 1985), thus neurons in larger animals must support greater growth demands. Given this enormous range in cell size, it seems likely that distinct mechanisms must exist to support growth in small and large neurons; however, whether neurons with extreme growth requirements such as Purkinje neurons have specialized machinery to support their growth demands remains unknown.

Size control in neurons depends, in part, on specification of neuronal type. Some neurons have an intrinsic growth program that operates largely independently of external influences. For example, the size and shape of some isolated retinal ganglion cells grown in culture is comparable to corresponding cells *in vivo*, suggesting that growth properties in these neurons are intrinsically encoded (Montague and Friedlander 1991). Likewise, following widespread genetic ablation of ganglion cells, spared ganglion cells adopt a normal size independent of contacts with other ganglion cells, further suggesting that size is intrinsically determined in ganglion cells (Lin et al. 2004). In some scenarios, expression of particular transcription factors dictates dendrite arbor size and complexity. For example, levels of the transcription factor *cut* dictate dendrite arbor size in *Drosophila* dendrite arborization (da) neurons; loss of *cut* reduces arbor size in da neurons with large dendrite arbors, whereas ectopic *cut* expression drives overgrowth of da neurons with small dendrite arbors (Grueber et al. 2003a). Similarly, levels of the MEC-3 transcription factor specify elaborate (low) or simple (high) dendrite arbors in *C. elegans* sensory

neurons (Smith et al. 2013). However, the downstream factors that facilitate growth, and whether they are materially different in neurons with small and large dendrite arbors remain unknown.

Drosophila peripheral nervous system (PNS) neurons have type-specific dendrite arbors that vary in size by several orders of magnitude in total dendrite length (Grueber et al. 2002), providing a tractable system to study dendrite growth control. Here we report our identification and characterization of *path*, which encodes a putative amino acid transporter that is broadly expressed in neurons and non-neuronal cells but is preferentially required for growth in neurons with large dendrite arbors. Dendrite growth in different types of neurons with large dendrite arbors arrests at the same value of total dendrite length in *path* mutants, despite the fact that dendrites in these neurons normally grow to very different sizes, suggesting that *path* defines a program required for extreme growth in neurons. Consistent with this notion, mutation of *path* impinges on nutrient responses and protein homeostasis in neurons with large arbors, but not in other cells. Altogether, our studies suggest that Path functions as part of a nutrient sensor in neurons and define a novel form of growth control required for extreme growth demands in neurons.

2.3 Materials and methods

2.3.1 Fly Husbandry

A list of alleles used in this study is available in the supplemental materials. EMS mutagenesis was conducted as previously described (Lee et al. 2015). Transgenic lines were generated using P-element mediated integration.

2.3.2 Live Imaging

Embryos were collected on yeasted grape juice agar and aged at 25˚C in a moist chamber. At the appropriate time, a single embryo/larva was mounted in 90% glycerol under coverslips sealed with grease and imaged on Leica SP5 microscope with a 40x 1.25NA lens. For quantitation of dendrite phenotypes, image stacks of dendrites in segments A3-A4 were captured from 8-10 larvae. For time-lapse analysis, larvae were imaged at the indicated time, recovered to yeasted agar plates with vented lids, aged at 25˚C, and imaged again.

2.3.3 Immunohistochemistry

Larval fillets were dissected/processed as described (Grueber et al. 2002) with the exception of tissue for anti-Path staining, which was fixed in 10% TCA for 15 minutes, washed 5x in PBS-Triton-X100 (0.3%) and then processes as other tissue. Samples were stained with the following antibodies: HRP conjugated with Cy2 or Cy3 (1:200; Jackson ImmunoResearch), mCD8 (1:100; Life Technologies), anti-Path (1:500), DAPI (50ng/mL; Life Technologies) and secondary antibodies from Jackson ImmunoResearch (1:250).

Surface Staining

Tissue was fixed in 4% Formaldehyde/PBS and subsequent washes and antibody incubations were conducted in the absence of detergent to prevent cell permeabilization.

2.3.4 Path antibody

Anti-Path antibodies were produced in guinea pigs using a KLH-conjugated peptide derived from the N-terminal cytosolic domain (KIQPRKSDTEQALAGN) common to all predicted Path polypeptides (Pierce Antibodies). Antibodies were affinity purified using the antigenic peptide. Specificity was confirmed by immunohistochemistry of *path* mutant body wall preparations.

2.3.5 Molecular Biology

UAS-path transgenes: The *path-RA* (path- *long)* and its derivatives were PCR amplified from cDNA clone RH24992 (Drosophila Genomics Resource Center); *path-RE* (path-short) and its derivatives were isolated via RT-PCR from larval body wall RNA. *ss-myr-GFP* transgene: The GMR15F10 *ss* enhancer (Pfeiffer et al. 2008) was PCR amplified and shuttled into a Gateway destination cassette (Life Technologies) that was cloned into pJFRC19 as a HindIII/SpeI fragment.

2.3.6 Luciferase Assays

120 hr AEL larvae were filleted in ice cold PBS (10 per sample) and body wall tissue was lysed with 1x Luciferase Cell Culture Lysis Reagent (Promega). Total protein concentration of each lysate was measured using a Quick Start Bradford Protein Assay (BIO-RAD), and the concentration of all samples were normalized by diluting lysates in Lysis Reagent, as needed. 20 µl of cell lysate was analyzed for Renilla luciferase using the Luciferase Assay System (Promega), and luminescence was measured using a Victor V Plate Reader (Perkin-Elmer). All values were corrected to blank wells. For measuring relative Renilla transcript levels, *SYBR* Green based quantitative RT–PCRs was used. RNA purification was performed with RNAqueous-Micro Total RNA Isolation Kit (Thermo Fisher). qRT–PCRs were done as

previously described. B-tubulin was used as a normalization control for experiments analyzing mRNAs. Primer sequences for Renilla: Ren F: GGGTGCTTGTTTGGCATTTC, Ren R: GGCCATTCATCCCATGATTC; b-tub F: AGACAAGATGGTTCAGGT; b-tub R: CGAGGCTCTCTACGATAT

2.3.7 Measurements

2D projections of Z-stacks were used for computer-assisted dendrite tracing with Neurolucida (MBF Bioscience), and features were measured using the traces. To monitor expression of GFP exon traps, we traced the outline of cells of interest in 2D projections of Z stacks using ImageJ and measured the mean pixel intensity within the cell. For these experiments, we imaged control and *path* mutant larvae using identical settings, including the same number and thickness of optical sections.

2.3.8 Statistical Analysis

Differences between group means were analyzed via ANOVA with a post hoc Dunnett's test; pairwise comparisons of group means were done with unpaired t-tests with Welch's correction.

Accessions

Microarray data is available at the NCBI Gene Expression Omnibus (accession: GSE64477).

2.4 Results

2.4.1 path is required for late stage dendrite growth

Drosophila dendrite arborization (da) neurons are born embryonically, and dendrites of these neurons grow continuously during larval development to maintain proportional body wall coverage (Jiang et al. 2014; Parrish et al. 2009). Different classes of da neurons cover different territories and, as a result, support different levels of growth (Fig. 1A, 1B)(Grueber et al. 2002; Parrish et al. 2009). Among these neurons, class I da (C1da) neurons have the simplest dendrite arbors and occupy the smallest territory whereas class IV da (C4da) neurons have the most complex arbors and occupy the largest territory; C4da dendrite length is nearly ten-fold greater than C1da dendrite length by the end of larval development (Fig. 1B).

We reasoned that if neurons with large dendrite arbors have specialized machinery to support increased growth demands, then mutations in such machinery would preferentially affect C4da dendrite growth. We therefore screened for mutations that affected growth of C4da dendrites but not C1da dendrites. Specifically, we EMS-mutagenized a *Drosophila* line bearing *ppk-CD4-tdTomato*, which labels C4da neurons, and screened mutants for defects in C4da dendrite arbor size. From this screen, we identified a homozygous viable mutant (*dendrite growth defective 50*; *dg50*) with severe C4da dendrite growth defects but no obvious effect on animal growth (Fig. 1C, 1D). In *dg50* mutants, early growth and patterning of C4da neurons proceed normally (Supplemental Fig. S1), but beginning in late first larval instar larvae, two growth defects are manifest. First, C4da dendrite length plateaus at ~3.5 mm, which *dg50* mutants reach by ~36-40 h after egg laying (AEL), whereas control C4da dendrites continue growing throughout larval development, reaching ~20 mm (Fig. 1D, 1E). Second, C4da dendrite arbors were remodeled after reaching their maximum length in *dg50* mutants: terminal dendrites

were progressively lost whereas primary dendrites continued to grow, maintaining a constant value of total dendrite length (Fig. 1D, Supplemental Fig. S2).

To determine whether *dg50* specifically affects growth in neurons with large dendrite arbors, we assayed *dg50* mutants for effects on growth of C1da and C3da neurons, which normally have small and medium-sized dendrite arbors, respectively (Fig. 1F, 1G). In wild type larvae, dendrites of dorsal C1da neurons (ddaD, ddaE) grew to a total length of 1.8 mm, on average, at 120 h AEL. C1da dendrites in *dg50* mutants grew to a comparable size and exhibited no measurable patterning defects. We also noted that *dg50* had no effect on dendrite growth in PNS neurons with even smaller dendrite arbors, including chordotonal neurons and bipolar dendrite neurons (Supplemental Fig. S3). Thus, *dg50* has no effect on dendrite growth in PNS neurons with small dendrite arbors.

Next, we monitored effects of *dg50* on growth of the C3da neurons ddaA and ddaF, which have medium-sized dendrite arbors (Fig. 1F, 1G). In control larvae, C3da dendrites reach a total length of 5.3 mm (ddaA) and 4.8 mm (ddaF), on average, at 120 h AEL. By contrast, C3da dendrites in *dg50* mutants grew to only 3.5 mm, comparable to the upper limit for C4da total dendrite length in *dg50* mutants. *dg50* therefore appears to impose an upper limit on dendrite growth in PNS neurons; in *dg50* mutants neurons with small dendrite arbors (bd, ch, C1da) are unaffected whereas dendrite growth in neurons with larger arbors (ddaA, ddaF, ddaC) arrests at a fixed dendrite length, despite the fact that these neurons normally grow to very different sizes.

To identify the molecular basis for these growth defects, we screened for chromosome deficiencies that failed to complement *dg50*. Heterozygosity for *dg50* had no effect on dendrite growth, but placing *dg50* in trans to *Df(3L)BSC773* phenocopied *dg50* homozygotes

(Supplemental Fig. S1), localizing *dg50* to a small interval and demonstrating that *dg50* is a recessive, loss-of-function allele. *Df(3L)BSC773* deletes 64 genes, including *path*, which has been implicated in growth control (Goberdhan et al. 2005), thus we tested whether *dg50* is allelic to *path*. Indeed, homozygosity for a P-element insertion allele of *path* ($path^{KG06640}$) or heteroallelic combination of $path^{KG06640}$ with *dg50* or *Df(3L)BSC773* similarly affected C4da dendrite growth (Supplemental Fig. S1). Further, *dg50* carries a 172 nucleotide deletion in *path* that causes a frameshift and premature stop, truncating the transmembrane domains. Thus, *dg50* should render Path nonfunctional (Fig. 1H). Finally, ubiquitous expression of GFP-tagged Path (*Actin-Gal4, UAS-pathA-GFP*) rescued *dg50* dendrite phenotypes (Supplemental Fig. S1), demonstrating that dendrite defects in *dg50* mutants were caused by loss of *path* function and that *UAS-pathA-GFP* is a functional transgene. We conclude that *dg50* is a loss-of-function allele of *path*.

path encodes an amino acid transporter of the solute carrier 36 (SLC36) family (Fig. 1H), many members of which are highly expressed in vertebrate nervous systems, including the two putative mammalian orthologs, SLC36A1 and SLC36A4 (Bermingham and Pennington 2004; Roshanbin et al. 2014; Sagné et al. 2001). SLC36 transporters appear to be involved in transport of amino acids and their derivatives, thus they may directly modulate cellular nutrient availability. However, requirements for SLC36 transporters in nervous system development have not been examined *in vivo*.

2.4.2 path is required for extreme dendrite growth in neurons

Our initial characterization of *path* suggested that neurons grow to a fixed limit in the absence of *path*. Since *path* transcript is maternally deposited (Tomancak et al. 2002), we examined whether maternal *path* supported dendrite growth in *path* zygotic null mutants. To this

end, we used the dominant female-sterile technique (Perrimon 1984) to generate homozygous mutant *path*^{dg50} germ-line clones and assayed for maternal *path* contribution to dendrite growth. Notably, C4da dendrites in larvae lacking both maternal and zygotic *path* function arrested at the same value of dendrite growth as zygotic *path* mutants (Supplemental Fig. S1), demonstrating that *path* function is indeed dispensable for dendrite growth up to this fixed limit. Taken together, these results suggest that da neurons can support dendrite growth up to a maximum of ~3.5 mm without *path*, but growth beyond this limit requires *path*.

In *path* mutants, dendrite patterning is altered to facilitate maximal extension of major dendrites. Whereas major dendrite branches continue to elongate throughout larval development in *path* mutants, overall dendrite length is unchanged after 36 h AEL and terminal dendrites are lost by retraction (Fig. 1D, Supplemental Fig. S2). This phenotype might reflect a deficit in branching or an intrinsic hierarchy in which primary dendrite growth predominates. We therefore investigated the relationship between dendrite patterning and *path*-dependent dendrite growth. To this end, we overexpressed the small GTPase Rac, which drives ectopic dendrite branching in C4da neurons (Lee et al. 2003), and monitored effects on dendrite growth in wild type and *path* mutant larvae. Although total dendrite length was unaffected, *rac* overexpression drove ectopic dendrite branching in both wild type and *path* mutant larvae (Fig. 2A), demonstrating that *path* mutant C4da neurons can support branching. Strikingly, this increase in terminal dendrite branching was accompanied by a significant decrease in primary dendrite growth in both control and *path* mutant larvae. As a result, distal portions of the territory normally covered by C4da neurons were completely devoid of dendrites. Thus, although *path* mutant C4da neurons can support dendrite branching, *path* affects dendrite growth independent of dendrite patterning and

in *path* mutants primary dendrite growth normally appears to be prioritized at the expense of terminal branching.

Dendrite growth in neurons with small arbors (e.g. C1da neurons) was unaffected by mutation of *path*, possibly because dendrite length in these neurons was below the threshold for sensitivity to *path* function. If this was indeed the case, increasing dendrite length beyond this threshold in C1da neurons should require *path* function. Ectopic expression of the homeodomain transcription factor *cut* drives exuberant dendrite growth in C1da neurons (Grueber et al. 2003a), therefore we monitored effects of *path* mutation on the ability of C1da neurons to support *cut*-induced exuberant dendrite growth. Consistent with prior reports, *UAS-cut* expression induced dendrite overgrowth in each of the C1da neurons, vpda, ddaD, and ddaE (Fig. 2B, Supplemental Fig. S4); we focused our analysis on vpda because our Gal4 drivers expressed most stably in that neuron. We found that two different C1da Gal4 drivers ($Gal4^{98b}$ and $Gal4^{221}$) became active at different time-points (1st instar larva and stage 17 embryo, respectively) and therefore supported different levels of *UAS-cut* induced dendrite growth (3.0 mm and 4.8 mm, respectively)(Fig. 2B). We reasoned that if *path* is required for dendrite growth beyond ~3.5 mm in da neurons, *path* mutation should affect *UAS-cut* induced dendrite growth in C1da neurons when driven by $Gal4^{221}$ but not $Gal4^{98b}$. This is precisely what we observed. Whereas *UAS-cut* expression induced dendrite overgrowth in all C1da neurons in *path* mutants, the extent of growth was constrained only when *UAS-cut* was driven by $Gal4^{221}$. The increased growth demands imposed by ectopic *cut* expression therefore require *path* only when dendrites grow beyond the empirically-determined threshold (~3.5mm), further demonstrating a role for *path* in supporting extreme dendrite growth. Different classes of da neurons develop at different rates (Parrish et al. 2009) and therefore reach this growth limit at different times (C4da neurons, 48hr AEL; C3da

neurons, 72hr AEL; *cut*-expressing C1da neurons, 96hr AEL). Thus, the growth limit for *path*-independent dendrite growth in C4da neurons appears to be independent of larval size and developmental progression.

Next, we investigated whether treatments that stimulate exuberant dendrite growth can modify the growth limit in *path* mutant larvae. Expression of *UAS-Pi3K92E* or *UAS-Raf* in C4da neurons drives excessive dendrite branch elongation while causing little effect on patterning of C4da dendrites (Fig. 2C), resulting in dendrite arbors with a 50% or 37% increase, respectively, in total dendrite length. However, mutation of *path* was epistatic to expression of either *Pi3K92E* or *Raf* in growth control of these neurons, with dendrite growth arresting at the same value in the absence or presence of these transgenes, further underscoring the notion that *path* mutation imparts a fixed growth limit on neurons (Fig. 2D).

2.4.3 path is a permissive factor for dendrite growth

Path is required to support growth in neurons with large dendritic arbors, so we wondered whether ectopic expression of path could promote exuberant growth in neurons with small dendrite arbors. To test this possibility, we overexpressed *path* (*UAS-pathA-GFP*) in C1da neurons of otherwise wild type larvae and monitored effects on dendrite growth. (Supplemental Fig. S5). Indeed, we found that overexpression of *path* could promote a modest but significant increase in C1da dendrite growth. By contrast, overexpression of *path* had no effect on the total dendrite length of C4da neurons. Given the relatively modest effect of *path* overexpression on C1da dendrites and the absence of any effect on C4da neurons, we conclude that the final size of dendritic arbors in these neurons are likely regulated by other factors, with *path* required to support growth beyond a fixed limit.

We next investigated the relationship between *path*-dependent and *path*-independent growth. To this end, we tested whether supplying *path* to *path*-deficient neurons after they reached the limit of *path*-independent growth was sufficient to support extreme dendrite growth. For these assays, we used *Heat Shock Gal4* (*HS-Gal4*) to inducibly and ubiquitously express *UAS-pathA-GFP* at different stages during larval development and monitored effects on C4da dendrite growth using live time-lapse microscopy. As described above, ubiquitous expression of *UAS-pathA-GFP* was sufficient to mitigate the dendrite growth defects of *path* mutants, but did not induce dendrite overgrowth, suggesting that *path* is a permissive factor for dendrite growth.

Dendrite defects in *path* mutants first appear after 36 h AEL (Fig. 1D), therefore we tested whether an early pulse of *UAS-pathA-GFP* expression (1 h heat shock @ 24 h AEL) would suffice for dendrite growth. Indeed, transient early *UAS-pathA-GFP* expression supported wild type growth in C4da neurons (Fig. 3A, 3B). Next, we assayed effects of resupplying *UAS-pathA-GFP* at different time-points during larval development: 48 h AEL, shortly after C4da neurons cross the threshold for *path*-dependent growth and growth defects first appear; 72 h AEL, when growth and patterning defects are manifest in *path* mutants; and 96 h, when wild type C4da dendrites have grown 400% more than *path* mutants. To our surprise, resupplying *UAS-pathA-GFP* at each time-point was sufficient to significantly rescue dendrite growth defects of *path* mutants (Fig. 3A, 3B). Thus, growth defects of *path* mutants are reversible. We note that resupplying path expression at 96 h AEL led to incomplete rescue at 144 h AEL (Fig. 3B), Prior studies have shown that structural plasticity in C4da neurons is progressively limited during larval development as a result of dendrite-substrate interactions (Grueber et al. 2003b; Jiang et al. 2014; Parrish et al. 2009; Sugimura et al. 2003); our findings suggest that this restriction in plasticity depends on proper dendrite growth during early larval stages. Remarkably, the rescued

neurons were comparable to wild type controls in size and pattern, even when *path* was resupplied after growth defects were manifest, suggesting that factors other than *path* determine the final size of C4da neurons.

We next used time-lapse microscopy to characterize dendrite growth in *path* mutant neurons before and after resupplying *path* expression. Prior to induction of *path* expression at 72 h, *path* mutant C4da dendrites exhibited severe growth deficits (Fig. 3C). However, 24 h after transient *path-GFP* expression, *path* mutant C4da neurons exhibited sprouting of new dendrites that grew extensively over the next 48 h, eventually regenerating wild type dendrite coverage in these neurons. Whereas *path* mutant C4da neurons exhibited no net growth over this time lapse, the "rescued" neurons exhibited a significant increase in growth rate and overall growth compared to wild type controls during this time lapse (Fig. 3C, 3D). Thus, altering the timing of *path* expression alters growth rate and timing but not the final size of dendrite arbors, suggesting that additional mechanisms exist that sense and/or constrain size in these neurons.

2.4.4 Path is ubiquitously expressed and localizes to endolysosomal compartments

To gain insight into Path's site of action and the basis for specificity of *path* mutant growth defects, we monitored distribution of Path *in vivo*. Since *path* mutants selectively affect growth in neurons with large dendrite arbors, we anticipated that Path would be selectively expressed in these neurons. However, in third instar larvae, punctate Path immunoreactivity was present in all cells of the body wall (Fig. 4A); this immunoreactivity was absent in $path^{dg50/Df}$ larvae (Fig. 4B, Supplemental Fig. S6), demonstrating the specificity of the antibody. In C4da neurons, Path was prominent in the soma and also present in axons and dendrites (Fig. 4A).

Next, we examined whether Path was present at different levels in neurons with small dendrite arbors and neurons with large dendrite arbors. This was not the case; somatic Path levels

were comparable in all da neurons (Fig. 4B). Although signal in neurites was obscured by epithelial Path expression, we observed no overt difference in Path levels in C1da and C4da dendrites. Likewise, Path levels were comparable in control and *UAS-cut* expressing C1da neurons (data not shown). Thus, Path levels do not appear to correlate with dendrite arbor size, consistent with Path functioning as a permissive factor for dendrite growth.

In the course of our analysis, we noted that ~0.5% of C4da neurons in *path* mutant larvae exhibited normal growth properties. These "escaper" C4da neurons retained detectable Path immunoreactivity (Supplemental Fig. S6), likely representing persistent maternally derived protein, indicating that low levels of neuronal Path are sufficient for extreme dendrite growth, and suggesting that Path functions cell-autonomously to support neuron growth. We noted an "all or none" response to loss of *path*: in neurons where detectable Path persisted, dendrite growth was comparable to wild type controls, whereas neurons without detectable Path did not grow beyond the empirically determined threshold for *path*-supported growth.

The epithelial expression of Path precluded high-resolution analysis of Path distribution in dendrites, therefore we focused on characterizing distribution of endogenous Path in C4da cell bodies. Mammalian SLC36A1 and SLC36A4 transporters localize to endolysosomal compartments (Roshanbin et al. 2014, 4; Wreden et al. 2003), and we likewise found that Path localized to structures labeled by endolysosomal markers in C4da neurons (Fig. 4C). To monitor Path distribution in neurites, we examined intracellular distribution of Path-GFP in C4da neurons of *path* mutants. Consistent with our antibody staining, Path-GFP was also distributed along axons and dendrites (Fig. 4D).

One model for Path function in dendrite growth control is that Path localizes to the plasma membrane where it senses or transports nutrients into the neuron. We therefore examined

Path distribution and topology using surface staining of C4da neurons expressing Path-GFP, reasoning that GFP should be surface-exposed if Path is targeted to the plasma membrane. As a negative control, we first assayed for surface-exposed GFP in C4da neurons expressing alpha-tubulin-GFP and observed no surface staining, demonstrating that the plasma membrane was not permeabilized in our staining protocol (Supplemental Fig. S5). By contrast, surface-exposed Path-GFP was detectable throughout C4da dendrite arbors (Fig. 4E). Path-GFP surface staining in dendrites was markedly higher than in axons or cell bodies, but surface staining of other antigens was likewise reduced in C4da axons and cell bodies (for example HRP immunoreactivity; Fig. 4E), likely a result of reduced accessibility due to glial wrapping, so we cannot conclusively say whether surface-exposed Path is enriched in dendrites. Overall, these results demonstrate that Path localizes to the cell surface in dendrites of C4da neurons and in endolysosomal compartments where it likely senses or transports amino acids to support dendrite growth.

2.4.5 path is required cell-autonomously for dendrite growth

Dendrite growth in PNS neurons depends on both cell-autonomous and non-autonomous cues, therefore we investigated the site of *path* action by generating single cell homozygous *path* mutant neuron clones in a heterozygous background using the MARCM approach (Lee and Luo 1999) and monitored effects on dendrite growth. As shown in Fig. 5, *path* mutant C4da MARCM clones exhibited growth defects identical to C4da neurons in *path* mutant larvae, suggesting that *path* functions cell-autonomously in C4da neurons to control dendrite growth (Fig. 5A, 5B). Consistent with this notion, resupplying *UAS-path-GFP* to *path* mutant C4da MARCM clones rescued the growth defects (Fig. 5A, 5B). Thus, *path* functions cell-autonomously to support growth in neurons with large dendrite arbors.

We next turned to a genetic rescue assay to define the minimal functional site for *path* to support dendrite growth, testing the ability of transgenic *path* expression in different tissues to rescue dendrite growth defects of *path* mutant larvae. Neuronal expression of *path*, using pan-neuronal, PNS-specific, or C4da-specific Gal4 drivers fully rescued the *path* mutant phenotype (Fig 5C, 5D). By contrast, *path* expression in other body wall tissues had no effect on C4da dendrite growth. Thus, *path* expression in C4da neurons is both necessary and sufficient for extreme dendrite growth.

The *path* locus encodes two predicted polypeptides: a short isoform and a long isoform with 13 additional amino acids on the N-terminal intracellular domain (Fig. 1H). Having shown that the long isoform (*path-A*) was sufficient for extreme dendrite growth, we next tested whether the short isoform (*path-E*) could likewise support extreme dendrite growth. Indeed, resupplying *UAS-pathE-GFP* to C4da neurons in *path* mutant larvae restored wild type dendrite growth (Fig. 5E, 5G). By contrast, removing the entire N-terminal intracellular domain (*UAS-pathDN*) abrogated Path function in dendrite growth and prevented Path localization to axons and dendrites (Fig. 5E-5G). Finally, the N-terminal domain alone (*UAS-pathADC)* had no activity in supporting dendrite growth, suggesting that the trans-membrane transporter domain is critical for *path* function. Thus, the N-terminal domain is necessary for Path function, perhaps by modulating Path localization, and/or interaction with accessory factors, but Path-long and -short are functionally equivalent for dendrite growth.

2.4.6 path regulates protein homeostasis to support dendrite growth

To identify molecular mechanisms of *path*-dependent growth in C4da neurons, we conducted microarray expression profiling of C4da neurons from wild type and *path* mutant larvae (Fig. 6A). We identified >2000 transcripts that were significantly deregulated in *path*

mutant C4da neurons, indicating that *path* exerts a strong influence on gene expression in these neurons (Supplemental Table S1). Pathway analysis indicated that genes associated with fatty acid metabolism and branched-chain amino acid degradation were significantly over-represented in the set of genes with decreased abundance in *path* mutant C4da neurons (Supplemental Table S2), consistent with *path* mutation eliciting a starvation response in C4da neurons and directly or indirectly regulating these pathways. Indeed, *path* mutant C4da neurons exhibited a striking increase in expression of *Drosophila 4E-BP* (*Thor*) (Supplemental Table S1), which is elevated in response to starvation (Teleman et al. 2005; Tettweiler et al. 2005). Additionally, *path* mutant C4da and to a lesser degree C3da neurons exhibited mitochondrial fusion, which occurs in many cell types after nutrient depletion (Rambold et al. 2011), whereas C1da neurons and epithelial cells did not (Fig. 6B and Supplemental Fig. S7). Thus, mutation of *path* induces an apparent starvation response in neurons with large dendrite arbors but not other cells in the body wall.

We noted that a large number of transcripts associated with translation were deregulated in C4da neurons of *path* mutants, and this was of particular interest for several reasons. First, among deregulated translation factors, translational repressors were, in general, increased in abundance in *path* mutants whereas positive regulators of translation were reduced in abundance (Fig. 6C), suggestive of a coherent response to reduce translational activity in C4da neurons. Second, transcription of translational machinery is coupled to nutrient availability (Mayer and Grummt 2006), thus reduced abundance of factors that promote translation was a further indication of a starvation response. Third, we noted that reporter expression (*ppk-CD4-tdTomato*) was attenuated in C4da neurons of *path* mutants despite the fact that *ppk* mRNA levels were apparently not affected (Fig. 6D and Supplemental Table S1). Thus, we hypothesized

that *path* mutation altered protein homeostasis in C4da neurons via effects on protein synthesis, stability, or both, contributing to growth defects.

To monitor effects of *path* mutation on protein homeostasis *in vivo* we used a collection of GFP protein traps that allows for visualization of proteins expressed from their endogenous loci in *Drosophila* (Morin et al. 2001). By comparing levels of these protein traps in wild type and *path* mutant backgrounds we aimed to gain insight into the apparent cellular specificity of growth defects in *path* mutants and to explore the generality of protein accumulation defects in *path* mutant C4da neurons. For these assays, we chose 11 protein traps that displayed a range of expression patterns encompassing the major cell types of the larval body wall (Fig. 6E, 6F). Additionally, we predominantly chose gene products whose mRNA expression in C4da neurons was unaffected by *path* (Supplemental Table S1); 3 traps of gene products with increased mRNA accumulation (sm, Gao, and Imp,) and 1 trap of a gene product with reduced mRNA accumulation (CG5174) in *path* mutant C4da neurons were exceptions to this criteria.

Overall, we observed striking concordance between *path*-dependent effects on cell growth and protein trap levels. Each of the 10 protein traps normally expressed in C4da neurons exhibited significantly reduced levels at 96 h AEL in *path* mutants, suggesting that *path* broadly promotes protein accumulation in these neurons. By contrast, these protein traps were expressed at comparable levels in wt and *path* mutant C4da neurons at 36 h AEL, prior to the onset of growth defects (Supplemental Fig. S8), after which time protein trap levels were progressively reduced. Therefore, expression of the protein traps closely follows the progression of growth defects in *path* mutant C4da neurons. In C3da neurons, levels of many protein traps were reduced as well, but the effect was less severe. By contrast, levels of protein traps in neurons with small dendrite arbors (C1da neurons, es neurons), peripheral glia, epidermal cells, and

muscle were unaffected by *path* mutation, demonstrating remarkable specificity in cell types with *path*-dependent effects on protein accumulation.

In principle, altered protein levels of *path* mutants could be manifest at the level of either synthesis (mRNA translation) or decay (protein stability). To more directly examine the relationship between *path* function and translation in C4da neurons *in vivo*, we turned to cell-type specific reporter transgene assays. Similar *in vivo* reporter approaches have been used to dissect tissue-specific functions of other translational regulators (Schleich et al. Nature 2014). We expressed a *UAS-Luciferase* reporter specifically in C4da neurons of *path* mutant larvae or WT controls and measured both protein and mRNA expression levels by Luciferase activity assays and qRT-PCR, respectively. This revealed only a modest decrease in mRNA levels in *path* mutants (Fig. 6G). In contrast, Luciferase activity decreased to background levels in *path* mutants. These data are consistent with a strong decrease in translational output per mRNA in *path* mutant C4da neurons.

To further assess the cellular specificity of the response to *path* mutation, we monitored effects of path mutation on growth of other larval cell types. However, larval cell types other than C4da/C3da neurons exhibited little or no dependence on *path* for growth (Fig. 6H). Finally, we used microarray analysis to survey gene expression responses to loss of *path* that were manifest across the larval body wall and observed minimal overlap with *path*-responsive changes in gene expression of C4da neurons (Fig. 6I, Supplemental Tables S3 and S4). We conclude that *path* mutation induces a starvation response and alters protein homeostasis specifically in neurons with extreme growth requirements (C4da and C3da neurons).

Our microarray analysis indicated that translational repressors including *pum* were upregulated in *path* mutant C4da neurons whereas core translational machinery was down-

regulated, thus we tested whether reducing *pum* function or increasing translational activity abrogated dendrite growth defects of *path* mutants. As previously reported (Ye et al. 2004), we found that *pum* overexpression strongly attenuated terminal dendrite growth in an otherwise wild type background, but *pum* overexpression failed to enhance the growth defect of path mutants (Fig. 7A), consistent with *pum* up-regulation contributing to growth defects of *path* mutants. Whereas RNAi knockdown of *pum* in C4da neurons of otherwise wild type larvae caused a modest growth deficit in C4da neurons, *pum(RNAi)* significantly increased dendrite growth in *path* mutant larvae (Fig. 7A), demonstrating that *pum* up-regulation is a functionally relevant output of *path*; up-regulation of other translational repressors (*aret*, *bru-3*, etc; Fig. 6C) may similarly contribute to *path* mutant dendrite growth defects.

As with *pum* overexpression, RNAi knockdown of core translational machinery (*Rpl22*) caused dendrite growth defects comparable to *path* mutants (Fig. 7B), but the effects of *Rpl22(RNAi)* and path mutation were not additive, consistent with *path* affecting dendrite growth by modulating translation. If the dendrite growth defects in *path* mutants were due to reduced translational output, we reasoned, then treatments that increase translation should mitigate the dendrite growth defect of *path* mutants. This is what we observed. Overexpression of either eIF4E, which promotes cap-dependent translation (Richter and Sonenberg 2005) and is down-regulated in path mutant C4da neurons (Supplemental Fig. S9), or a constitutively active form of the Ribosomal protein S6 kinase (CA-S6k), which promotes cell growth by increasing translational activity, increased C4da dendrite growth in *path* mutants (Fig. 7B). We note that the efficacy of these treatments in rescuing growth defects of *path* mutant neurons was limited, and this was likely due in part to the growth-inhibitory effect of up-regulated translational repressors

(Fig. 6C, 7A). Altogether, these results suggest that Path regulates dendrite growth – at least in part – via effects on translation.

The best characterized substrates for SLC36 transporters are amino acids (Thwaites and Anderson 2011) and SLC36 transporters can modulate TORC1 activity in cultured cells (Heublein et al. 2010), therefore we hypothesized that Path supports dendrite growth by modulating TORC1 activity in response to amino acids. If Path was functioning as a nutrient sensor for TORC1, we reasoned that TORC1 inactivation should mimic loss of *path* and activation of TORC1 should bypass requirements for *path*. This is not what we observed. First, loss of neuronal TORC1 function (*Tor* mutation, *Tor* dominant negative, *Raptor* mutation, *RagA* dominant negative) led to a less severe growth defect in C4da neurons than loss of *path* function (Supplemental Fig. S10), suggesting that *path* likely engages growth machinery other than just TORC1. Second, overexpression of *Rheb*, which can bypass the nutrient requirement for cell growth (Garami et al. 2003; Saucedo et al. 2003), *Tor*, *raptor*, or a constitutive active version of *Akt*, which can activate TORC2 in response to amino acid starvation under certain conditions (Tato et al. 2011), had no positive effect on dendrite growth of *path* mutants (Supplemental Fig. S10). However, co-expression of *UAS-path* and *UAS-Rheb* had a synergistic effect on dendrite growth (Fig. 7C), suggesting that *path* can stimulate dendrite growth together with TORC1. We conclude that Path likely functions through TORC1 as well as additional pathways to support the extreme growth requirements of neurons with large dendrite arbors.

2.5 Discussion

Neurons exhibit striking diversity in size and shape, but whether large neurons have specialized machinery to support their growth remains largely unknown. Our identification and characterization of Path demonstrates that, at least in *Drosophila*, neurons with large dendrite arbors have additional requirements to meet extreme growth demands. In neurons with large dendrite arbors, the response to *path* mutation is complex – despite manifesting signs of starvation and defects in protein homeostasis, primary dendrites continue to grow. Thus, dendrite patterning appears to be hierarchical and context dependent: in *path* mutants, neurons lack the ability to generate material for overall arbor expansion, hence material is preferentially allocated to facilitate primary dendrite elongation.

Independent of *path*, dendrites of PNS neurons grow to a maximum of ~3.5 mm, and growth beyond this limit requires *path*. How this limit is determined is currently unknown. One possibility is that the limit may be the result of some cellular commodity being exhausted in the absence of *path* function. If this is the case, *path*-independent and –dependent growth programs could utilize much of the same cellular machinery. Consistent with this scenario, neurons that do not require *path* for normal dendrite growth do require *path* for exuberant growth and hence have the machinery necessary for *path*-dependent growth. By extension, *path* may be broadly engaged in response to extreme growth demands and/or stress in neurons and non-neuronal cells, although *path* is dispensable for growth of most larval cell types under laboratory conditions.

Unexpectedly, the timing and pattern of C4da dendrite growth are remarkably labile. In the absence of *path* activity, dendrites grow to a maximum of ~3.5 mm and persist at that size even as arbors are remodeled to maximize primary dendrite elongation. Resupplying *path* to these neurons, even after several days of growth arrest, completely reversed the growth defects,

despite the fact that structural plasticity in C4da dendrites, as in many other systems, is progressively limited (Grueber et al. 2003b; Parrish et al. 2009; Ramoa et al. 1988; Sugimura et al. 2003). Our findings suggest that restriction of structural plasticity in C4da neurons depends on the extent of dendrite growth during early developmental stages; it remains to be seen whether a similar relationship is manifest in other systems. Interestingly, resupplying *path* expression following several days of growth arrest led to more rapid dendrite growth than at any period in wild type development, suggesting that growth-inhibitory cues or other signaling pathways that coordinate dendrite growth and animal growth normally temper dendrite growth at earlier developmental stages.

How might Path regulate dendrite growth? The most straightforward model is that Path is required for transmembrane transport of essential amino acids, which in turn modulate activity of mTORC1 and other amino acid responsive signaling pathways. Path localizes to the cell surface and endolysomal compartments, thus it could be involved in transporting amino acids into the cell or out of the lysosome. Several lines of evidence suggest that either scenario is unlikely. First, although one vertebrate Path counterpart, SLC36A1, promotes amino acid transport out of lysosomes and, as a result, antagonizes mTORC1 activity (Zoncu et al. 2011), Path is most closely related to SLC36A4 (Schiöth et al. 2013), which has no effect on lysosomal amino acid content. Second, Path is most active at neutral pH (Goberdhan et al. 2005), thus it seems unlikely that it is involved in amino acid transport out of lysosomes. Third, although Path displays high affinity for a variety of amino acids, it exhibits minimal processivity in transport assays (Goberdhan et al. 2005), so it seems unlikely that it would substantially contribute to amino acid flux.

While it's possible that Path requires an unidentified co-factor for maximal transport activity, an alternative explanation is that Path may function as a transceptor, a transporter-like protein with a receptor function, to regulate signaling in response to metabolites independent of its transport capacity (Thevelein and Voordeckers 2009). Examples of transceptors include the System A amino acid transporter SNAT2, which regulates transcription in response to amino acid binding (Hyde et al. 2007) and GLUT2, a sugar transporter that has transport-independent functions as a receptor for extracellular glucose (Stolarczyk et al. 2010). Thus, Path could function at the cell surface to report on environmental conditions, gating downstream signaling in response to extracellular amino acid availability. In this model, low levels of extracellular amino acids or absence of Path would signal the cell to marshal its resources and arrest dendrite growth whereas high levels of amino acids would activate signaling that regulates protein homeostasis, supporting extreme dendrite growth. With this in mind, it will be intriguing to further characterize the N-terminal intracellular domain, as the N-terminal domain is a likely site for protein-protein interactions and is required for Path function.

Many degenerative disorders preferentially affect neurons with large axons/dendrites including Purkinje neurons, Betz cells, motoneurons, and sensory neurons. Thus, it's plausible that defects in growth machinery that contribute to extreme neuron growth contribute to pathology in these diseases. Path orthologs are present in vertebrates (Schiöth et al. 2013), but their *in vivo* function remains unknown. Interestingly, two mammalian SLC36 transporters, SLC36A1 and SLC36A4, are highly expressed in the nervous system (Bermingham and Pennington 2004; Roshanbin et al. 2014; Sagné et al. 2001). Thus, it will be of great interest to determine whether these SLC36 transporters are required for extreme dendrite growth similar to Path.

2.6 References

Bermingham JR, Pennington J. 2004. Organization and expression of the SLC36 cluster of amino acid transporter genes. *Mamm Genome* **15**: 114–125.

Bloomfield SA, Hitchcock PF. 1991. Dendritic arbors of large-field ganglion cells show scaled growth during expansion of the goldfish retina: a study of morphometric and electrotonic properties. *J Neurosci* **11**: 910–917.

Fiala, JC, Spacek, J, Harrish, Kristen M. 2008. Dendrite structure. In *Dendrites* (eds. Stuart, Spruston, Nelson, and Hausser), pp. 1–41, Oxford University Press, New York.

Garami A, Zwartkruis FJT, Nobukuni T, Joaquin M, Roccio M, Stocker H, Kozma SC, Hafen E, Bos JL, Thomas G. 2003. Insulin activation of Rheb, a mediator of mTOR/S6K/4E-BP signaling, is inhibited by TSC1 and 2. *Mol Cell* **11**: 1457–1466.

Goberdhan DCI, Meredith D, Boyd CAR, Wilson C. 2005. PAT-related amino acid transporters regulate growth via a novel mechanism that does not require bulk transport of amino acids. *Development* **132**: 2365–2375.

Grueber WB, Jan LY, Jan YN. 2003a. Different levels of the homeodomain protein cut regulate distinct dendrite branching patterns of Drosophila multidendritic neurons. *Cell* **112**: 805–818.

Grueber WB, Jan LY, Jan YN. 2002. Tiling of the Drosophila epidermis by multidendritic sensory neurons. *Development* **129**: 2867–2878.

Grueber WB, Ye B, Moore AW, Jan LY, Jan YN. 2003b. Dendrites of distinct classes of Drosophila sensory neurons show different capacities for homotypic repulsion. *Curr Biol* **13**: 618–626.

Hall MN, Raff M, Thomas G, eds. 2004. *Cell Growth: Control of Cell Size*. Cold Spring Harbor Press, Cold Spring Harbor, NY.

Heublein S, Kazi S, Ogmundsdóttir MH, Attwood EV, Kala S, Boyd CAR, Wilson C, Goberdhan DCI. 2010. Proton-assisted amino-acid transporters are conserved regulators of proliferation and amino-acid-dependent mTORC1 activation. *Oncogene* **29**: 4068–4079.

Hyde R, Cwiklinski EL, MacAulay K, Taylor PM, Hundal HS. 2007. Distinct sensor pathways in the hierarchical control of SNAT2, a putative amino acid transceptor, by amino acid availability. *J Biol Chem* **282**: 19788–19798.

Jiang N, Soba P, Parker E, Kim CC, Parrish JZ. 2014. The microRNA bantam regulates a developmental transition in epithelial cells that restricts sensory dendrite growth. *Development* **141**: 2657–2668.

Lee A, Li W, Xu K, Bogert BA, Su K, Gao F-B. 2003. Control of dendritic development by the Drosophila fragile X-related gene involves the small GTPase Rac1. *Development* **130**: 5543–5552.

Lee J, Peng Y, Lin W-Y, Parrish JZ. 2015. Coordinate control of terminal dendrite patterning and dynamics by the membrane protein Raw. *Development* **142**: 162–173.

Lee T, Luo L. 1999. Mosaic analysis with a repressible cell marker for studies of gene function in neuronal morphogenesis. *Neuron* **22**: 451–461.

Lin B, Wang SW, Masland RH. 2004. Retinal ganglion cell type, size, and spacing can be specified independent of homotypic dendritic contacts. *Neuron* **43**: 475–485.

Mayer C, Grummt I. 2006. Ribosome biogenesis and cell growth: mTOR coordinates transcription by all three classes of nuclear RNA polymerases. *Oncogene* **25**: 6384–6391.

Montague PR, Friedlander MJ. 1991. Morphogenesis and territorial coverage by isolated mammalian retinal ganglion cells. *J Neurosci* **11**: 1440–1457.

Morin X, Daneman R, Zavortink M, Chia W. 2001. A protein trap strategy to detect GFP-tagged proteins expressed from their endogenous loci in Drosophila. *Proc Natl Acad Sci U S A* **98**: 15050–15055.

Parrish JZ, Xu P, Kim CC, Jan LY, Jan YN. 2009. The microRNA bantam functions in epithelial cells to regulate scaling growth of dendrite arbors in drosophila sensory neurons. *Neuron* **63**: 788–802.

Perrimon N. 1984. Clonal Analysis of Dominant Female-Sterile, Germline-Dependent Mutations in *Drosophila Melanogaster*. *Genetics* **108**: 927–939.

Pfeiffer BD, Jenett A, Hammonds AS, Ngo T-TB, Misra S, Murphy C, Scully A, Carlson JW, Wan KH, Laverty TR, et al. 2008. Tools for neuroanatomy and neurogenetics in Drosophila. *Proc Natl Acad Sci U S A* **105**: 9715–9720.

Purves D, Lichtman JW. 1985. Geometrical differences among homologous neurons in mammals. *Science* **228**: 298–302.

Rambold AS, Kostelecky B, Elia N, Lippincott-Schwartz J. 2011. Tubular network formation protects mitochondria from autophagosomal degradation during nutrient starvation. *Proc Natl Acad Sci U S A* **108**: 10190–10195.

Ramoa AS, Campbell G, Shatz CJ. 1988. Dendritic growth and remodeling of cat retinal ganglion cells during fetal and postnatal development. *J Neurosci* **8**: 4239–4261.

Richter JD, Sonenberg N. 2005. Regulation of cap-dependent translation by eIF4E inhibitory proteins. *Nature* **433**: 477–480.

Roshanbin S, Hellsten SV, Tafreshiha A, Zhu Y, Raine A, Fredriksson R. 2014. PAT4 is abundantly expressed in excitatory and inhibitory neurons as well as epithelial cells. *Brain Res* **1557**: 12–25.

Sagné C, Agulhon C, Ravassard P, Darmon M, Hamon M, El Mestikawy S, Gasnier B, Giros B. 2001. Identification and characterization of a lysosomal transporter for small neutral amino acids. *Proc Natl Acad Sci U S A* **98**: 7206–7211.

Saucedo LJ, Gao X, Chiarelli DA, Li L, Pan D, Edgar BA. 2003. Rheb promotes cell growth as a component of the insulin/TOR signalling network. *Nat Cell Biol* **5**: 566–571.

Schiöth HB, Roshanbin S, Hägglund MGA, Fredriksson R. 2013. Evolutionary origin of amino acid transporter families SLC32, SLC36 and SLC38 and physiological, pathological and therapeutic aspects. *Mol Aspects Med* **34**: 571–585.

Schleich S, Strassburger K, Janiesch PC, Koledachkina T, Miller KK, Haneke K, Cheng YS, Kuchler K, Stoecklin G, Duncan KE, Teleman AA. 2014. DENR-MCT-1 promotes translational re-initiation downstream of uORFs to control tissue growth. *Nature* **512**: 208-212

Smith CJ, O'Brien T, Chatzigeorgiou M, Spencer WC, Feingold-Link E, Husson SJ, Hori S, Mitani S, Gottschalk A, Schafer WR, et al. 2013. Sensory neuron fates are distinguished by a transcriptional switch that regulates dendrite branch stabilization. *Neuron* **79**: 266–280.

Stolarczyk E, Guissard C, Michau A, Even PC, Grosfeld A, Serradas P, Lorsignol A, Pénicaud L, Brot-Laroche E, Leturque A, et al. 2010. Detection of extracellular glucose by GLUT2 contributes to hypothalamic control of food intake. *Am J Physiol Endocrinol Metab* **298**: E1078–1087.

Sugimura K, Yamamoto M, Niwa R, Satoh D, Goto S, Taniguchi M, Hayashi S, Uemura T. 2003. Distinct developmental modes and lesion-induced reactions of dendrites of two classes of Drosophila sensory neurons. *J Neurosci* **23**: 3752–3760.

Tato I, Bartrons R, Ventura F, Rosa JL. 2011. Amino acids activate mammalian target of rapamycin complex 2 (mTORC2) via PI3K/Akt signaling. *J Biol Chem* **286**: 6128–6142.

Teleman AA, Chen Y-W, Cohen SM. 2005. 4E-BP functions as a metabolic brake used under stress conditions but not during normal growth. *Genes Dev* **19**: 1844–1848.

Tettweiler G, Miron M, Jenkins M, Sonenberg N, Lasko PF. 2005. Starvation and oxidative stress resistance in Drosophila are mediated through the eIF4E-binding protein, d4E-BP. *Genes Dev* **19**: 1840–1843.

Thevelein JM, Voordeckers K. 2009. Functioning and evolutionary significance of nutrient transceptors. *Mol Biol Evol* **26**: 2407–2414.

Thwaites DT, Anderson CMH. 2011. The SLC36 family of proton-coupled amino acid transporters and their potential role in drug transport. *Br J Pharmacol* **164**: 1802–1816.

Tomancak P, Beaton A, Weiszmann R, Kwan E, Shu S, Lewis SE, Richards S, Ashburner M, Hartenstein V, Celniker SE, et al. 2002. Systematic determination of patterns of gene expression during Drosophila embryogenesis. *Genome Biol* **3**: RESEARCH0088.

Tusher VG, Tibshirani R, Chu G. 2001. Significance analysis of microarrays applied to the ionizing radiation response. *Proc Natl Acad Sci U S A* **98**: 5116–5121.

Wreden CC, Johnson J, Tran C, Seal RP, Copenhagen DR, Reimer RJ, Edwards RH. 2003. The H+-coupled electrogenic lysosomal amino acid transporter LYAAT1 localizes to the axon and plasma membrane of hippocampal neurons. *J Neurosci* **23**: 1265–1275.

Ye B, Petritsch C, Clark IE, Gavis ER, Jan LY, Jan YN. 2004. Nanos and Pumilio are essential for dendrite morphogenesis in Drosophila peripheral neurons. *Curr Biol* **14**: 314–321.

Zoncu R, Bar-Peled L, Efeyan A, Wang S, Sancak Y, Sabatini DM. 2011. mTORC1 senses lysosomal amino acids through an inside-out mechanism that requires the vacuolar H(+)-ATPase. *Science* **334**: 678–683.

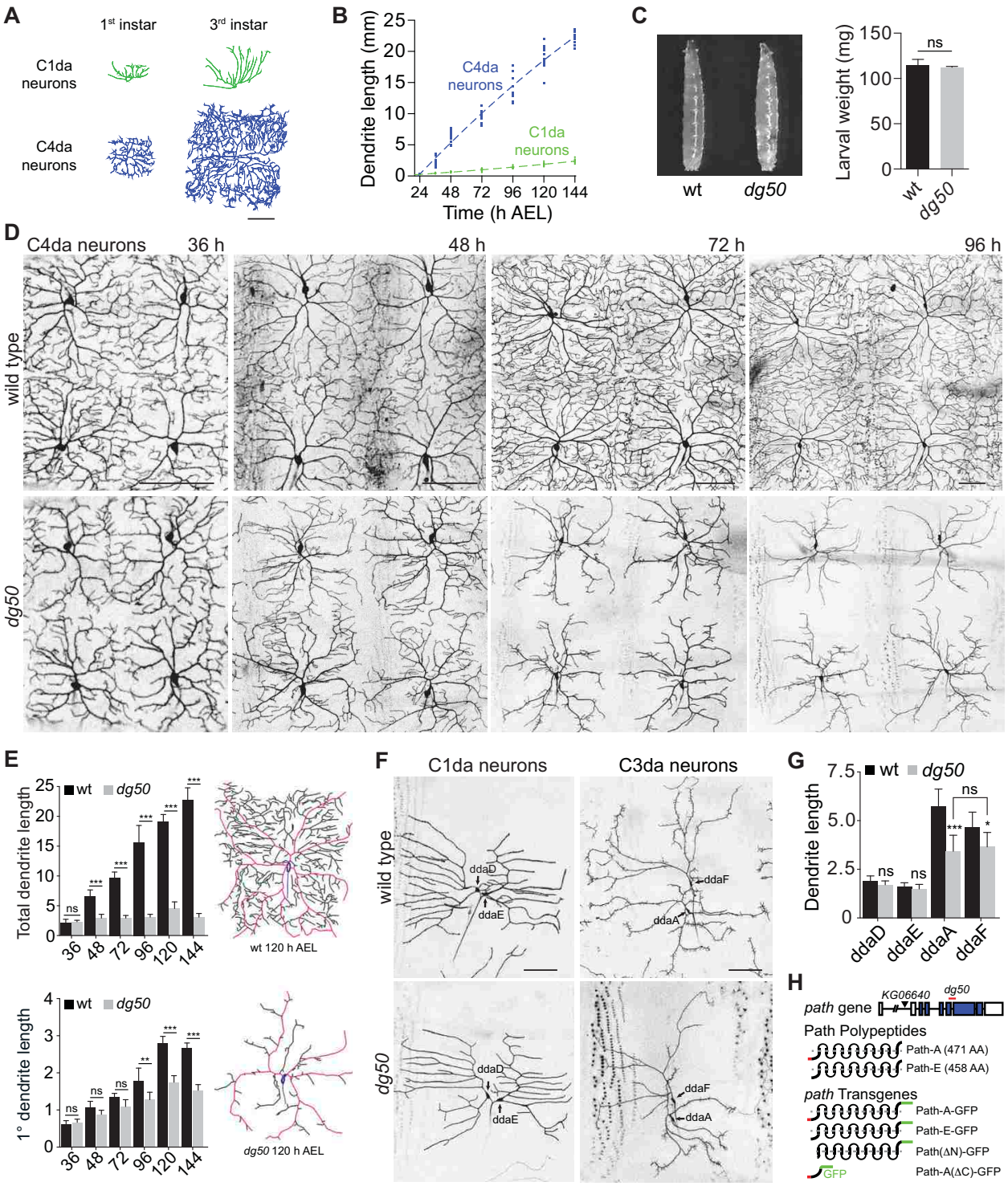
A
1st instar
3rd instar
C1da neurons
C4da neurons
B
Dendrite length (mm)
C4da neurons
C1da neurons
Time (h AEL)
C
wt
dg50
Larval weight (mg)
ns
D
C4da neurons
36 h
48 h
72 h
96 h
wild type
dg50
E
Total dendrite length
wt
dg50
wt 120 h AEL
1° dendrite length
dg50 120 h AEL
F
C1da neurons
C3da neurons
wild type
dg50
ddaD
ddaE
ddaF
ddaA
G
Dendrite length
ddaD
ddaE
ddaA
ddaF
H
path gene
KG06640
dg50
Path Polypeptides
Path-A (471 AA)
Path-E (458 AA)
path Transgenes
Path-A-GFP
Path-E-GFP
Path(ΔN)-GFP
Path-A(ΔC)-GFP
GFP

Figure 1. Identification of a novel regulator of dendrite growth.

(A-B) Growth control in da neurons. (A) Traces of representative C1da and C4da neurons in 1st instar and 3rd instar larvae. (B) Plots depicting C1da (green) and C4da (blue) dendrite growth during larval development. Points mark measurements from individual neurons. *n*=10, each time-point. (C-E) *path* regulates dendrite growth in C4da neurons. (C) *dg50* is dispensable for larval growth. *Left*, wild type (wt) and *dg50* mutant larvae at 120 h AEL; *right*, weight of wt and *dg50* mutant larvae. Mean and standard deviation for 5 independent measurements (80 larvae each) are shown. (D) Time-course of dendrite growth in C4da neurons (*ppk-CD4-tdTomato*) at 36, 48, 72, and 96 hr AEL in wt control and *dg50* mutants. (E) Mean total dendrite length and primary dendrite length (in millimiters) of individual ddaC C4da neurons of the indicated genotype at the indicated time are shown. *n* = 10 neurons for each time-point. Traces of representative C4da neurons from 120 h AEL wild type and *dg50* mutant larvae are shown with primary dendrites shaded in magenta. (F-G) Effects of *dg50* on dendrite growth in different classes of da neurons. (F) Dendrites of C1da neurons (*$Gal4^{98b}$, UAS-CD4-tdGFP*) and C3da neurons (*ss-myrGFP)* in wt control and *dg50* mutant larvae are shown. (G) Mean total dendrite length of C1da and C3da neurons of the indicated genotype. *n* = 10 neurons for each. **P*<0.05, ***P* <0.01, ****P* <0.001; ns, not significant compared to wt controls; one-way ANOVA with a post-hoc Dunnett's test. In this and all subsequent figures, dorsal is up, anterior is left. Scale bars, 50 mm. (H) Schematic depicting the *path* locus including alleles used in this study, Path polypeptides that differ by 13 amino acids at the N-terminus (red), and *path* transgenes used in this study. Boxes indicate trans-membrane domains and hatched gray line represents a membrane.

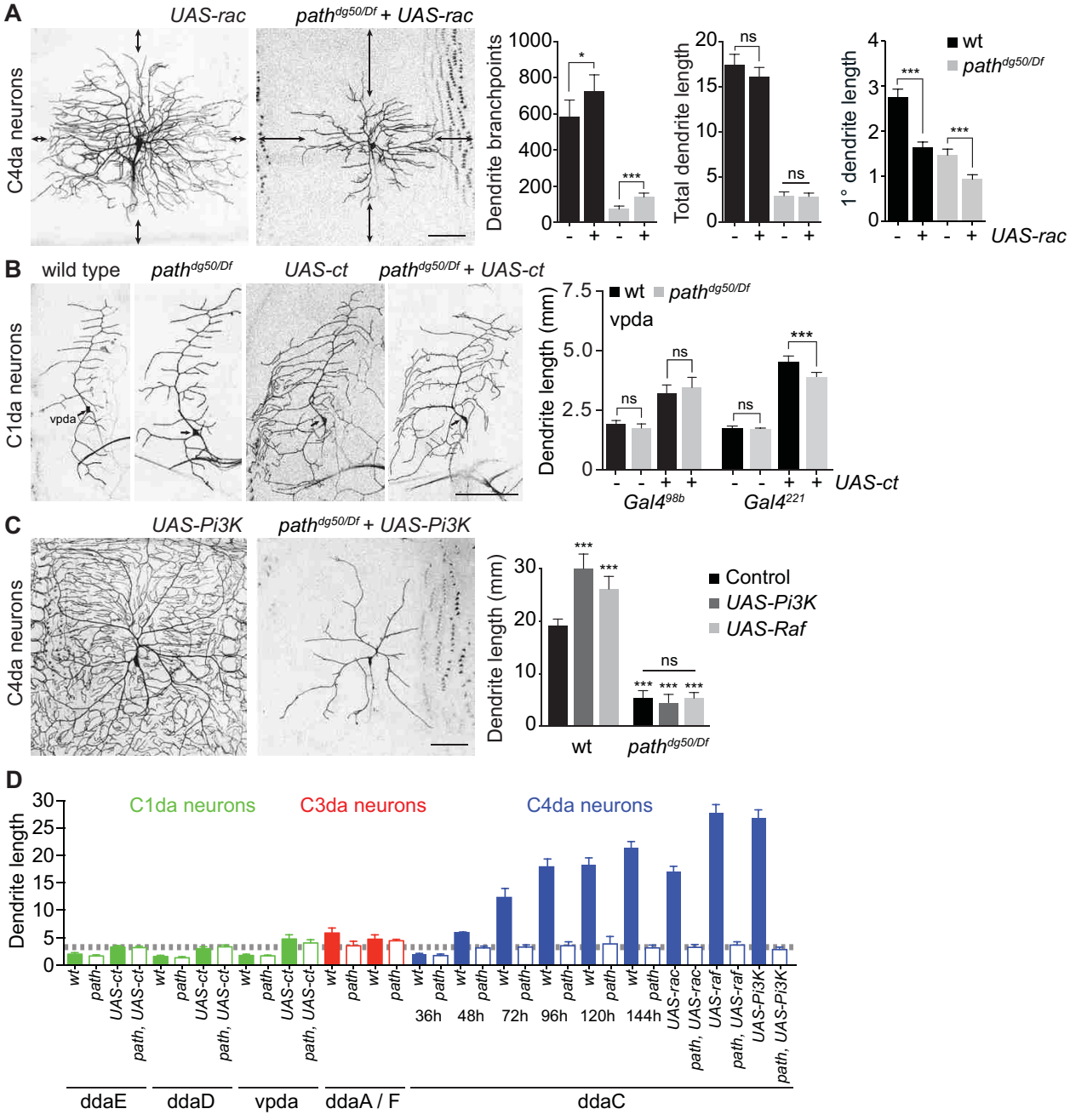
A
UAS-rac
path^dg50/Df + UAS-rac
C4da neurons
Dendrite branchpoints
Total dendrite length
1° dendrite length
wt
path^dg50/Df
UAS-rac
B
wild type
path^dg50/Df
UAS-ct
path^dg50/Df + UAS-ct
C1da neurons
vpda
Dendrite length (mm)
UAS-ct
Gal4^98b
Gal4^221
C
UAS-Pi3K
path^dg50/Df + UAS-Pi3K
C4da neurons
Control
UAS-Pi3K
UAS-Raf
D
Dendrite length
C1da neurons
C3da neurons
C4da neurons
36h
48h
72h
96h
120h
144h
ddaE
ddaD
vpda
ddaA / F
ddaC

Figure 2. *path* is required for dendrite growth above a fixed limit.

(A) *path* affects dendrite growth independent of dendrite patterning. *Left*, representative images of wt or *path* mutant C4da neurons expressing *UAS-rac* (*ppk-Gal4, UAS-rac*). *Right*, quantification of dendrite branching and length in the indicated genotypes. Arrows mark uncovered territory. **P* <0.05, ****P* <0.001, ns, not significant compared to controls that do not express *UAS-Rac*; unpaired t-tests with Welch's correction. (B) Forced overgrowth in C1da dendrites requires *path*. C1da neurons (vpda) are shown for the indicated genotypes. *UAS-ct* expression induces dendrite overgrowth in C1da neurons of wt and *path* mutant larvae, but this overgrowth is limited in *path* mutants. Quantification shows mean dendrite length and standard deviation in vpda C1da neurons of the indicated genotype. (C) *path* is epistatic to treatments that increase the C4da dendrite growth. *Left*, representative images of wt or *path* mutant C4da neurons expressing *UAS-Pi3K92E*. *Right*, quantification of dendrite growth in wt or *path* mutant larvae expressing *UAS-Pi3K92E* or *UAS-Raf* in C4da neurons. ****P* <0.001, ns, not significant compared to wt controls unless otherwise indicated in (B) and (C); one-way ANOVA with a post-hoc Dunnett's test. $n = 10$ neurons for each genotype. Scale bars, 50 mm. (D) Summary of dendrite measurements highlighting the upper limit for *path*-independent dendrite growth (hatched gray line).

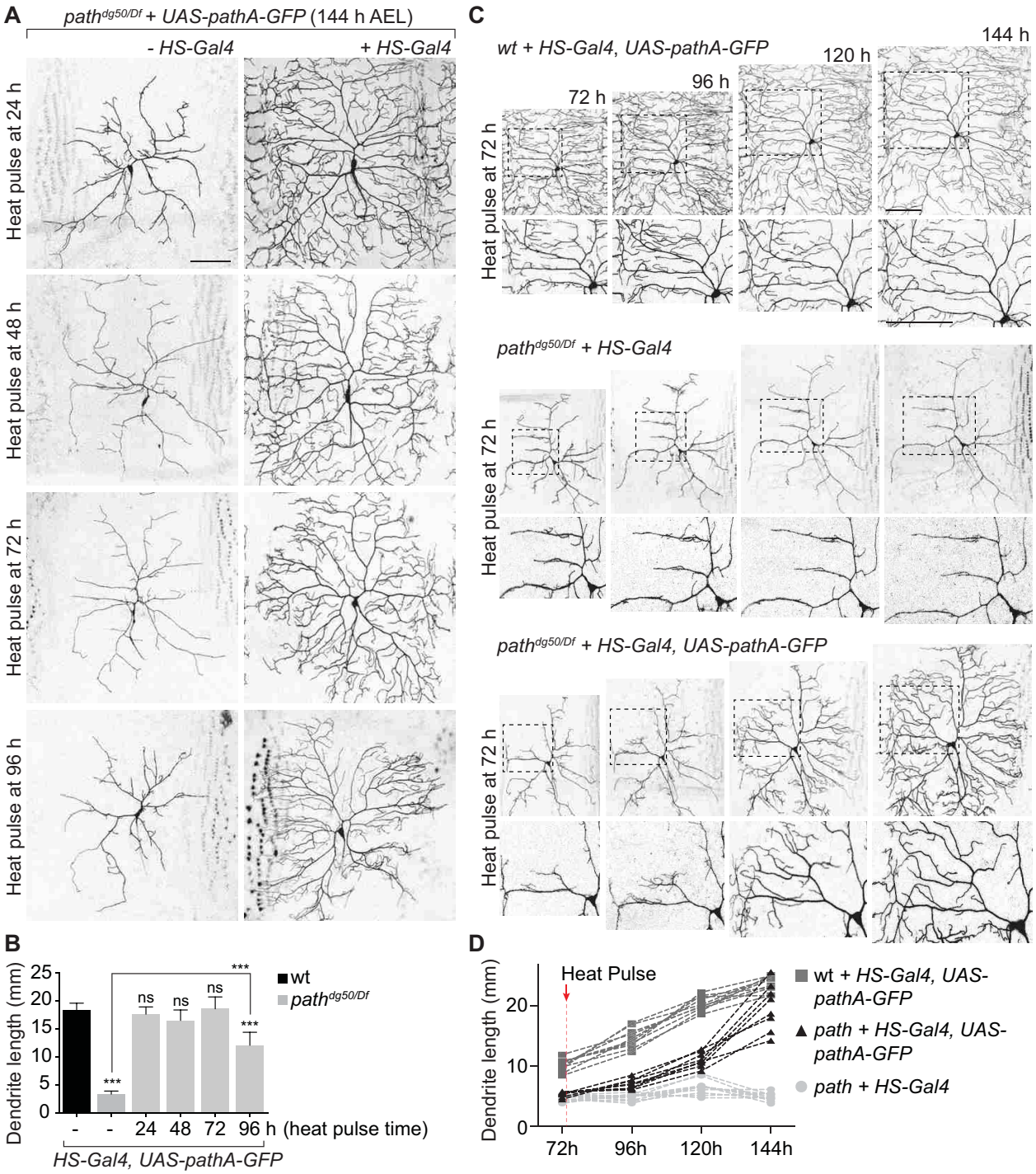
A
path^dg50/Df + UAS-pathA-GFP (144 h AEL)
- HS-Gal4
+ HS-Gal4
Heat pulse at 24 h
Heat pulse at 48 h
Heat pulse at 72 h
Heat pulse at 96 h
B
Dendrite length (mm)
25
20
15
10
5
0
***
ns
ns
ns
***
***
wt
path^dg50/Df
- - 24 48 72 96 h (heat pulse time)
HS-Gal4, UAS-pathA-GFP
C
wt + HS-Gal4, UAS-pathA-GFP
72 h
96 h
120 h
144 h
Heat pulse at 72 h
path^dg50/Df + HS-Gal4
path^dg50/Df + HS-Gal4, UAS-pathA-GFP
D
Heat Pulse
Dendrite length (mm)
20
10
0
72h
96h
120h
144h
wt + HS-Gal4, UAS-pathA-GFP
path + HS-Gal4, UAS-pathA-GFP
path + HS-Gal4

Figure 3. *path* is a permissive factor for dendrite growth.

(A-B) Growth defects of *path* mutants are reversible. *path* mutant (*path*^{dg50}/*Df(3L)BSC773*) larvae carrying a *path* rescue transgene (*UAS-pathA-GFP*) without (left) or with (right) a heat-inducible *Gal4* driver (*HS-Gal4*) were heat shocked for 1 h at 37°C at the indicated time and effects on dendrite growth were assessed at 144 h AEL using *ppk-CD4-tdTomato* to label C4da dendrites. (B) Quantification of C4da dendrite length in *path* mutants at 144 h AEL after resupplying *UAS-pathA-GFP* at the indicated times. n = 8 neurons for each genotype. (C-D) Resupplying *path* to *path* mutants induces heterochronic growth. (C) Time-lapse imaging of dendrite growth prior to a 1 h heat shock (72 h AEL, *left*), 24 h after heat shock (96 h AEL), 48 h after heat shock (120 h AEL), and 72 h after heat shock (144 h AEL) in larvae of the indicated genotype. (D) Plot depicting growth profile of C4da dendrites in the indicated genotypes following induction of *path* expression. Note that *path* expression induces rapid late-stage growth in *path* mutants. n = 5 neurons for each genotype. *P <0.05, **P <0.01, ***P <0.001; ns, not significant compared to wt controls unless otherwise indicated; one-way ANOVA with a post-hoc Dunnett's test. Scale bars, 50 mm.

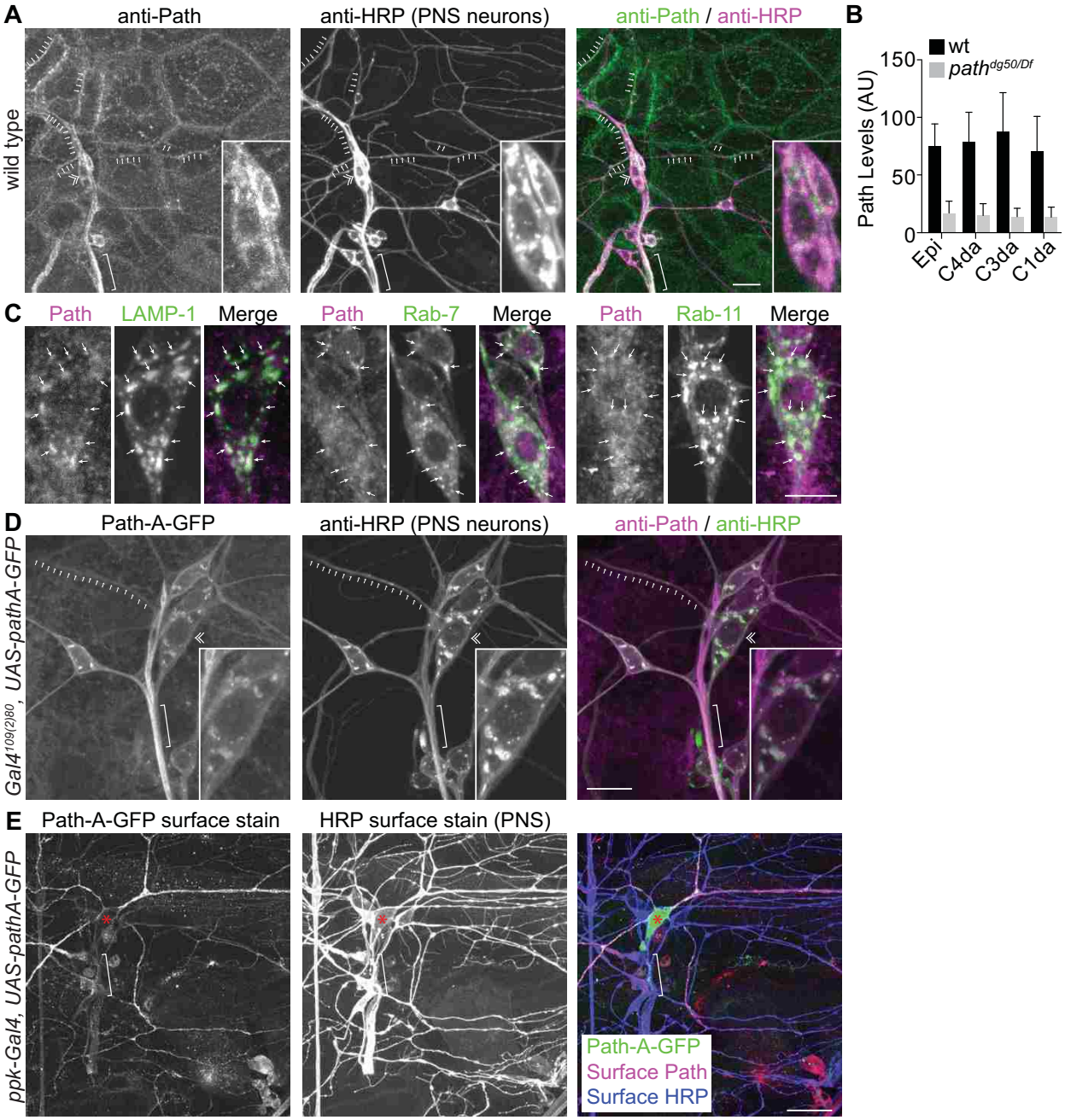
A
anti-Path
anti-HRP (PNS neurons)
anti-Path / anti-HRP
wild type
B
wt
path^dg50/Df
Path Levels (AU)
150
100
50
0
Epi
C4da
C3da
C1da
C
Path
LAMP-1
Merge
Path
Rab-7
Merge
Path
Rab-11
Merge
D
Path-A-GFP
anti-HRP (PNS neurons)
anti-Path / anti-HRP
Gal4^109(2)80, UAS-pathA-GFP
E
Path-A-GFP surface stain
HRP surface stain (PNS)
ppk-Gal4, UAS-pathA-GFP
Path-A-GFP
Surface Path
Surface HRP

Figure 4. Path is broadly expressed and localizes to the cell surface and endolysosomal compartments.

(A) Anti-Path immunostaining of a wt 3rd instar fillet reveals expression throughout the body wall. Path localizes to punctate structures within cells and accumulates at junctional domains and in PNS dendrites (arrows) and axons (brackets). Double chevron marks C4da cell body. (B) Quantification of Path levels in different classes of da neurons. Mean pixel intensity and standard deviation for Path immunoreactivity in body wall epithelial cells (epi) and PNS neurons are shown. n = 20 cells each. (C) Path co-localizes with endolysosomal markers. Images depict co-localization of endogenous Path with GFP-LAMP, Rab-7-GFP or Rab-11-GFP. (D) Path-GFP localizes to axons and dendrites. Representative images of Path-A-GFP and HRP (to label sensory neurons) staining are shown. Inset shows magnified view of the C4da soma. (E) Path-A-GFP localizes to the plasma membrane in dendrites. Surface-exposed GFP as revealed by immunostaining under non-permeabilizing conditions (Path-A-GFP surface stain) is shown for a $path^{dg50/Df}$ mutant expressing *UAS-pathA-GFP* in C4da neurons. Scale bars: 10 mm in (C), 50 mm in other panels.

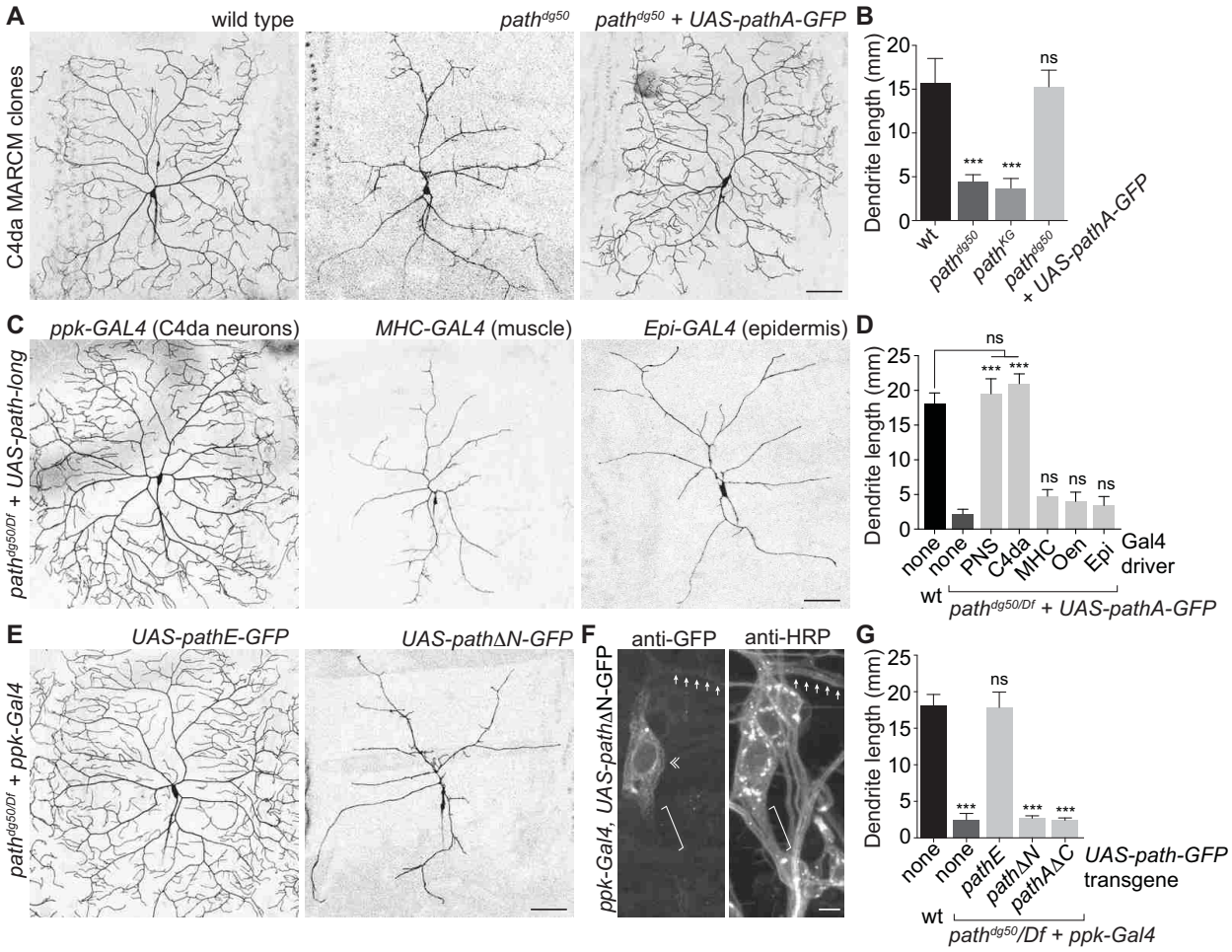

Figure 5. *path* is required cell-autonomously for extreme dendrite growth.

(A-B) *path* is required in neurons for dendrite growth. (A) Representative wild type control, $path^{dg50}$, and $path^{dg50}$ + *UAS-path-GFP* ddaC C4da MARCM clones are shown. (B) Quantification of total dendrite length for ddaC MARCM clones of the indicated genotypes. $n \geq$ 8 ddaC MARCM clones for each. (C-D) Neuronal *path* expression is sufficient for extreme dendrite growth. (C) The ability of *UAS-path-GFP* expression directed by a variety of Gal4 drivers to rescue dendrite growth defects of *path* mutants was assayed at 120 hr AEL. Representative images of rescue with the *ppk-gal4*, *MHC-gal4* and *A58-gal4* drivers are shown (D) Quantification of rescue activity of Gal4 drivers at 120 hr AEL. Gal4 drivers used to drive *UAS-path-A-GFP* are as follows: none, no Gal4 driver; PNS, *21-7-Gal4*; C4da, *ppk-Gal4*; MHC,

MHC-Gal4; Oen (Oenocytes), *OK72-Gal4*; Epi, *A58-Gal4*.. *n* = 5 neurons for each genotype. (E-G) The N-terminal domain is required for Path function. (E) Representative images of C4da neurons from *path* mutant larvae expressing *UAS-pathE-GFP*, the short isoform of *path,* (left) or a version of *path* lacking the N-terminal intracellular domain, *UAS-pathDN-GFP*. (F) The N-terminal domain influences Path localization. Antibody staining shows distribution of PathDN-GFP in C4da neurons (da neurons labeled by anti-HRP immunoreactivity). Arrows mark dendrites, double chevron marks C4da soma, bracket marks axon. (G) Quantification of rescue activity of neuronal expression of the indicated transgenes in *path* mutant larvae. *n* = 8 neurons for each genotype. Error bars represent standard deviation. ***P <0.001; ns, not significant compared to wt controls unless otherwise indicated in (B) and (G), compared to *path* mutants in (D); one-way ANOVA with a post-hoc Dunnett's test. Scale bars: 50 mm in (A-E), 10 mm in (F).

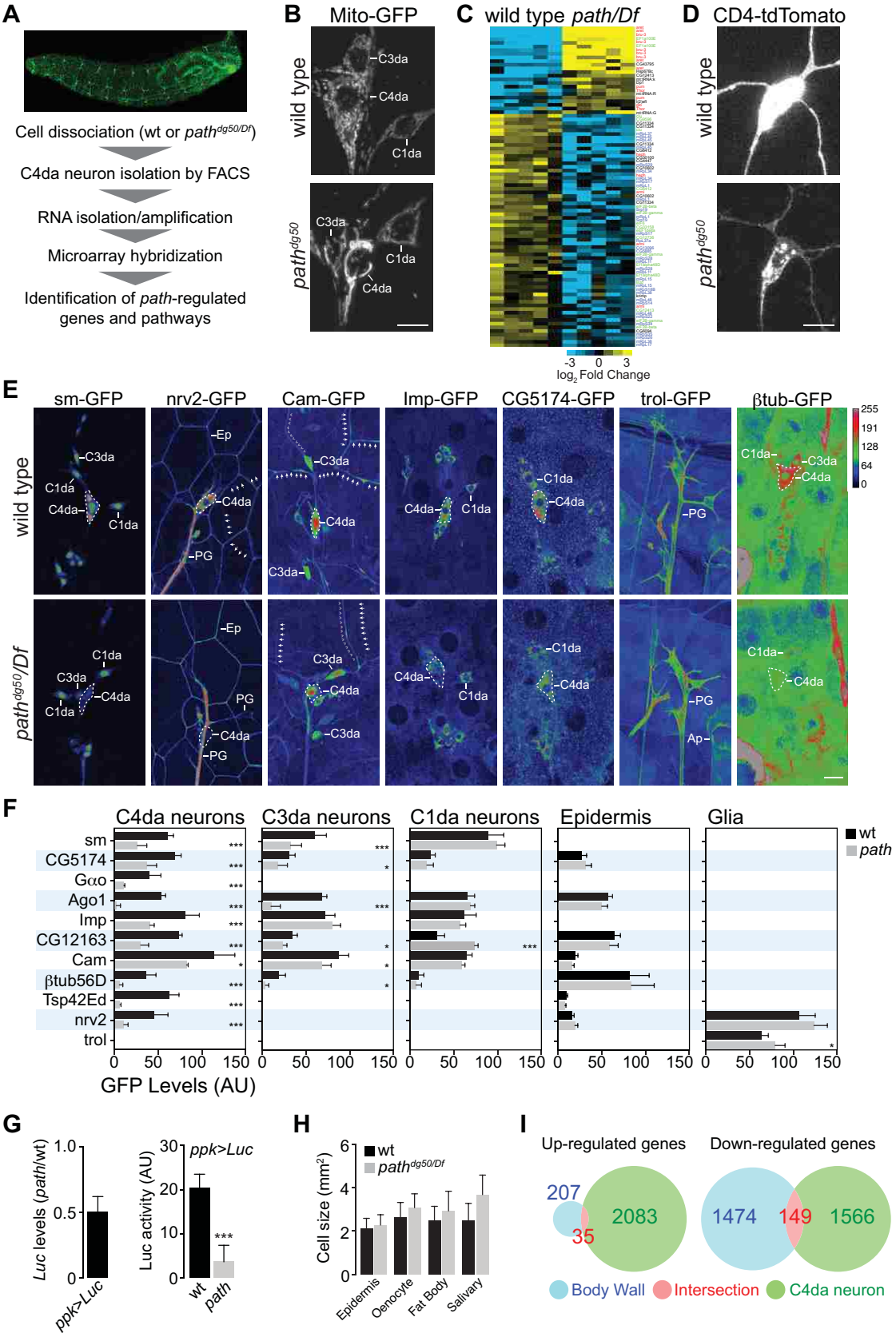
A
Cell dissociation (wt or path^dg50/Df)
C4da neuron isolation by FACS
RNA isolation/amplification
Microarray hybridization
Identification of path-regulated genes and pathways
B
Mito-GFP
wild type
path^dg50
C3da
C4da
C1da
C
wild type path/Df
-3 0 3
log2 Fold Change
D
CD4-tdTomato
wild type
path^dg50
E
sm-GFP
nrv2-GFP
Cam-GFP
Imp-GFP
CG5174-GFP
trol-GFP
βtub-GFP
wild type
path^dg50/Df
Ep
PG
Ap
255
191
128
64
0
F
C4da neurons
C3da neurons
C1da neurons
Epidermis
Glia
wt
path
sm
CG5174
Gαo
Ago1
Imp
CG12163
Cam
βtub56D
Tsp42Ed
nrv2
trol
GFP Levels (AU)
G
Luc levels (path/wt)
ppk>Luc
Luc activity (AU)
wt
path
H
Cell size (mm2)
Epidermis
Oenocyte
Fat Body
Salivary
I
Up-regulated genes
Down-regulated genes
207
35
2083
1474
149
1566
Body Wall
Intersection
C4da neuron

Figure 6. Path affects nutrient signaling and protein homeostasis in C4da neurons.

(A) Workflow for microarray expression profiling of *path* mutant C4da neurons. (B) *path* affects mitochondria morphology in C4da neurons. PNS neurons from wild type control (top) and *path* mutant larvae expressing mitochondrial-targeted GFP (*UAS-mito-GFP*) are shown. Levels of apparent mitochondrial fusion (high, C4da neurons; low, C3da neurons; none, C1da neurons) correlate with severity of dendrite growth defects in *path* mutants. (C) Heat map depicting *path*-regulated transcripts involved in translation. Significantly deregulated transcripts were identified using SAM analysis with a false discovery rate of 0.01 (Tusher et al. 2001). Transcripts are color-coded according to gene function as follows: red, translation inhibitor; green, translation initiation/elongation; blue, core translational machinery; black, unknown. (D-F) *path* affects protein homeostasis in C4da neurons. (D) Levels of the *ppk-CD4-tdTomato* reporter are reduced in *path* mutants, although *ppk* transcription is not affected (Supplemental Table S1). C4da neurons in age-matched wt (top) and *path* mutant (bottom) larvae expressing *ppk-CD4-tdTomato* were imaged under identical conditions. (E) Representative images depicting expression levels of 7 GFP exon trap lines in wt or *path* mutant larvae at 120 h AEL. Images are pseudocolored according to a lookup table (key, top right), C4da cell bodies are outlined with a hatched white line, and cells of interest labeled by each exon trap are indicated (C1da, C3da, and C4da neurons; Ep, epithelial cells; PG, peripheral glia; Ap, apodeme). Arrows mark C4da dendrites and double chevrons mark C3da dendrites. Exon traps were imaged under identical conditions in wt and *path* mutant larvae. (F) Mean expression intensity of exon traps in the indicated cell types. $n \geq 8$ cells for each bar. *$P<0.05$, ***$P<0.001$; ns, not significant compared to wt controls; one-way ANOVA with a post-hoc Dunnett's test. Error bars, standard deviation. Scale bars, 50 mm. (G) Cell size measurements for the indicated cell types in wt or *path* mutant larvae. Cells were

labeled with a membrane reporter (*UAS-mCD8-GFP*) and cell size (2D area) was measured by tracing plasma membranes and measuring area of the resulting polygons. Mean and standard deviation for 100 cells of each genotype are shown. (H) Venn diagram depicting transcriptional changes manifest in the entire body wall (blue) and C4da neurons (green) of *path* mutant larvae; the region of intersection is shown in red.

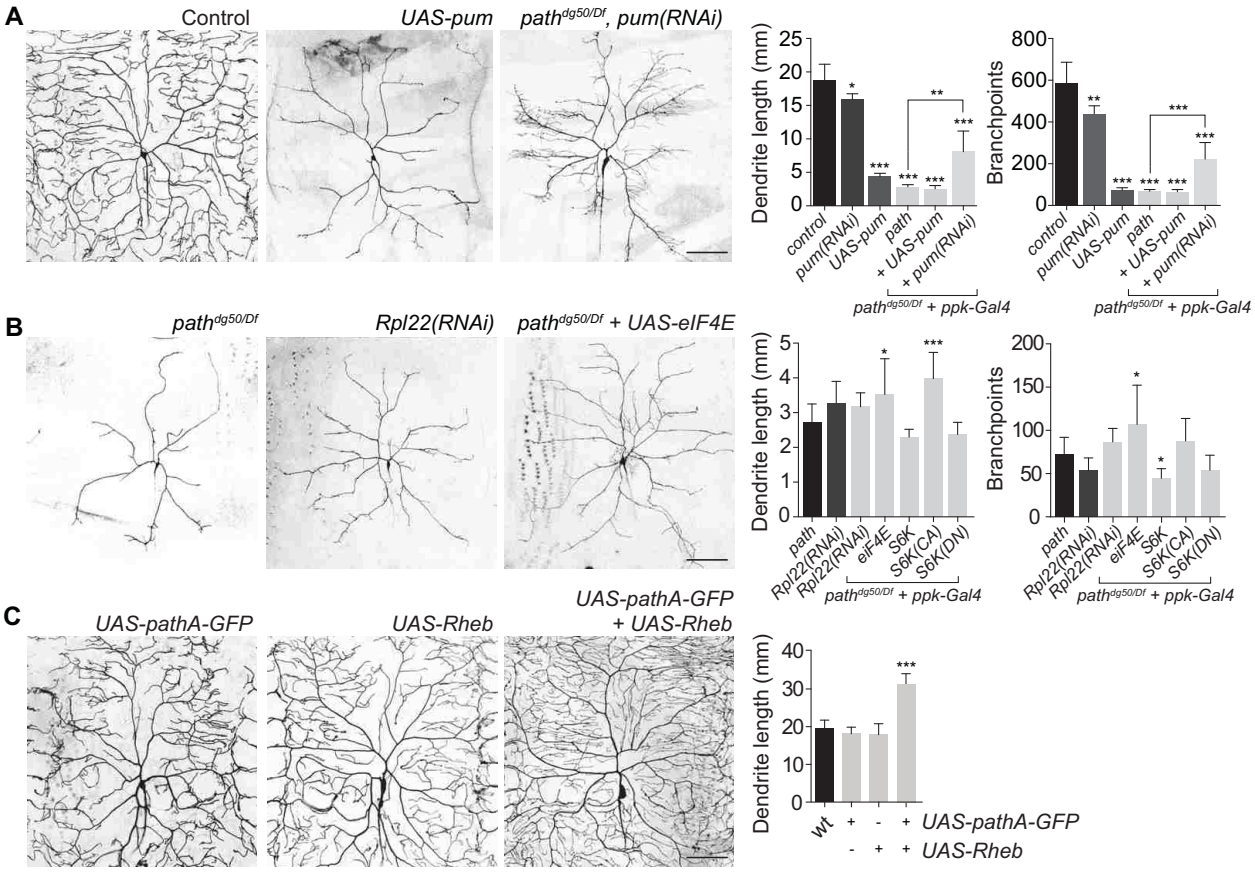

Figure 7. Path regulates dendrite growth via effects on translation.

(A) Increased translational repression contributes to growth defects of *path* mutants. Representative images of C4da dendrites are shown for a wt control, neuronal expression of *UAS-pum* or *UAS-pum(RNAi),* and *path* mutant larvae expressing *UAS-pum(RNAi)* in neurons. Quantification of dendrite growth phenotypes is shown for the indicated genotypes. (B) Reduced translational capacity likely contributes to dendrite growth defects in *path* mutants. RNAi of core translational machinery such as *Rpl22* causes growth defects similar to *path*, whereas overexpression of *eIF4e* partially mitigates *path* mutant growth defects. Quantification of dendrite growth phenotypes is shown for the indicated genotypes. (C) *path* can cooperate with TORC1 to promote dendrite growth. *Left*, representative C4da neurons expressing *UAS-pathA-GFP*, *UAS-Rheb*, or both are shown. Right, quantification of effects of *UAS-pathA-GFP* and/or

UAS-Rheb expression on C4da dendrite growth. $n \geq 7$ cells for each bar. *$P<0.05$, **$P<0.01$, ***$P<0.001$; ns, not significant compared to wt controls in (A) and (C) and *path* mutants in (B); one-way ANOVA with a post-hoc Dunnett's test. Error bars, standard deviation. Scale bars, 50 mm.

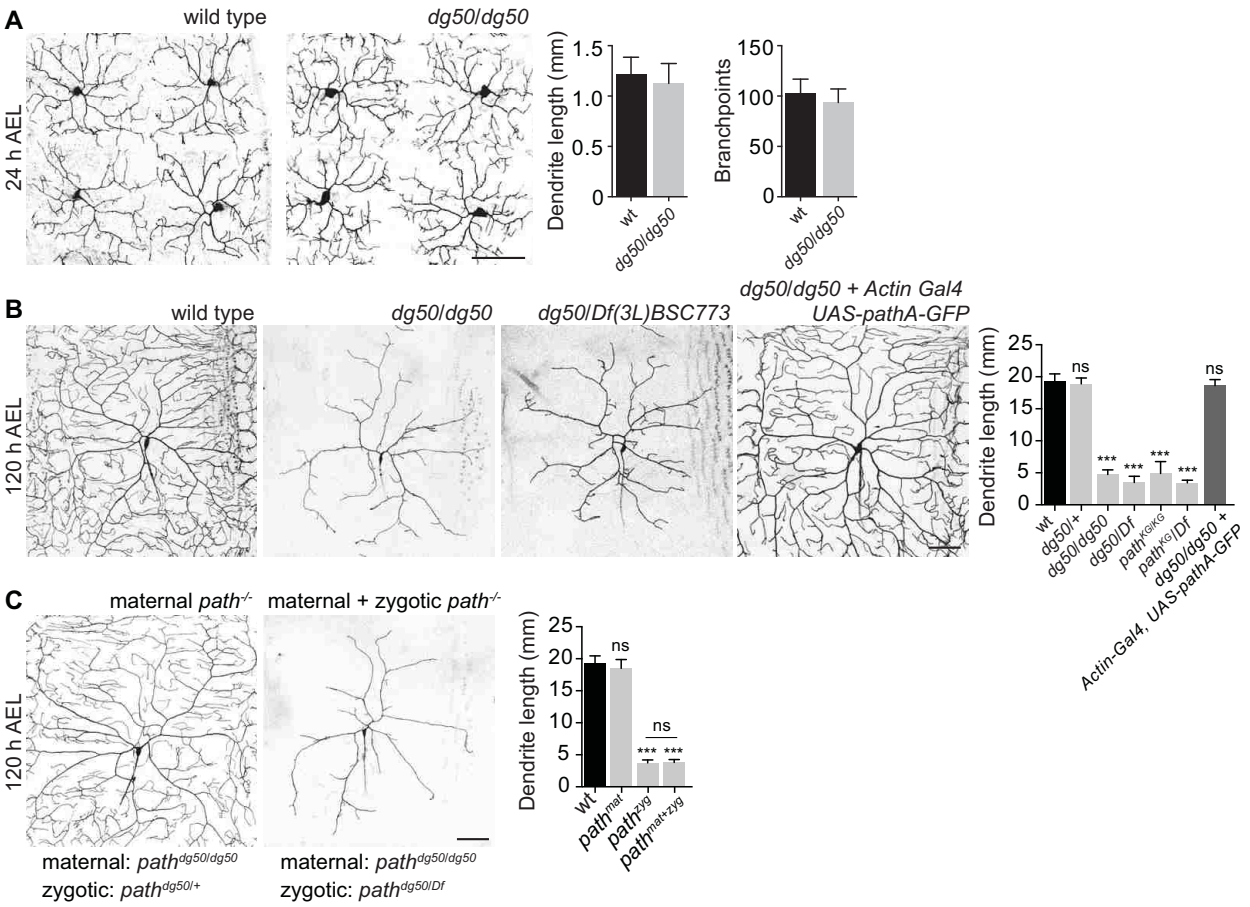

Figure S1. Supplement to Figure 1.

(A) Early dendrite growth proceeds normally in dg50 mutants. Repre- sentative images of C4da neurons (*ppk-CD4-tdTomato*) in wt control and *dg50* mutants at 24 h AEL are shown. Quantification of dendrite length and branching is shown at right (n=8 neurons, each genotype). (B) *dg50* is a loss-of-function allele of *path*. Representative images of C4da neurons and quantification of dendrite length (mean and standard deviation) are shown for the indicated genotypes at 120 h AEL (n=8 neurons, each genotype). (C) Maternal *path* does not influence larval dendrite growth. Images of C4da neurons in larvae derived from $path^{dg50}$ germline clones are shown. In larvae with zygotic *path* function (left), no dendrite growth defects are apparent, whereas larvae lacking maternal and zygotic *path* (center) are indistinguishable from zygotic

path mutants alone. Mean total dendrite length is shown for the indi- cated geneotypes. Error bars represent standard deviation. $n = 8$ neurons for each. ***$P<0.001$; ns, not significant relative to wt controls; one-way ANOVA with a post-hoc Dunnett's test. Scale bars, 50μm.

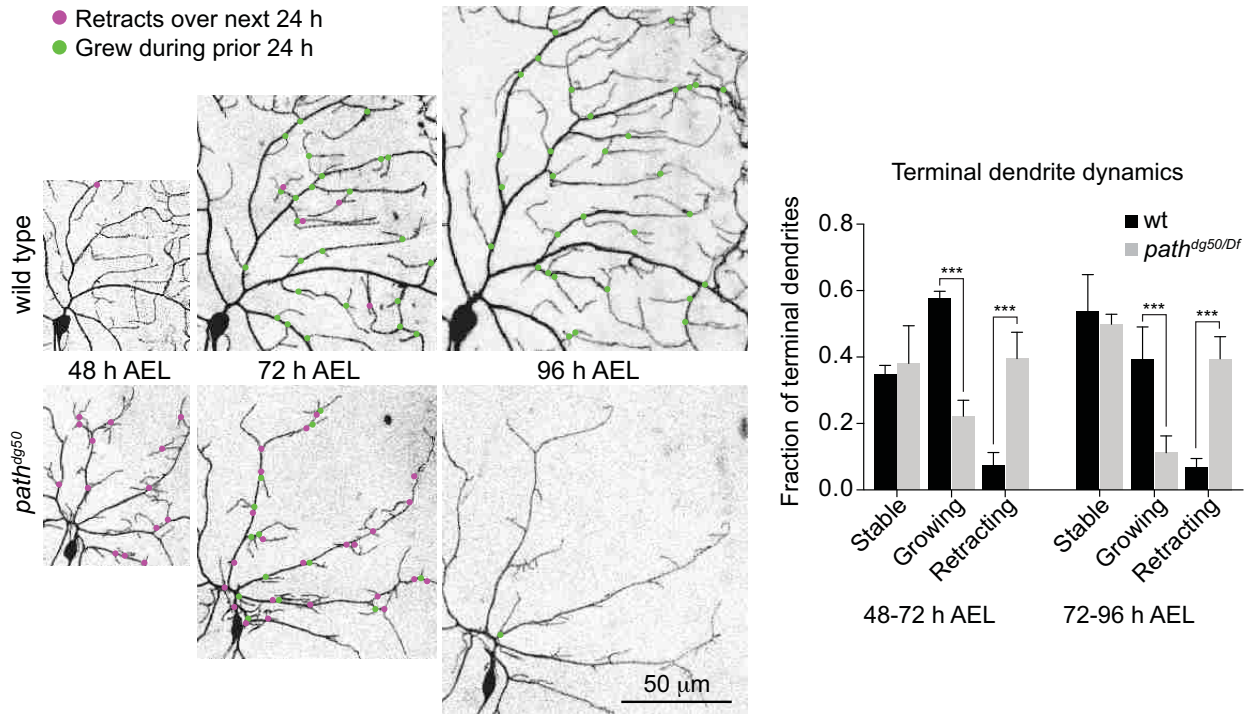

Figure S2. Time-lapse analysis of dendrite branch dynamics in path mutants.

C4da neurons (*ppk-CD4tdTomato*) from segment A3 were imaged at 48 h, 72 h, and 96 h AEL in wt control and *path*$^{dg50/Df}$ mutant larvae and terminal dendrite branch dynamics were monitored in the dorsal posterior quadrant of the arbor (corresponding to a 100x120 micron region of interest at 96 h AEL). To monitor dendrite dynamics, images of dendrite arbors from 2 time points (48-72 h and 72-96 h AEL) were overlayed, and terminal dendrites that exhibited changes in length >2μm were scored as dynamic terminals. Representative time-lapse series of wt and *path* mutant neurons are shown. Terminal branches that retract over the following 24 h period are marked at the base of the branch by a magenta circle and terminal dendrites that grew over the prior 24 h are marked by a green circle. 6 neurons each for wt and *path* mutants were imaged, and the proportion of stable, growing, and retracting terminal branches was calculated for each neuron. ***P<.001, one-way ANOVA with a post-hoc Tukey's test.

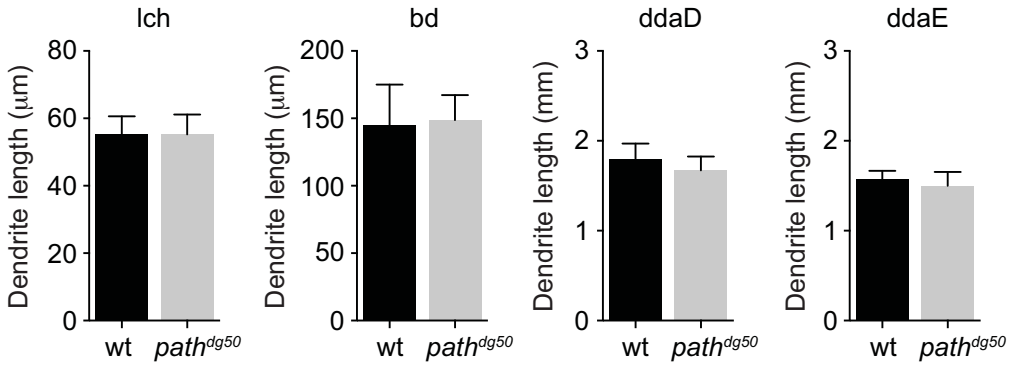

Figure S3. path is dispensable for dendrite growth in neurons with small dendrite arbors.

Quantification of total dendrite length (mean and standard deviation) for lch, bd, ddaD, and ddaE MARCM clones is shown for the indicated genotypes. *n*>8 MARCM clones for each. Dendrite length not significantly differ between wt control and *path* mutant larvae for lch, bd, ddaD or ddaE neurons, unpaired t-test with Welch's correction.

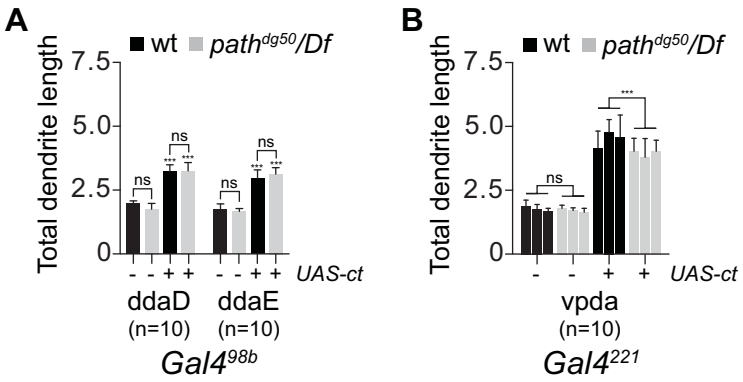

Figure S4. Effects of ct overexpression on dendrite growth in class I neurons.

(A) Total dendrite lenght for ddaD and ddaE in animals of the indicated genotype. (B) Total dendrite length for vpda in animals of the indicated genotype. Results from 3 independent experiments are shown (n = 10 neurons each bar). Bars represent mean values and error bars represent standard deviation. ***P<0.001; ns, not significant; one-way ANOVA with a post-hoc Dunnett's test.

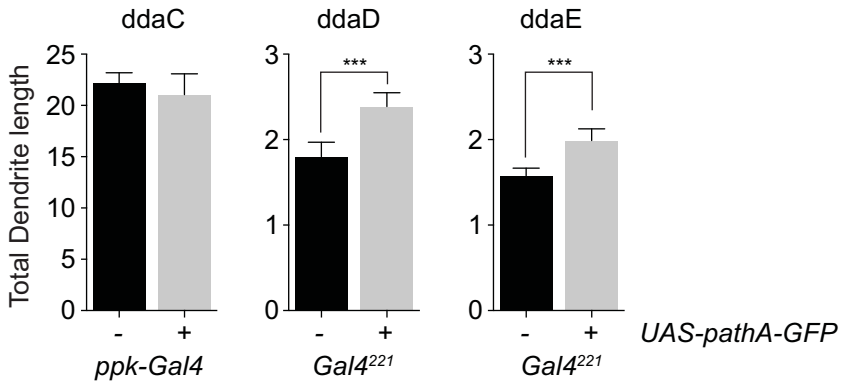

Figure S5. Overexpression of path can drive exuberant dendrite growth in neurons with small dendrite arbors.

Quantification of total dendrite length for control (*Gal4/+*) or *path*-overexpressing (*Gal4/UAS-pathA-GFP*) C4da neurons (ddaC) and C1da neurons (ddaD and ddaE). Mean and standard deviation of measurements from $n>8$ cells are shown for each genotype. ***$P<.001$, unpaired t-test with Welch's correction.

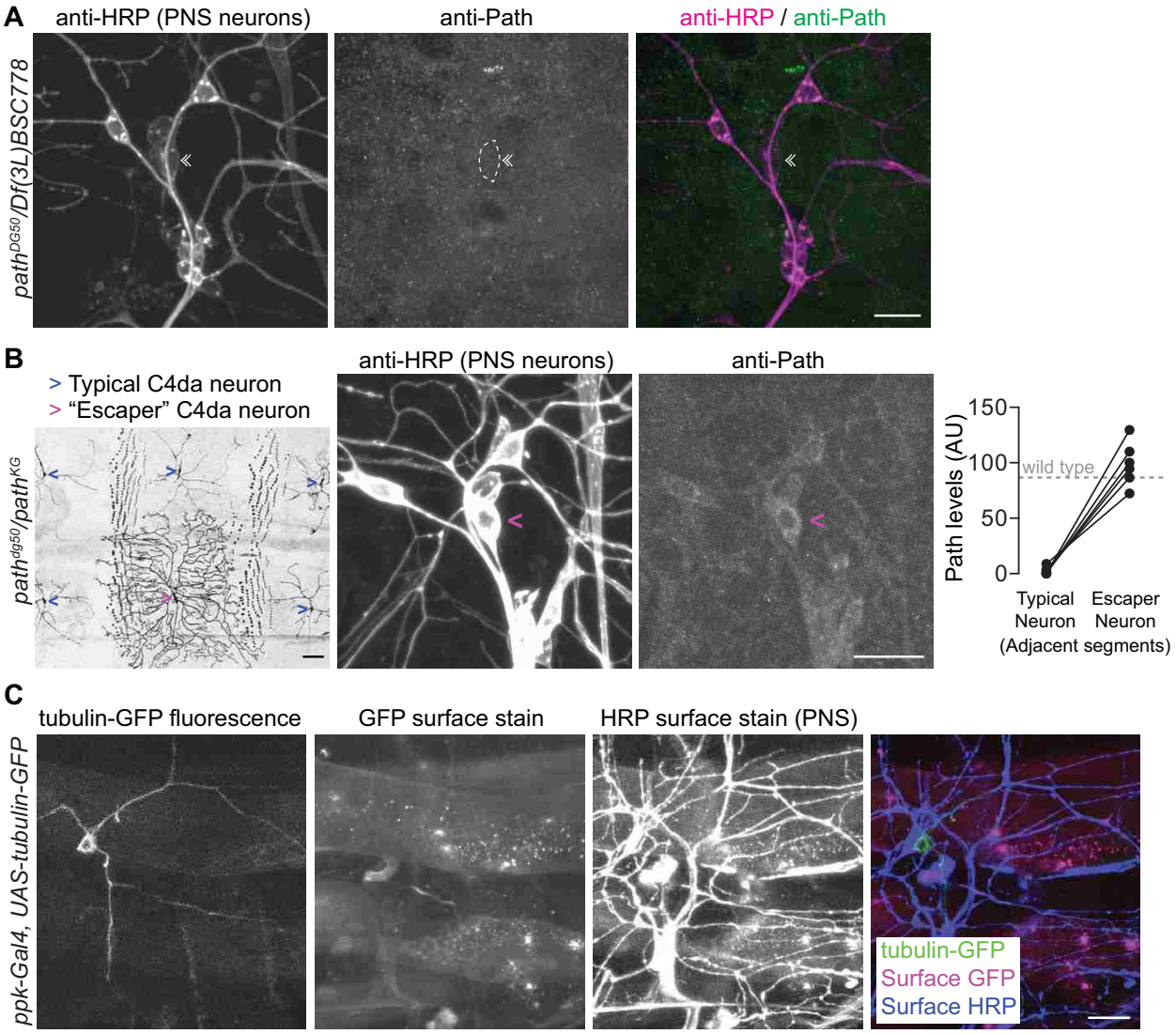

Figure S6. Supplement to Figure 4.

(A) Specificity of anti-Path antibody. (B) Low levels of Path support dendrite growth. (B) An example of a rare "escaper" neuron in a *path* mutant larva (marked by the magenta carat) surrounded by neurons exhibiting the stereotypical *path* mutant growth defect (blue carats). Approximately 0.5% of C4da neurons exhibit normal growth in path mutant larvae, and these "escaper" neurons exhibit significant perdurance of Path protein. Anti-Path immunostaining of one such "escaper" neuron is shown, and levels (arbitrary units, AU) of Path immunoreactivity are shown for an escaper neuron and a typical *path* mutant neuron from adjacent segments in 10

different animals. Neurons from the same animal are connected by a line. (C) Control for surface staining. Total GFP fluorescence (after formaldehyde fixation), GFP surface stain (staining in non-permeabilizing conditions), and HRP surface staining (as a positive control) are shown for a C4da neuron expressing α-tubulin-GFP, which should not be surface exposed. Scale bars, 50 μm.

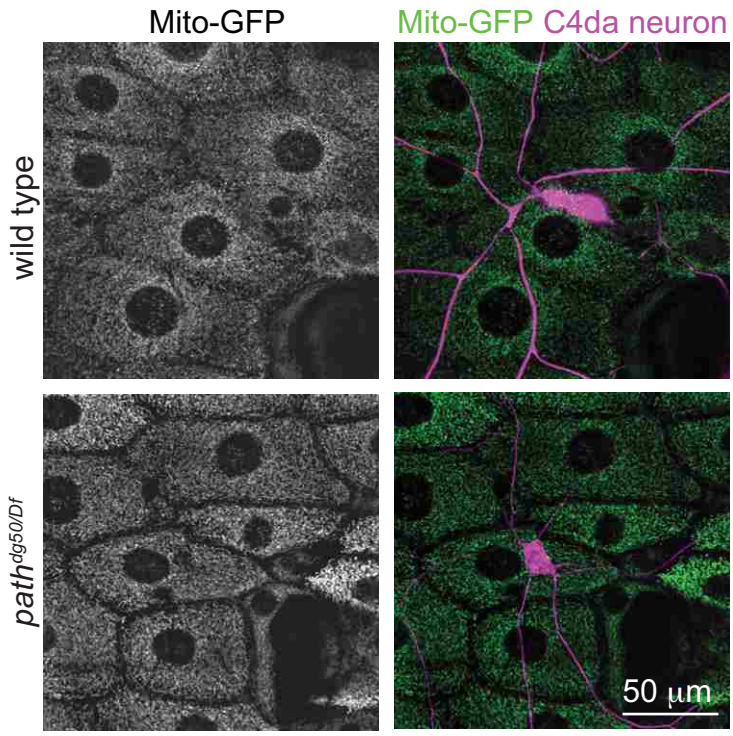

Figure S7. Supplement to Figure 6.

Images of wild type or *path* mutant larvae expressing mitochondrial-targeted GFP in epithelial cells (*A58-Gal4, UAS-mitoGFP*) and Tomato in C4da neurons (*ppk-CD4tdTomato*). Whereas *path* mutant C4da neurons exhibit striking alterations in mitochondrial morphology (Fig. 6), wild type and *path* mutant larvae exhibit comparable epithelial mitochondria morphology.

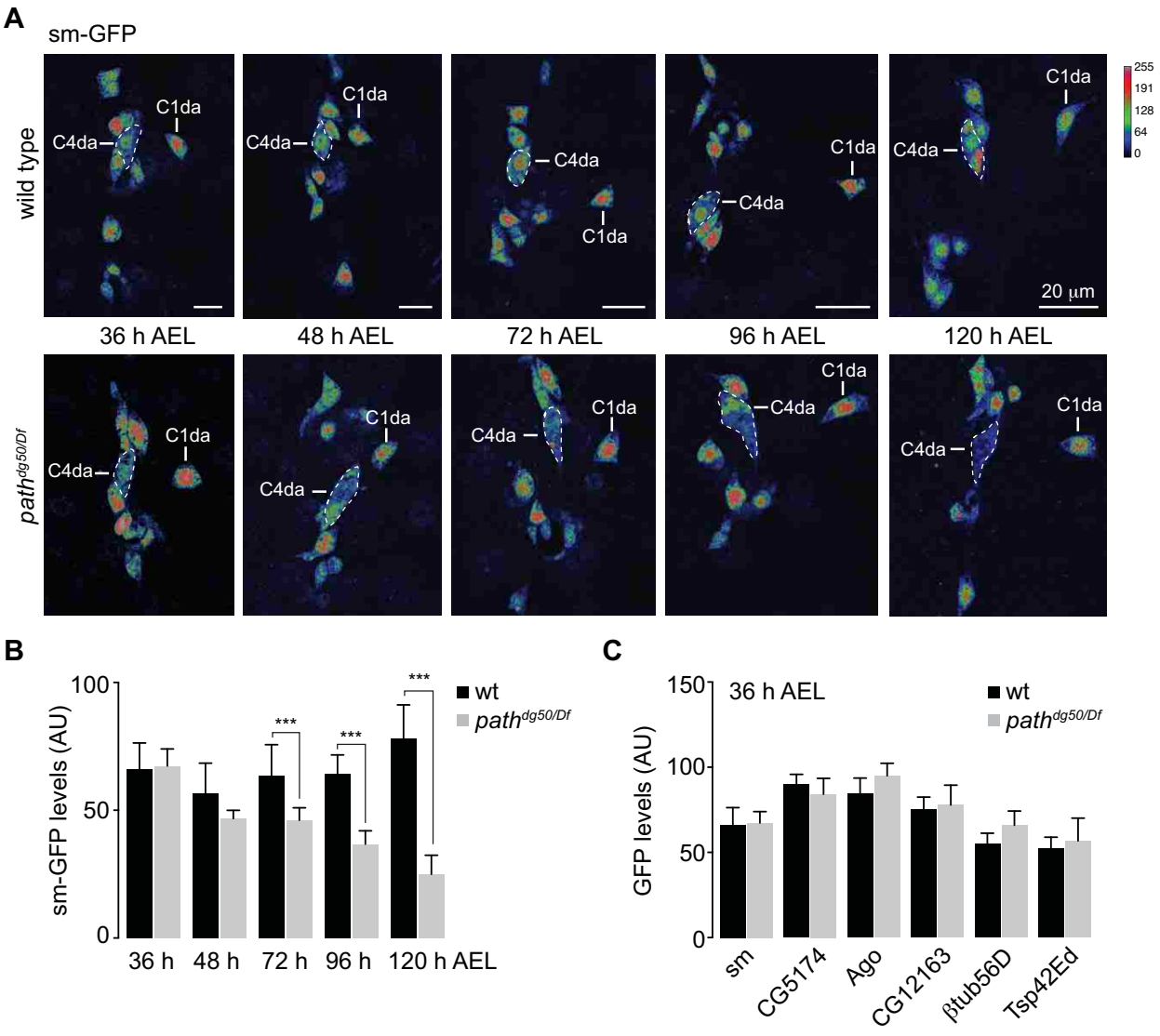

Figure S8. Supplement to Figure 6.

(A) Time-course of sm-GFP expression in wild type control and *path* mutant larvae. C4da and C1da neurons are marked in each image and C4da neuron cell bodies are outlined with a white hatched line. All images were captured using live confocal microscopy and levels were assessed by measuring mean pixel intensity in cells of interest. Images are pseudocolored according to a lookup table (key, top right). (B) Plot depicting sm-GFP levels in C4da neurons over a developmental time-course in wt control and *path* mutant larvae. $n>10$ cells for each bar. ***$P<.001$ relative to time-matched wt control, one-way ANOVA with a post-hoc Tukey's test.

(C) Plot depicting GFP levels for the indicated exon traps at 36 h AEL in wt control and *path* mutant larvae. $n>10$ cells for each bar. GFP levels for each of the exon traps did not significantly differ between wt control and *path* mutant larvae at 36 h AEL, unpaired t-test with Welch's correction.

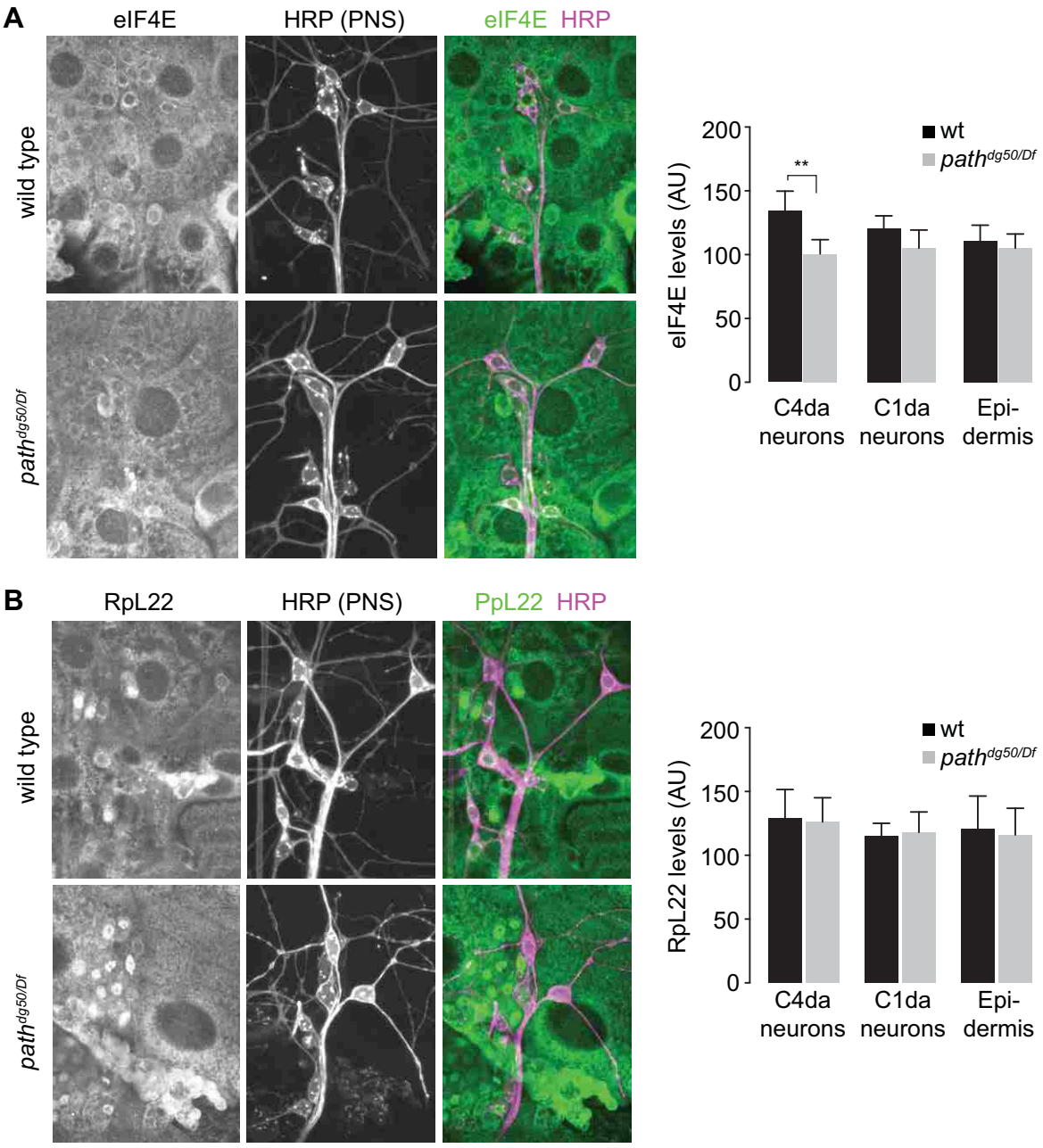

Figure S9. Supplement to Figure 7.

(A) eIF4E and (B) Rpl22 levels in wild type control and *path*$^{dg50/Df}$ mutant larvae. Third instar larvae (96 h AEL) were stained with antibodies to eIF4E (A) or RpL22 (B) and HRP (to label PNS neurons). eIF4E (A) and Rpl22 (B) signal intensities were measured in 2D projections of confocal stacks. Control and *path* mutant fillets were processed identically (stained in the same

tube, imaged using identical settings). Mean values and standard deviation for intensity measurements of 10 cells for each cell type/genotype combination shown. ***P<.001, one-way ANOVA with a post-hoc Tukey's test.

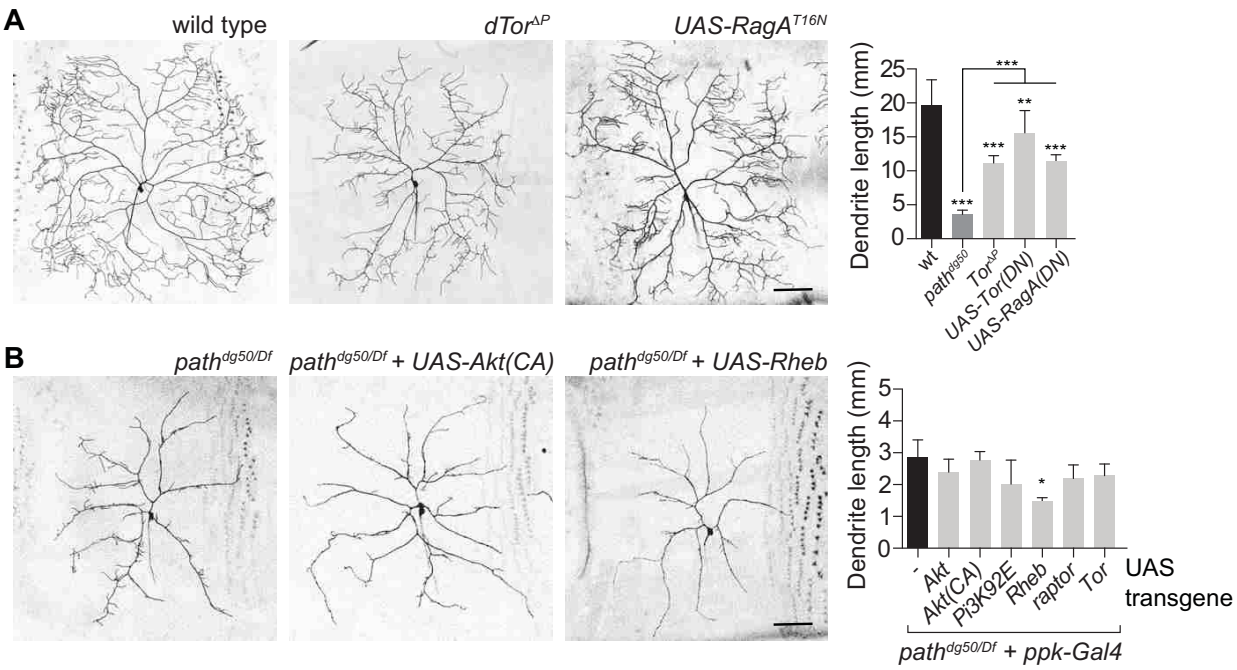

Figure S10. Relationship between Path and TORC1 in dendrite growth.

(A) Effect of TORC1 inactivation on C4da dendrite growth. Representative images of wild type control, *dTor* mutant, or RagA dominant-negative expressing C4da MARCM clones are shown. Quantification depicts mean total dendrite length for the indicated genotypes ($n > 6$ neurons for each). (B) Assaying rescue activity of TORC1 activation on C4da growth defects in *path* mutants. The indicated transgenes were expressed in C4da neurons of *path* mutants. Quantification depicts mean total dendrite length for the indicated genotypes ($n > 8$ neurons for each). *$P<0.05$; **$P<0.01$; ***$P<0.001$; ns, not significant; one-way ANOVA with a post-hoc Dunnett's test. Scale bars, 50μm.

Chapter 3 Functions of the SLC36 transporter Pathetic in growth control

3.1 Abstract

Neurons exhibit extreme diversity in size, but whether large neurons have specialized mechanisms to support their growth is largely unknown. Recently, we identified the SLC36 transporter Pathetic (Path) as a factor required for extreme dendrite growth in neurons. Path is broadly expressed, but only neurons with large dendrite arbors or small neurons that are forced to grow large require path for their growth. To gain insight into the basis of growth control by path, we generated additional alleles of path and further examined the apparent specificity of growth defects in path mutants. Here, we confirm our prior finding that loss of path function imposes an upper limit on neuron growth, and additionally report that path likely limits overall neurite length rather than dendrite length alone. Using a GFP knock-in allele of path, we identify additional tissues where path likely functions in nutrient sensing and possibly growth control. Finally, we demonstrate that path regulates translational capacity in a cell type that does not normally require path for growth, suggesting that path may confer robustness on growth programs by buffering translational output. Altogether, these studies suggest that Path is a nutrient sensor with widespread function in Drosophila.

3.2 Introduction

Neurons exhibit extreme diversity in size, but how growth programs are tailored to meet the respective demands of small and large neurons is largely unknown. From a genetic screen for mutations that differentially affected growth in *Drosophila* sensory neurons with different sized dendrite arbors, we identified *pathetic (path)* as a gene that selectively affects dendrite growth in neurons with large dendrite arbors.[1] In *path* mutants, dendrite growth arrests at a fixed upper

limit of dendrite length in neurons that normally have differently sized arbors. While *path* is normally dispensable for growth in neurons with small dendrite arbors, forcing these neurons to elaborate complex dendrite arbors reveals that these neurons likewise require *path* for growth beyond the same upper limit of dendrite growth. Thus, *path* appears to define a pathway required to support extreme growth demands in neurons.

How does *path* modulate neuron growth? *path* encodes an SLC36 family transporter that paradoxically displays very low transport capacity under physiological conditions[2,3] leading to the model that Path functions similar to other transporter-related receptors (tranceptors) to regulate signaling in response to metabolites. Examples of transceptors include the System A amino acid transporter SNAT2, which regulates transcription in response to amino acid binding[4] and GLUT2, a sugar transporter that has transport-independent functions as a receptor for extracellular glucose.[5] With respect to growth control in neurons, Path regulates translational capacity,[1] but how Path couples nutrient status to translational control is unknown. One model that has been proposed is that Path functions as a nutrient sensor for the target of rapamycin complex 1 (TORC1).[2] In support of this model, one study demonstrated that SLC36A1 and Path can interact with components of the Ragulator complex,[6] which links amino acid availability to TORC1 activation.[7] However, other studies have yielded different results. For example, proteomic analysis of SLC36-interacting proteins failed to identify interactions between SLC36 transporters and Ragulator or TORC1 components,[8] and SLC36A1 overexpression antagonizes TORC1 activation in some contexts.[9] Furthermore, we found no evidence of interactions between Path and TORC1 in developmental control of neuron growth,[1] though gain-of-function experiments suggest that Path can promote neuron growth together with TORC1.

Several prominent questions remain regarding the function of Path and other SLC36 family transporters in growth control. First, the nature of interactions between Path and TORC1 and whether these interactions differ according to cell type or cellular state merits further study. Second, although Path is broadly expressed in neurons and non-neuronal cells, mutation of *path* affects growth in neurons with large dendrite arbors, but not in other cells. Whether this apparent specificity reflects cellular differences in Path function, regulation, or redundancy with other SLC36 transporters is unknown. Finally, the nature of the metabolites that elicit Path-dependent signaling *in vivo* remain elusive, though amino acids are the most likely candidates. As a first step to answering these questions, we generated new alleles of *path* that facilitate functional analysis of the gene product *in vivo*. Here, we provide additional support for the notion that *path* is required for growth above a fixed limit in neurons. Using a functional GFP knock-in allele of *path* we provide an overview of Path expression and localization in well-fed larvae, defining likely sites of Path function. Finally, we provide evidence that Path regulates translational output in non-neuronal cells.

3.3 Materials and Methods

3.3.1 Fly stocks

The following alleles were used in this study: w^{1118} (FBal0018157), $path^{dg50}$ (FBal0305310), $path^{GFP}$ (this study), $path^{\Delta}$ (this study), *Df(3L)BSC773* (FBab0045882), *ppk-CD4-tdTomato* (FBti0143432), *ppk.hs-mCD8.3xEGFP* (FBtp0065837), *UAS-Rluc-Fluc*bicistronic reporter (FBtp0108905), *A58-Gal4* (FBti0072310), and *vas-Cas9* (FBti0160473).

3.3.2 Generation of path alleles

The *path* knockout allele and GFP-tagged *path* knock-in allele were engineered using CRISPR/Cas9 mediated gene editing.[11]Two target sites were selected just outside of the coding region of the shortest isoform, *path-RE*, which includes the four exons shared by all *path* isoforms, using the CRISPR Optimal Target Finder (http://tools.flycrispr.molbio.wisc.edu/targetFinder/).[11] chiRNA plasmids were generated by insertion of annealed oligonucleotides into the BbsI site of pU6-BbsI-chiRNA.[10] The donor vector for the *path* knockout allele was cloned by restriction digest, inserting 5′ and 3′ 1kb homology arms into the NheI and SapI sites, respectively, of the pHD-DsRed plasmid.[14] The donor vector for the *path-GFP* knock-in allele was cloned by Gibson assembly, using the knockout donor vector as a backbone, with GFP fused in-frame with the C-terminal end of *path* and the LoxP-flanked dsRed marker following the GFP stop codon, all internal to the mutated CRISPR target sites. chiRNA and pHD-DsRed plasmids were co-injected into embryos expressing Cas9 in the germline (BL55821: *y[1] M{vas-Cas9.RFP-}ZH-2A w[1118]/FM7a, P{w[+mC]=Tb[1]}FM7-A*).

Primers used were as follows:

path chiRNA 1 sense: cttcgtacacaactgaaactcgcca

path chiRNA 1 antisense: aaactggcgagtttcagttgtgtac

path chiRNA 2 sense: cttcgtacttcaccatttaggagag

path chiRNA 2 antisense: aaacctctcctaaatggtgaagtac

path homology arm 1 forward: gccagctagccaaacgaatggaaaagtcgtg

path homology arm 1 reverse: ctcagctagcccacggaatcgaagcggtttcttatatgctg

path homology arm 2 forward: gaacgctcttcatatgagaggctccgctttctag

path homology arm 2 reverse: cgcggctcttccgaccttctgaatatgtaatatggac

path-GFP backbone forward: cttcaccacttaggagagagcctccgctttctagataaaatc

path-GFP backbone reverse: ctgaaactcgccacactatcgaagcggtttcttatatgctg

path-GFP coding region forward: ccgcttcgatagtgtggcgagtttcagttgtgtacagacg

path-GFP coding region reverse: cgaagttatctatttgtatagttcatccatgcc

path-GFP loxP dsRed forward: ggcatggatgaactatacaaatagataacttcgtataatgtatgc

path-GFP loxP dsRed reverse: gcggaggctctctcctaagtggtgaagtatataacttcgtatagc

3.3.3 Live imaging

Larvae were mounted in 90% glycerol under coverslips sealed with grease and imaged on Leica SP5 microscope with a 20x/0.8NA lens (Fig. 2A) or a 40x 1.25NA lens (all other images).

3.3.4 Luciferase assays

Luciferase assays were as described.[1] Briefly, larvae were filleted in ice cold PBS, lysed in 1x Luciferase Cell Culture Lysis Reagent (Promega), and protein concentrations were measured and normalized. 20 µl of cell lysate was analyzed for Renilla luciferase using the Luciferase Assay System (Promega), and luminescence was measured using a Victor V Plate Reader (Perkin-Elmer). All values were corrected to blank wells and normalized for protein input. For qPCR, RNA was isolated using the RNAqueous Micro kit (LifeTechnologies), reverse transcribed into cDNA, and transcript levels quantified in SYBR Select (Life Technologies) on an ABI StepOne Plus instrument (Life Technologies). Primers used were Renilla F, GGGTGCTTGTTTGGCATTTC; Renilla R: GGCCATTCATCCCATGATTC; β-tubulin F, AGACAAGATGGTTCAGGT; β-tubulin R, CGAGGCTCTCTACGATAT. Data was analyzed by the Pfaffl method.[27]

3.3.5 Measurements

2D projections of Z-stacks were used for computer-assisted dendrite tracing with Neurolucida (MBF Bioscience), and features were measured using the traces. For these experiments, we imaged control and *path* mutant larvae using identical settings, including the same number and thickness of optical sections.

3.3.6 Statistical analysis

Differences between group means were analyzed via ANOVA with Tukey's HSD *post hoc* analysis; pairwise comparisons of group means were done with unpaired t-tests with Welch's correction.

3.4 Results

3.4.1 Path is required for dendrite growth beyond a fixed limit

We previously found that *path* is required for dendrite growth above a fixed limit in PNS neurons, but appears to be dispensable for growth of other larval tissues.[1] Our prior analyses made use of a nonsense mutation ($path^{dg50}$) that behaved as a strong loss of function with regard to dendrite growth, however this allele retained coding sequences for the entire N-terminal intracellular domain. We therefore set out to assay whether the truncated protein encoded by this allele provided residual activity for dendrite growth, animal viability or growth of other cell types. To this end, we used CRISPR-Cas9-mediated genome editing[10,11] to generate a deletion allele of *path* ($path^{\Delta}$) that removed the entire short isoform, leaving coding sequences for the first 16 amino acids of the long isoform of *path* but no other portion of the protein (Fig. 1A). Similar to$path^{dg50}$, larvae homozygous for the $path^{\Delta}$ allele were also viable and had no significant defects in overall larval growth (data not shown). Likewise, $path^{\Delta}$ caused severe defects in C4da

dendrite growth on its own or in combination with a chromosomal deficiency [*Df(3L)BSC773*; hereafter referred to as *Df*] that spans the entire *path* locus (Fig. 1B). Notably, dendrites of C4da neurons arrested at the same fixed value of total dendrite length in $path^{dg50/Df}$ and $path^{\Delta/Df}$ mutant larvae (Fig. 1C), strongly suggesting that this represents a complete loss-of-function phenotype. Given that this allele of *path* is viable, it should be possible to use this allele for systematic analysis of *path* function in other contexts as well.

Whereas PNS neurons require *path* for extreme growth, *path* is dispensable for cell growth in body wall epithelial cells, oenocytes, fat bodies, and salivary glands, as well as overall animal growth in larva and adult flies under well-fed laboratory conditions.[1] However, we cannot rule out a role for *path* in imparting robustness to growth programs, or modulating growth programs under stressful conditions (see below). In contrast to our observations, a prior study relying on a P-element insertion allele of *path* ($path^{KG06640}$) reported that *path* influenced overall animal growth.[2] Although we found that $path^{KG06640}$ is a strong hypomorphic *path* allele, we observed no overt effects of *path* mutation on animal growth in any allelic combination[1]. Notably, our studies included $path^{KG06640}$ as well as 2 molecularly defined amorphic *path* alleles. We therefore speculate that second-site mutations may have contributed to the reported effects of $path^{KG06640}$ on animal growth. Alternatively, *path* function in animal growth could be responsive to nutrients that differed in the food sources in the prior study and our more recent studies. Nevertheless, we conclude that under well-fed conditions, *path* is dispensable for overall animal growth.

3.4.2 Path regulates overall neuron size

Path localizes to both axons and dendrites, and our working model for *path* function in neuronal growth control is that Path regulates translational capacity of neurons. With this in

mind, it's unclear how Path could selectively regulate dendrite growth. Our prior studies indicated that *path* is required for dendrite growth beyond a fixed limit; whether *path* similarly affects axon growth has not been investigated. We therefore wanted to determine whether *path* was responsive to growth demands of dendrites alone or axons and dendrites.

Axon outgrowth precedes dendrite development in *Drosophila* embryonic PNS neurons, with axons innervating targets in the ventral nerve cord (VNC) (Fig. 2A). Because the VNC is located anteriorly, larval sensory neurons in posterior segments have longer axons than corresponding neurons in anterior segments. If *path* is setting an upper limit on dendrite growth, as we previously hypothesized,[1] we would expect dendrites of C4da neurons in different segments to arrest at the same fixed value of dendrite length. In contrast, if *path* is responsive to growth demands of axons and dendrites, dendrites in PNS neurons with longer axons should be more severely affected by loss of *path*. Our prior analysis of *path* function in dendrite growth involved PNS neurons located in a fixed position along the anterior-posterior (AP) axis,[1] which therefore had axons of the same length, so we examined whether C4da dendrite growth was more severely affected in PNS neurons located in posterior segments of *path* mutants (Fig. 2A). To this end, we measured dendrite length of C4da neurons in 3 abdominal segments (A2, A5, A8) and compared mean dendrite lengths of neurons in segment A2 to those in A5 and A8. We found that C4da neurons in posterior segments had significantly shorter dendrites and fewer dendritic branches in *path* mutant larvae (Fig. 2B-C), consistent with the notion that *path* mutation sets an upper limit on total neurite length rather than dendrite length alone.

3.4.3 path is required for axon growth

We next assayed for growth defects in axons by visualizing terminal axonal arbors of C4da neurons. We measured coverage area of axonal arbors of C4da neurons in all segments and

compared mean coverage area of wild type controls to *path* mutants. Whereas axonal arbors of *path* mutant C4da neurons were indistinguishable from wild type controls prior to 48 h after egg laying (AEL), *path* mutant axonal arbors exhibited progressive growth defects by 144 h AEL (Fig. 3A, 3B). We further compared mean coverage area of axonal arbors of C4da neurons in the same 3 abdominal segments (A2, A5, A8) as we compared for the dendritic arbors. We found by 144 h AEL, C4da neurons in posterior segments exhibited severe defects in axon growth in *path* mutant larvae (Fig. 3C). By contrast, we observed no effect on the overall axon length or terminal arbor of motor neurons that innervate dorsal muscles (data not shown), possibly because the total neurite length of motor axons and dendrites is below the threshold for *path*-dependent growth. We conclude that mutations in *path* likely impose an upper limit on overall neurite (axon and dendrite) growth, rather than setting an upper limit on dendrite length alone, and that *path* function is dispensable for growth below this limit.

3.4.4 path affects presynapse formation and nociceptive escape response

Drosophila larval da neurons activate motor responses to various sensory cues. For example, activation of C4da sensory neurons through mechanical sting, heat, ultraviolet light, or blue light causes a nociceptive rolling escape. Our collaborator has recently identified second-order interneuron A08n that directly maintain synapses with C4da neurons (Soba laboratory, unpublished). As the initial synapse responsible for the rolling escape behavior, forming precise synapse between C4da axons and A08n dendrites is critical for the following sensori-motor circuitry. Therefore, we visualized presynaptic protein synaptobrevin (Syb) in C4da axons by using Syb-GFP and monitored whether synaptic contact is lost in *path* mutants. We measured coverage area of Syb-GFP containing presynaptic vesicles in all segments and compared mean coverage area of wild type controls to *path* mutants. Similar to what we found for the axonal

arbors, the Syb-GFP containing presynaptic vesicles of *path* mutants were indistinguishable from controls prior to 48 h AEL, but *path* mutants severely decreased presynaptic Syb protein levels by 144 h AEL (Fig. 4A, 4B). We also compared coverage area of Syb-GFP containing presynaptic vesicles in A2, A5, and A8 abdominal segments. By 144 h AEL, *path* mutants largely affected the Syb-GFP containing presynapse formation in posterior segments (Fig. 4C).

Since the direct synapses of C4da axons to A08n dendrites were lost in *path* mutants, we assumed that the nociceptive escape response in *path* mutants would be lost too. The mechanical-nociception assays using Von Frey filament validated our thoughts. By 120 h AEL, the nociceptive escape in *path* mutants were lost, with only 3% of rolling compared to 52% of rolling in controls (Soba laboratory, unpublished). We concluded that *path* function is required for axon growth and functional C4da – A08n circuit formation.

3.4.5 Path is differentially expressed in different larval tissues

One prominent model for SLC36 transporter function in growth control is that SLC36 transporters serve as nutrient sensors for TORC1.[12] Two predictions of this model are that SLC36 transporters should be responsive to amino acids and that they should localize to lysosomes, where TORC1 is activated.[9] In support of the first prediction, some SLC36 transporters bind amino acids with a high degree of specificity,[2,3,13,14] though different SLC36 transporters show different binding preferences and markedly different transport properties. Confounding the potential link to TORC1, different SLC36 transporters appear to localize differently. Whereas SLC36A1 is most active at acidic pH and predominantly localizes to lysosomes,[14] Path and its closest vertebrate counterpart SLC36A4 are most active at neutral pH and appear to localize to the plasma membrane and a number of intracellular compartments.[1,15] However, analysis of SLC36 protein distribution has relied on antibody

staining, which can be confounded by lack of antibody specificity, artifacts of fixation, and tracking of ectopically expressed epitope-tagged proteins, which may or may not reflect endogenous expression patterns. Thus, it remains to be conclusively determined whether Path or other SLC36 transporters localize to appropriate cellular compartments to function as nutrient sensors for TORC1.

We next set out to characterize Path expression and distribution *in vivo*. To facilitate *in vivo* analysis of SLC36 transporter expression, localization, and dynamic trafficking we used CRISPR-Cas9-mediated genome editing[10,11] to generate a GFP insertion allele ($path^{GFP}$) containing the coding sequence for GFP inserted immediately upstream of the stop codon in the last coding exon of *path* (Fig. 1A). Our prior studies demonstrated that addition of GFP to the Path C-terminus does not interfere with the function of *path* transgenes[1], and we found addition of GFP to the C-terminus of the endogenous locus had no detectable effects on *path* function *in vivo*. First, heterozygosity for $path^{GFP}$ or placing $path^{GFP}$ in trans to $path^{dg50}$ or*Df(3L)BSC773* had no effect on dendrite growth. Further, we noted no obvious differences in developmental timing, body size, or fecundity of $path^{GFP}$ homozygotes compared to wild type or $path^{GFP/+}$ controls. We therefore concluded that $path^{GFP}$ is a functional allele and that we could use $path^{GFP}$ to monitor endogenous distribution and dynamics of an SLC36 transporter for the first time in a living animal.

For our initial characterization of $path^{GFP}$ we monitored GFP distribution in well-fed third instar larvae, as the neuronal growth defects we previously described were analyzed in well-fed animals.[1] In third instar larvae, $Path^{GFP}$ was broadly expressed (Fig. 5A), consistent with our prior antibody staining results[1]. However, $Path^{GFP}$ accumulated to different levels in different tissues, suggesting that Path regulation varies according to tissue type. Within the body wall,

Path^{GFP} was most highly expressed in epithelial cells, where it accumulated at junctional domains, consistent with plasma membrane localization (Fig. 5B), and sensory neurons, where it was present in axons, cell bodies, and throughout dendrite arbors (Fig. 5B).

Although our phenotypic analysis of *path* mutants has focused on growth control in the PNS, Path^{GFP} was expressed at the highest levels in the larval brain and the digestive system. Within the larval brain, Path^{GFP} expression was especially high in surface glia (Fig. 5C), suggesting that Path may participate in glial growth control or nutrient sensing. Notably, a P-element insertion allele of *path* causes increased sensitivity to ethanol-induced sedation and increased ethanol-induced hyperactivity,[16] therefore we speculate that Path may function in glia to modulate these behavioral responses to alcohol in*Drosophila*. Additionally, glial cells form the blood-brain barrier (BBB) in *Drosophila*, providing a barrier to solute diffusion and serving roles in nutrient uptake for the brain,[17] so it will be intriguing to determine whether *path* contributes to BBB function. It should be noted that although there have been no reports on expression or localization of SLC36 at the vertebrate BBB, other members of the β group of SLCs (neutral amino acid transporters) localize to the BBB.[18,19]

Path^{GFP} was also present at high levels in the digestive system, thus it seems plausible that Path may function as an intestinal nutrient sensor. Although candidate receptors for carbohydrate sensing in the gut have been identified,[20–22] little is known about the nature of intestinal amino acid sensing programs. Within the digestive system, Path^{GFP} was present at the highest levels in the proventriculus (Fig. 5A, D), a structure involved in food maceration as well as insect innate immunity[23]; whether Path functions in processes other than nutrient sensing remains to be determined. In the midgut, Path^{GFP} strongly labeled small clusters of cells (arrows, Fig. 5D) that likely correspond to adult midgut progenitor cells (AMPs). AMPs give rise

to all of the cells of the adult midgut including intestinal stem cells,[24] therefore it is conceivable that Path functions as a nutrient sensor to regulate proliferation of these precursors.

Finally, we note that Path^{GFP} adopted a similar distribution in most cell types: the majority of the protein was predominantly confined to plasma membrane domains (Fig. 5B, E), but low levels of Path^{GFP} were present in intracellular puncta (Fig. 5B′, E′). Thus, at least in well-fed larvae, negligible amounts of Path appear to localize to lysosomal compartments. Thus, although we cannot rule out a role for Path in TORC1 activation, our results suggest that the connection may be indirect. Notably, some SLC36 transporters can be dynamically trafficked in a nutrient-dependent manner in cultured cells,[6] but similar trafficking patterns have not yet been demonstrated *in vivo*.

3.4.6 Path regulates translational capacity in non-neuronal tissues

path regulates neuron growth by modulating translational output of PNS neurons.[1] Paradoxically, Path is widely expressed but growth defects are manifest specifically in sensory neurons. We therefore wanted to test the hypothesis that *path*regulates translational output in sensory neurons but not other cell types. For these studies we focused on larval body wall epidermis for the following reasons: Path is expressed at high levels in these cells and *path* mutation had no significant effect on size of these cells.[1] We expressed a *UAS-Luciferase* reporter specifically in epithelial cells of wild type control or *path* mutant larvae and measured protein and mRNA expression levels by Luciferase activity assays and qRT-PCR, respectively. To our surprise, *path* mutation caused a significant decrease in epithelial Luciferase activity while causing only a modest decrease in mRNA levels (Fig. 6A), suggesting that *path* regulates translational capacity in epithelial cells as well as neurons. Although it

remains to be determined whether *path* similarly regulates translational output in other cell types, we speculate that Path is broadly utilized to couple nutrient conditions to translational output.

3.4.7 *path* is essential for the survival of adult *Drosophila melanogaster*

To gain insight into the functions of Path, we examined the influences of Path in adult survival. *path* mutant led to a dramatically shortened life span, with an ~73 % reduction in the median life span: 17 days for *path* flies, 24 days for *path* + *UAS-path-GFP*, and 62 days for wildtype control (Fig. 7A). We further discovered that there were sex differences in the effect of *path* on life span. In wildtype flies, female medium life span was 63 days, and male medium life span was 59 days. However, in *path* mutant flies, female medium life span was 28 days, and male medium life span was only 12 days. *path* female flies lived 55% shorter than wildtype females, whereas *path* males lived dramatically 80% shorter than wildtype males (Fig. 7B). Next, we used genetic rescue assay to define the functional site for path to support adult survival. Ubiquitous expression of Path (Actin-Gal4, UAS-path-GFP) rescued the short life span of *path*, showing that the shortened life span in *path* mutants was caused by loss of path function (medium life span: 61 days for *path* + Actin>*path-GFP*, and 62 days for wildtype control). In contrast, neuronal expression of Path using C4da-specific (medium life span of *path* + ppk>*path-GFP*: 43 days), or PNS-specific (medium life span of *path* + 109280>*path-GFP*: 46 days) Gal4 drivers did not fully rescued the *path* mutant survival (Fig. 7C). Interestingly, path expression in other tissues, such as epithelium, hemocytes, salivary gland, or oenocytes, also partially rescued the *path* mutant life span (Fig. 7D). These results suggest that neuronal Path and Path in other tissues coordinately regulate life span in adult *Drosophila*.

3.5 Discussion

How growth programs are tailored to meet the demands of large neurons is largely unknown. Here, we demonstrate that the SLC36 transporter Path is required for growth of axons and dendrites in large neurons. Although the precise mechanism of action remains to be determined, the amino-terminal intracellular domain is essential for Path function in neuron growth control,[1] and we hypothesize that Path transduces nutrient signals via protein-protein interactions between its N-terminal intracellular domain and unidentified signaling proteins to modulate translational output (Fig. 6B). In light of prior studies suggesting a link between SLC36 transporters and TORC1 signaling[2,6,12] and our observation that co-overexpression of Path and Rheb potentiates dendrite growth,[1] we propose that Path may promote neuron growth, in part, through regulation of TORC1 activity. However, given our observations that Path primarily localizes to the plasma membrane and that mutations in TORC1 components cause more modest neuron growth deficits than mutation of *path*, it seems likely that Path engages downstream pathways other than TORC1 to promote neuron growth. Although the identity of these pathways is currently unknown, eukaryotic initiation factor 2 (eIF2) activity is regulated by a suite of kinases (eIF2K) that tune translation levels in response to environmental stresses, including amino acid deficiency.[25]

Although Path is broadly expressed, *path* is dispensable for growth in most cell types under well-fed laboratory conditions. One prediction of this observation is that Path selectively affects translation in large neurons. Our results from this study refute this notion; cells that do not require *path* for growth still require *path* for maximum translational output. How can we explain the disparity in growth phenotypes between neurons and other cells? First, Path may play a more significant role in translational control of neurons than other cell types. *Drosophila* has

several uncharacterized genes that encode SLC36 transporters, and these gene products may function redundantly to control growth together with Path in some cell types. Consistent with this notion, overexpression of *CG1139*, which encodes another SLC36 transporter, drives ommatidial overgrowth in the eye.[2] Second, the residual translational capacity in *path* mutants is likely sufficient to support normal growth in many cell types, at least under certain conditions. Similarly, loss of *Drosophila* 4E-BP (*Thor*) function reduces overall translation without any obvious effect on animal growth in well-fed conditions.[26] Intriguingly, environmental stresses such as hypoxia or starvation uncover a requirement for *Thor* in growth control. Similarly, we predict that stresses that compromise translational efficiency should sensitize cells to a requirement for *path* function, therefore an exciting future direction will be to determine whether *path* exerts state-dependent functions on growth control.

3.6 References

1. Lin W-Y, Williams C, Yan C, Koledachkina T, Luedke K, Dalton J, Bloomsburg S, Morrison N, Duncan KE, Kim CC, et al. The SLC36 transporter Pathetic is required for extreme dendrite growth in Drosophila sensory neurons. Genes Dev 2015; 29:1120–35.

2. Goberdhan DCI, Meredith D, Boyd CAR, Wilson C. PAT-related amino acid transporters regulate growth via a novel mechanism that does not require bulk transport of amino acids. Dev Camb Engl 2005; 132:2365–75.

3. Pillai SM, Meredith D. SLC36A4 (hPAT4) is a high affinity amino acid transporter when expressed in Xenopus laevis oocytes. J Biol Chem 2011; 286:2455–60.

4. Hyde R, Cwiklinski EL, MacAulay K, Taylor PM, Hundal HS. Distinct sensor pathways in the hierarchical control of SNAT2, a putative amino acid transceptor, by amino acid availability. J Biol Chem 2007; 282:19788–98.

5. Stolarczyk E, Guissard C, Michau A, Even PC, Grosfeld A, Serradas P, Lorsignol A, Pénicaud L, Brot-Laroche E, Leturque A, et al. Detection of extracellular glucose by GLUT2 contributes to hypothalamic control of food intake. Am J Physiol Endocrinol Metab 2010; 298:E1078–87.

6. Ögmundsdóttir MH, Heublein S, Kazi S, Reynolds B, Visvalingam SM, Shaw MK, Goberdhan DCI. Proton-assisted amino acid transporter PAT1 complexes with Rag GTPases and activates TORC1 on late endosomal and lysosomal membranes. PloS One 2012; 7:e36616.

7. Sancak Y, Bar-Peled L, Zoncu R, Markhard AL, Nada S, Sabatini DM. Ragulator-Rag complex targets mTORC1 to the lysosomal surface and is necessary for its activation by amino acids. Cell 2010; 141:290–303.

8. Rebsamen M, Pochini L, Stasyk T, de Araújo MEG, Galluccio M, Kandasamy RK, Snijder B, Fauster A, Rudashevskaya EL, Bruckner M, et al. SLC38A9 is a component of the lysosomal amino acid sensing machinery that controls mTORC1. Nature 2015; 519:477–81.

9. Zoncu R, Bar-Peled L, Efeyan A, Wang S, Sancak Y, Sabatini DM. mTORC1 senses lysosomal amino acids through an inside-out mechanism that requires the vacuolar H(+)-ATPase. Science 2011; 334:678–83.

10. Gratz SJ, Cummings AM, Nguyen JN, Hamm DC, Donohue LK, Harrison MM, Wildonger J, O'Connor-Giles KM. Genome engineering of Drosophila with the CRISPR RNA-guided Cas9 nuclease. Genetics 2013; 194:1029–35.

11. Gratz SJ, Ukken FP, Rubinstein CD, Thiede G, Donohue LK, Cummings AM, O'Connor-Giles KM. Highly specific and efficient CRISPR/Cas9-catalyzed homology-directed repair in Drosophila. Genetics 2014; 196:961–71.

12. Heublein S, Kazi S, Ogmundsdóttir MH, Attwood EV, Kala S, Boyd CAR, Wilson C, Goberdhan DCI. Proton-assisted amino-acid transporters are conserved regulators of proliferation and amino-acid-dependent mTORC1 activation. Oncogene 2010; 29:4068–79.

13. Boll M, Daniel H, Gasnier B. The SLC36 family: proton-coupled transporters for the absorption of selected amino acids from extracellular and intracellular proteolysis. Pflüg Arch Eur J Physiol 2004; 447:776–9.

14. Wreden CC, Johnson J, Tran C, Seal RP, Copenhagen DR, Reimer RJ, Edwards RH. The H+-coupled electrogenic lysosomal amino acid transporter LYAAT1 localizes to the axon and plasma membrane of hippocampal neurons. J Neurosci Off J Soc Neurosci 2003; 23:1265–75.

15. Roshanbin S, Hellsten SV, Tafreshiha A, Zhu Y, Raine A, Fredriksson R. PAT4 is abundantly expressed in excitatory and inhibitory neurons as well as epithelial cells. Brain Res 2014; 1557:12–25.

16. Devineni AV, McClure KD, Guarnieri DJ, Corl AB, Wolf FW, Eddison M, Heberlein U. The genetic relationships between ethanol preference, acute ethanol sensitivity, and ethanol tolerance in Drosophila melanogaster. Fly (Austin) 2011; 5:191–9.

17. Limmer S, Weiler A, Volkenhoff A, Babatz F, Klämbt C. The Drosophila blood-brain barrier: development and function of a glial endothelium. Front Neurosci 2014; 8:365.

18. Geier EG, Chen EC, Webb A, Papp AC, Yee SW, Sadee W, Giacomini KM. Profiling solute carrier transporters in the human blood-brain barrier. Clin Pharmacol Ther 2013; 94:636–9.

19. Sundberg BE, Wååg E, Jacobsson JA, Stephansson O, Rumaks J, Svirskis S, Alsiö J, Roman E, Ebendal T, Klusa V, et al. The evolutionary history and tissue mapping of amino acid transporters belonging to solute carrier families SLC32, SLC36, and SLC38. J Mol Neurosci MN 2008; 35:179–93.

20. Miguel-Aliaga I. Nerveless and gutsy: intestinal nutrient sensing from invertebrates to humans. Semin Cell Dev Biol 2012; 23:614–20.

21. Mishra D, Miyamoto T, Rezenom YH, Broussard A, Yavuz A, Slone J, Russell DH, Amrein H. The molecular basis of sugar sensing in Drosophila larvae. Curr Biol CB 2013; 23:1466–71.

22. Miyamoto T, Slone J, Song X, Amrein H. A fructose receptor functions as a nutrient sensor in the Drosophila brain. Cell 2012; 151:1113–25.

23. Hao Z, Kasumba I, Aksoy S. Proventriculus (cardia) plays a crucial role in immunity in tsetse fly (Diptera: Glossinidiae). Insect Biochem Mol Biol 2003; 33:1155–64.

24. Jiang H, Edgar BA. Intestinal stem cells in the adult Drosophila midgut. Exp Cell Res 2011; 317:2780–8.

25. Wek RC, Jiang H-Y, Anthony TG. Coping with stress: eIF2 kinases and translational control. Biochem Soc Trans 2006; 34:7–11.

26. Teleman AA, Chen Y-W, Cohen SM. 4E-BP functions as a metabolic brake used under stress conditions but not during normal growth. Genes Dev 2005; 19:1844–8.

27. Pfaffl MW. A new mathematical model for relative quantification in real-time RT-PCR. Nucleic Acids Res 2001; 29:e45.

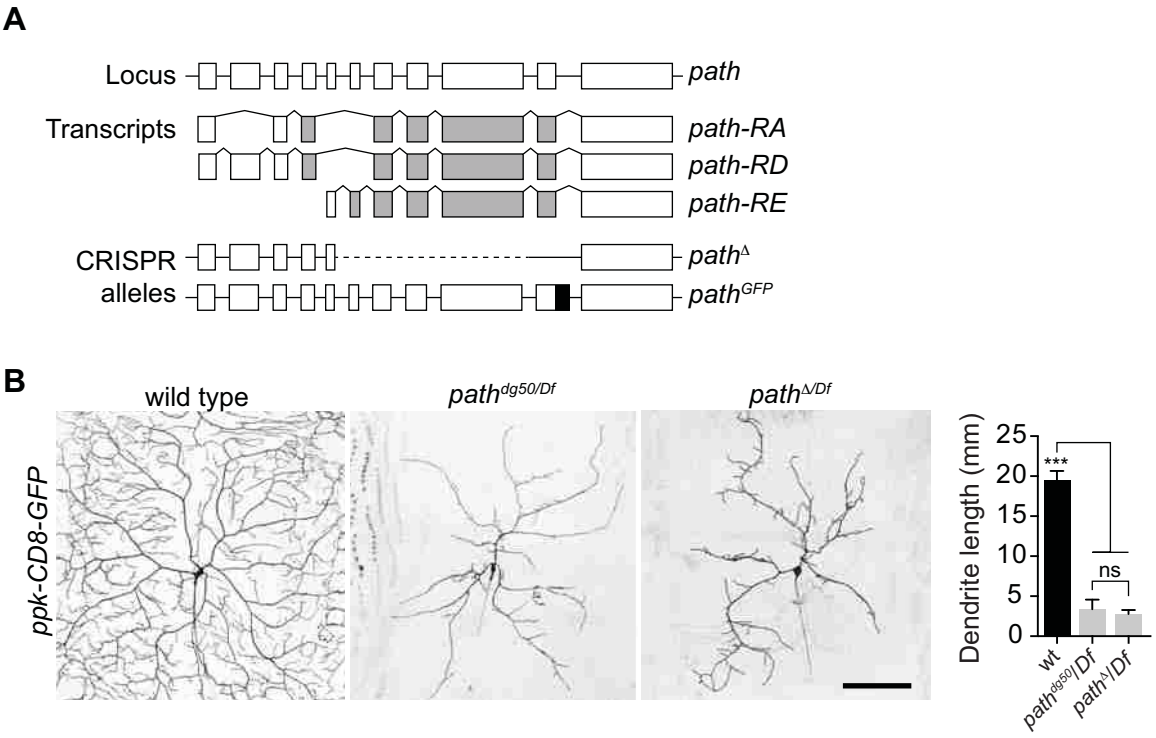

Figure 1. Generation of new *path* alleles.

(A) Schematic of the *path* locus, *path* transcripts, and new alleles generated by CRISPR-based genome engineering. Lines depict introns and boxes depict exons (empty boxes, non-coding; shaded, protein coding). The *path* locus encodes three documented transcripts and two polypeptides with alternative 5′ coding exons yielding different intracellular domains. The $path^{\Delta}$ allele deletes the entire *path-RE*transcript including the four coding exons shared by all *path* transcripts and the $path^{GFP}$ allele contains GFP coding sequences fused in-frame upstream of the Path stop codon. (B) $path^{\Delta}$ is a loss-of-function allele. *Left*, representative images C4da neurons in wild type or *path* mutant larvae. *Right*, quantification of dendrite length in the indicated genotypes (n>6 neurons for each genotype). Dendrite lengths of $path^{dg50/Df}$ and $path^{\Delta/Df}$ mutants are significantly different from wild type controls (***, <0.001*P*) but not significantly different from one another (ns), one-way analysis of variance

(ANOVA) with Tukey's HSD *post hoc* analysis. Scale bar, 100 μm. Genotypes: wt; *w^{118}/ppk-CD8-GFP; $path^{dg50}$/Df: w^{118}/ppk-CD8-GFP;; $path^{dg50}$/DF(3L)BSC773; $path^{\Delta}$/Df: w^{118}/ppk-CD8-GFP; $path^{\Delta}$/DF(3L)BSC773*.

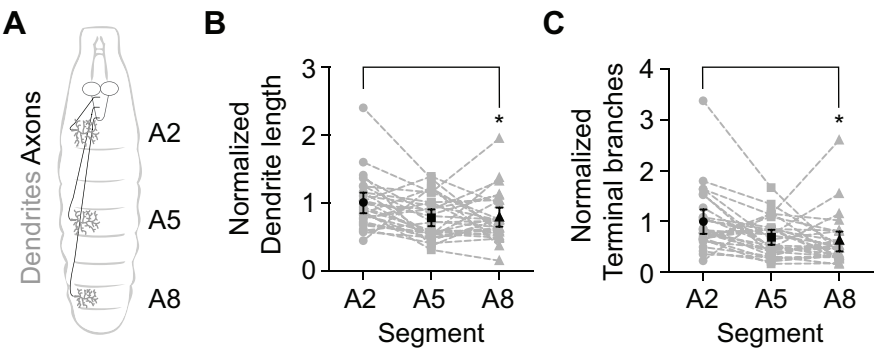

Figure 2. *path* imposes a limit on total neurite length.

(A) Schematic depiction of axon (black) and dendrite (grey) arbors of C4da neurons in abdominal segments A2, A5, and A8. Sensory neurons in more posterior segments have longer axons. Plots depict relative C4da dendrite length (B) and branch number (C) in abdominal segments A2, A5, and A8 in each of 30 $path^{dg50}/Df$ larvae. Values are normalized to mean values for segment A2. Dashed lines connect data points derived from the same larva, black points mark the mean for each segment, and error bars represent the standard deviation. *$p < 0.05$, two-way analysis of variance (ANOVA) with Tukey's HSD *post hoc* analysis.

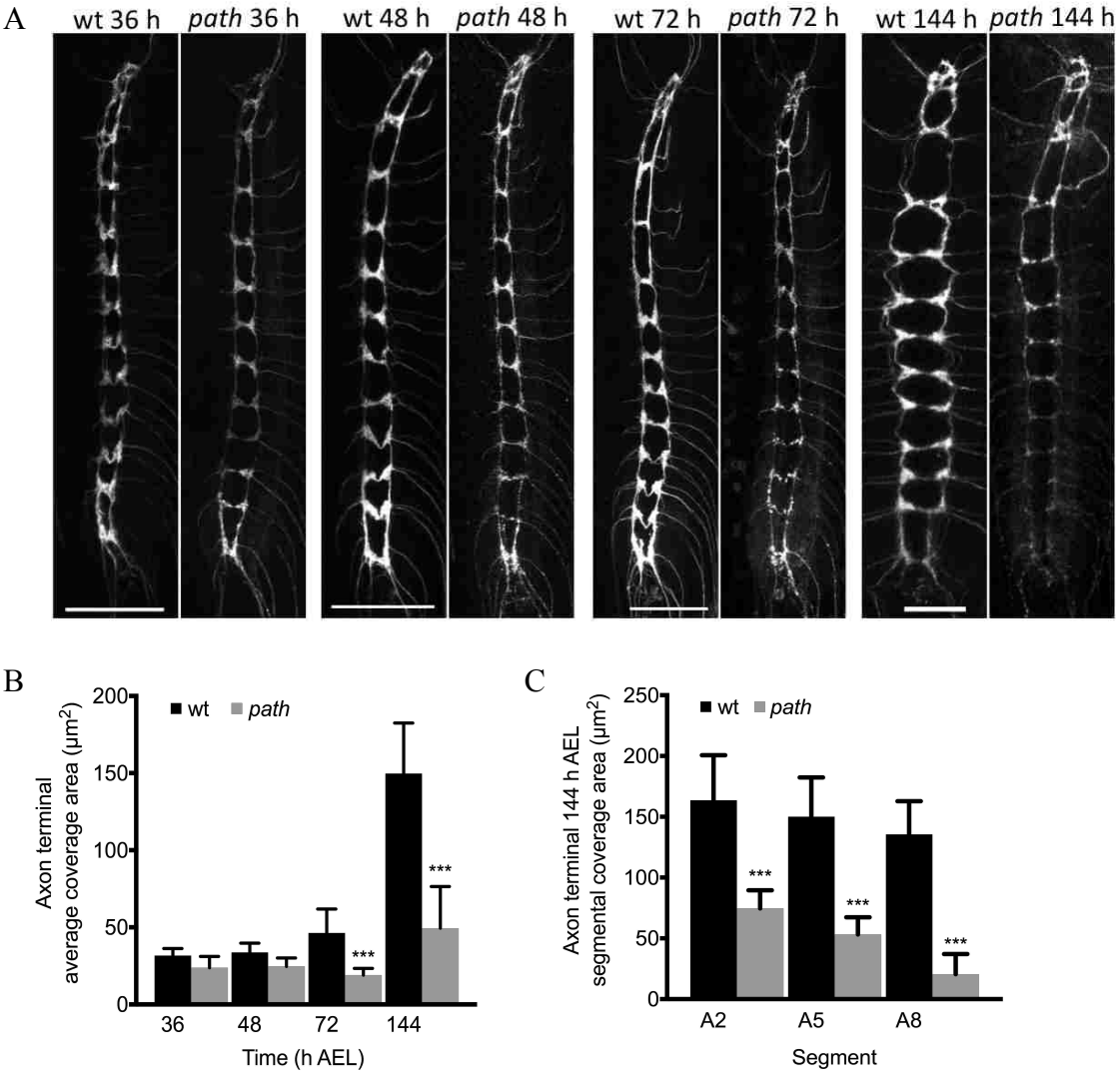

Figure 3. *path* is required for axon growth of C4da neurons.

(A) Time course of axonal arbors of C4da neurons at 36, 48, 72, and 144 h AEL in wild-type control and $path^{dg50}$ mutant larvae. Anterior is up, scale bars are 50 mm. Genotype: wt: w^{118};; *ppk-CD4-tdTomato; path:* w^{118};; $path^{dg50}$, *ppk-CD4-tdTomato*. (B) Mean coverage area of axonal arbors of C4da neurons in all segments of the indicated genotype at the indicated times are shown. n = 10 neurons for each time point. (C) Mean coverage area of axonal arbors of C4da neurons in abdominal segments A2, A5, and A8 of the indicated genotype at 144 h AEL are shown. n = 10 neurons for each time point.

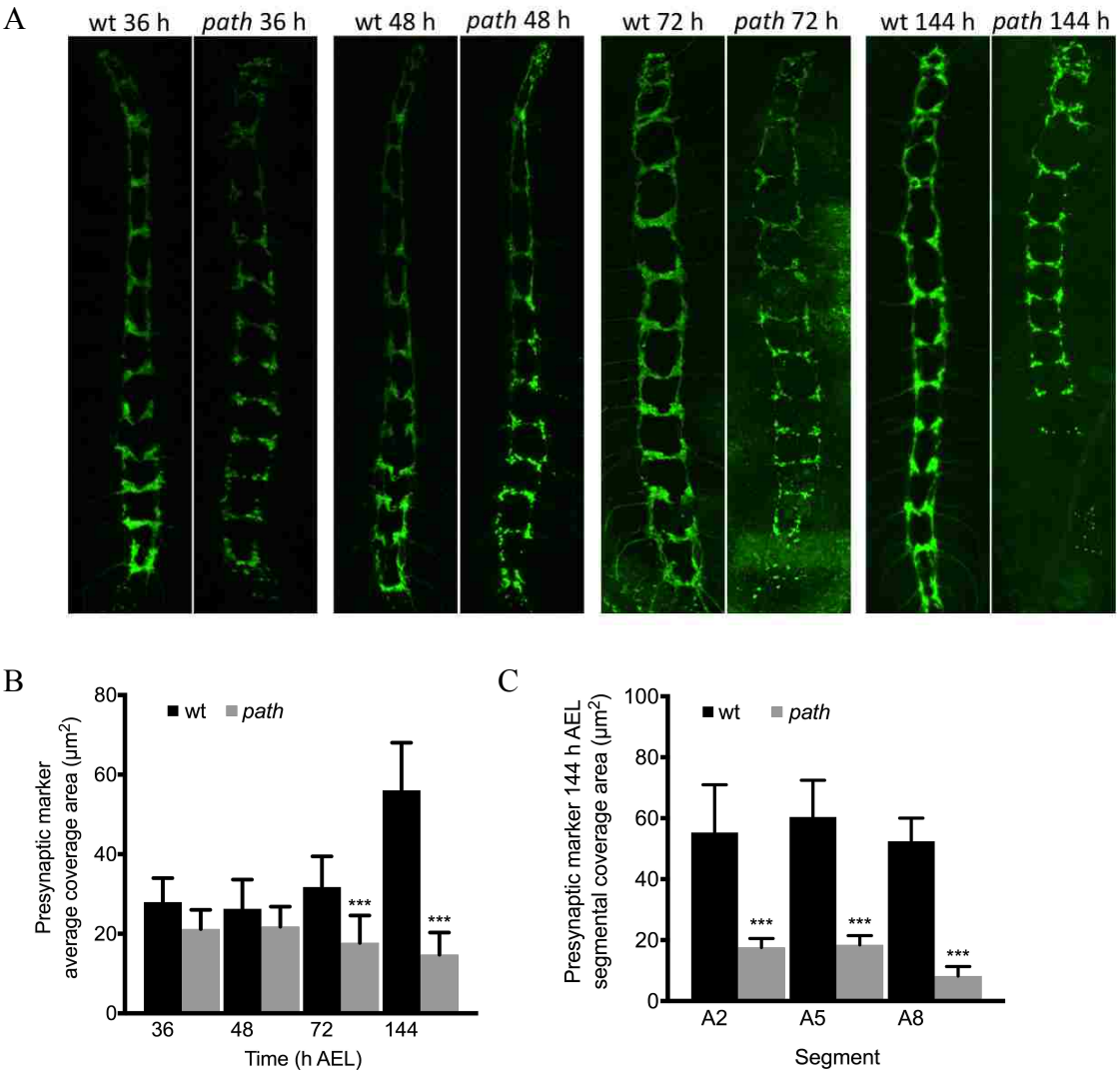

Figure 4. *path* is required for proper presynapse formation.

(A) Time course of Syb-GFP containing presynaptic vesicles of C4da axons at 36, 48, 72, and 144 h AEL in wild-type control and *path*^{dg50} mutant larvae. (B) Mean coverage area of Syb-GFP containing presynaptic vesicles in all segments of the indicated genotype at the indicated times are shown. n = 10 neurons for each time point. (C) Mean coverage area of Syb-GFP containing presynaptic vesicles in abdominal segments A2, A5, and A8 of the indicated genotype at 144 h AEL are shown. n = 10 neurons for each time point.

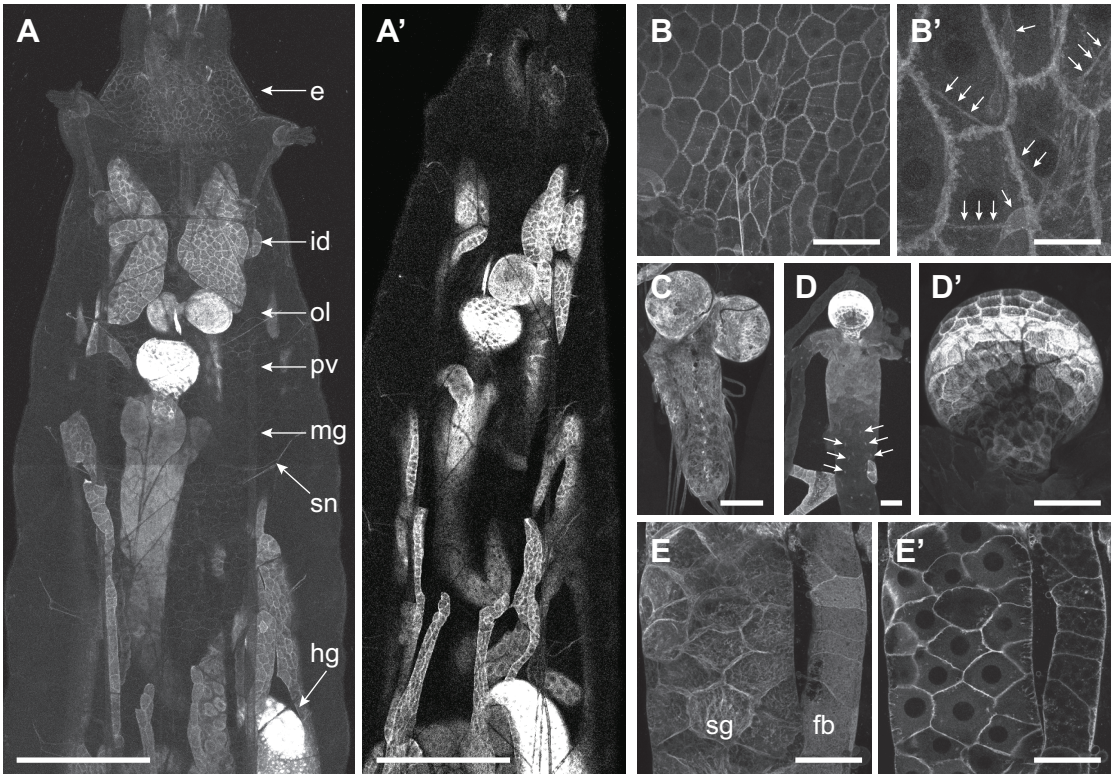

Figure 5. Path^{GFP} expression in larvae.

(A) Path^{GFP} is broadly expressed in larvae but present at different levels in different tissues. Abbreviations: e, epidermis; fb, fat body; hg, hindgut; id, imaginal discs; mg, midgut; ol, optic lobe; pv, proventriculus; sg, salivary glands; sn, segmental nerves. Scale bars: 500 μm in A, 100 μm in all other panels except for B' (25 μm). (B) Path^{GFP} expression in the body wall, where Path^{GFP} accumulates most notably at cell-cell junctions in epithelial cells and is present in cell bodies and dendrites of sensory neurons (B', arrows). Path^{GFP} is expressed at high levels in the ventral nerve cord (C), most notably in glia, and in the digestive system (D) where levels are highest in the proventriculus (D'). Arrows in (D) mark cell clusters that likely correspond to adult midgut progenitor cells. Surface (E) and medial (E) cross-sectional views of Path^{GFP} expression in a salivary gland and fat body illustrating that Path^{GFP} is largely confined to the area of the plasma membrane in most cell types. Genotype:*w*^{118}*;; path*^{GFP}/+.

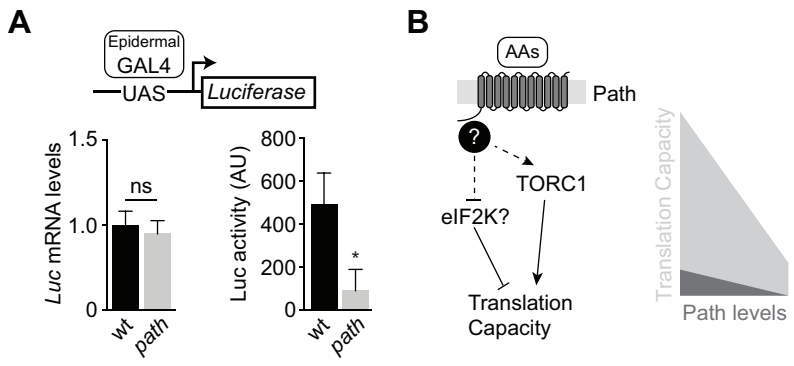

Figure 6. *path* regulates translational capacity.

(A) *path* is required for maximum translational output in non-neuronal cells. *Luciferase* mRNA levels and Luciferase activity were assayed in larval body wall extracts of wild type and *path* mutants expressing a *UAS-Rluc-Fluc* bicistronic reporter transgene in epithelial cells (*A58-Gal4*). mRNA levels reflect ΔΔCt values for *Luciferase* relative to β-*tubulin* in larval body wall lysates (n=6). For Luciferase activity, the mean and standard deviation from 6 samples is shown. ns, not significant (>0.05*P*), *<0.05*P*, unpaired t-test with Welch's correction. Genotypes: wt, w^{118}*;UAS-RLucFluc/+; A58-Gal4/+; path,* w^{118}*; UAS-RLucFluc/+; A58-Gal4,* $path^{dg50}$*/DF(3L)BSC773*. (B) Putative pathway (left) and model (right) for Path-mediated control of translational capacity. The N-terminal intracellular domain of Path plays a critical role in growth control, perhaps by linking Path to currently unknown signaling molecules (question mark). Some evidence supports a role for TORC1 downstream of Path, but we speculate that additional pathways, possibly including eIF2 kinases, contribute to translational control by Path. Though a baseline level of translation occurs even in the absence of Path protein, Path is required for maximal translational output.

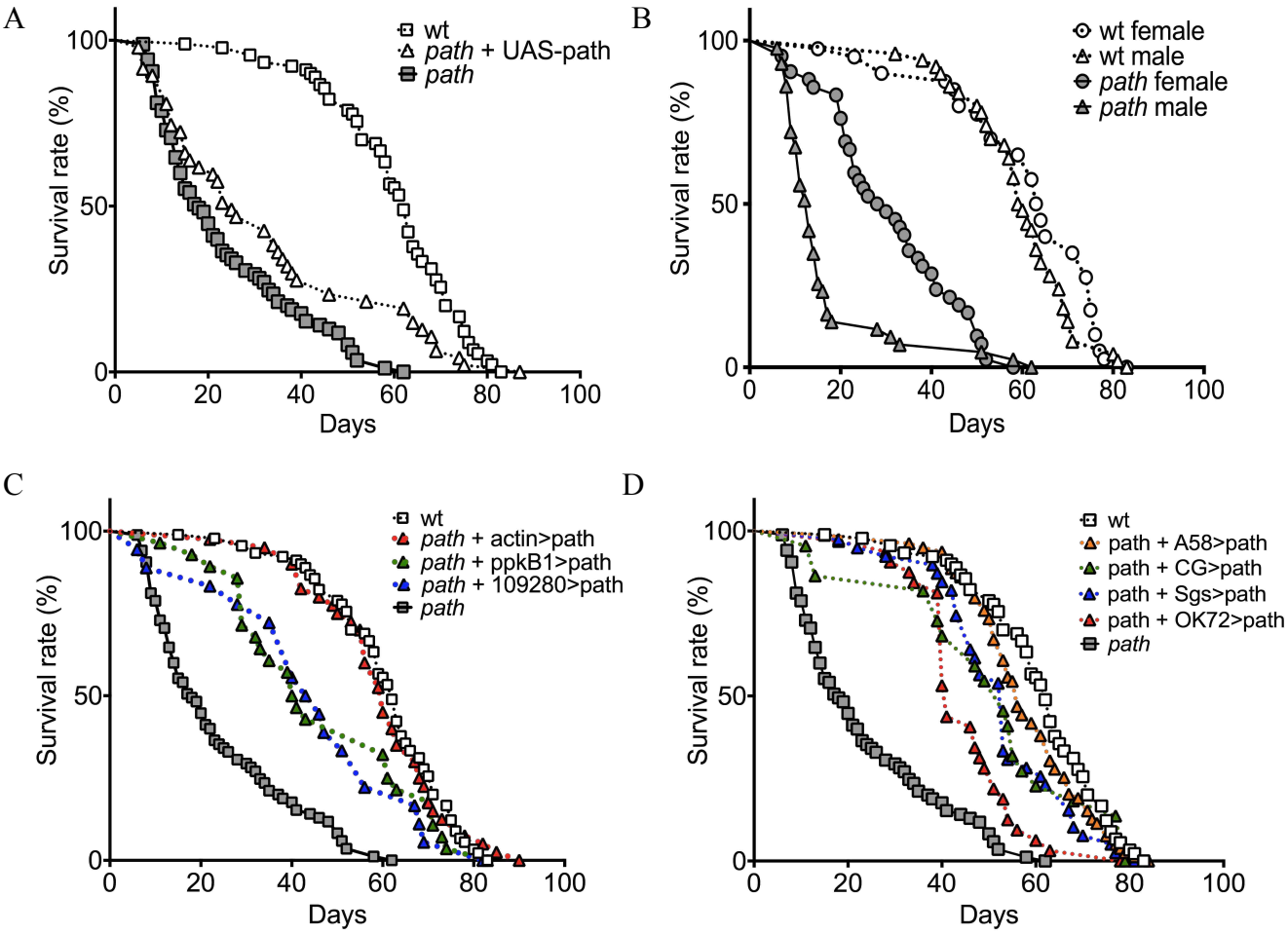

Figure 7. *path* is essential for the survival of adult *Drosophila melanogaster*.

(A-B) *path* regulates lifespan in adult *Drosophila melanogaster*. (A) Cumulative survival curves for adult *Drosophila melanogaster* wild type control, *path* ^{dg50} + *UAS-path-GFP* control, and *path*^{dg50} are shown. Each curve represents the average profile of 100 flies per genotype. (B) Cumulative survival curves for female and male adult *Drosophila melanogaster* of wild type control and *path*^{dg50} are separately shown. (C-D) *path* expression is sufficient for adult lifespan. (C) Cumulative survival curves of *UAS-path-GFP* expression directed by a variety of neuronal-Gal4 drivers to rescue lifespan defects of *path* mutants: ubiquitous, *actin-Gal4*; md neurons, *109280-Gal4*; C4da, *ppk-Gal4.* (D) Cumulative survival curves of *UAS-path-GFP* expression

directed by a variety of non-neuronal-Gal4 drivers to rescue lifespan defects of *path* mutants: epithelium, *A58-Gal4*; hemocytes, *CG-Gal4*; salivary gland, *SGS-Gal4*; oenocytes, *OK72-Gal4*.